ADSORPTION OF BINARY GAS MIXTURES

ON WET FRUITLAND COAL AND

COMPRESSIBILITY FACTOR

PREDICTIONS

By

SURESH BABU VELLANKI

Bachelor of Engineering

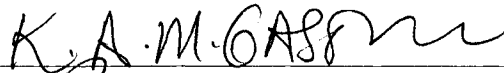Birla Institute of Technology and Sciences

Rajasthan, India
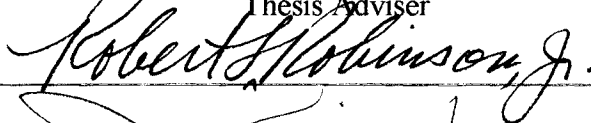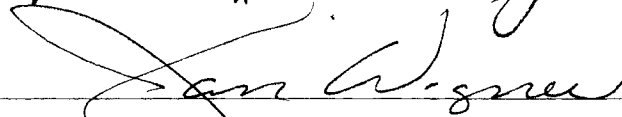
1991

ADSORPTION OF BINARY GAS MIXTURES

ON WET FRUITLAND COAL AND

COMPRESSIBILITY FACTOR

PREDICTIONS

Thesis Approved:

_____
Thesis Adviser

_____

_____

_____
Dean of the Graduate College

PREFACE

This study consists of two sections. The first section deals with the measurement and correlation of adsorption data for methane, nitrogen, and carbon dioxide binary mixtures on wet Fruitland coal at 115°F and pressures to 1800 psia. The extended Langmuir model was employed to correlate the present data. In addition, new mixing rules were incorporated in the model to lend it greater flexibility. In the second section, five equations-of-state (EOS) models were evaluated for their ability to predict the compressibility factors of methane, nitrogen, and carbon dioxide. The effect of reoptimizing the EOS parameters was also investigated.

I would like to extend my sincere thanks and expression of gratitude to my advisor and mentor Dr. K. A. M. Gasem, for his wisdom, understanding and guidance during the different stages of this work. I have always been impressed with his teaching skills and rank him as one of the best teachers I have come across.

I would like to thank my co-advisor Dr. R. L. Robinson, Jr. for his intelligent guidance and critical assessment of my work, which made me strive for excellence. I would also like to thank Dr. Jan Wagner for serving in my thesis committee and for his valuable suggestions.

My special thanks go to my dear friends, especially Sriram and Rohit, for their encouragement and understanding during my graduate study at OSU. I also extend my thanks and appreciation to Charles Baker, Pat Swart and Vickie Karman for their help.

My greatest appreciation, thanks and love go to my family members, especially my parents and brothers for their encouragement and moral support during the course of this work.

TABLE OF CONTENTS

LIST OF TABLES

Table   Page

SECTION 1

SECTION 2

LIST OF FIGURES

Figure   Page

SECTION 1

SECTION 2

NOMENCLATURE

a	cubic equation-of-state (EOS) parameter, BWR EOS parameter, PRG EOS parameter, molar area
A	Helmholtz energy
%AAD	average absolute percentage deviation
AAD	average absolute deviation
A_o	BWR EOS parameter
b	cubic EOS parameter, BWR EOS parameter, PRG EOS parameter
b_i	co-efficients of the modifying function of MSPHCT EOS
B	Langmuir adsorption constant
B_o	BWR EOS parameter
c	degrees of freedom parameter, BWR EOS
C_o	BWR EOS parameter
d	BWR EOS parameter
D_o	BWR EOS parameter
E_o	BWR EOS parameter
F_t	SPHCT modifying function
G	Gibbs function
H	enthalpy
L	amount adsorbed per unit of adsorbent upon the completion of a hypothetical monolayer
m_i	PR EOS parameters
n	number of moles

N	number of terms, number of particular species
P	pressure
p_i, p_f	initial and final pressure
Q	PRG EOS parameter
R	gas constant
RMSE	root mean square error
S	entropy
SS	objective function
T	temperature
$\tilde{T}$	reduced temperature (T/T^*)
v	specific volume
$\tilde{v}$	partial molar volume
u	PRG EOS parameter
U	internal energy
V	volume
WRMS	weighted root mean square error
w	PRG EOS parameter
x_i	adsorbate mole fraction
z	feed gas mole fraction
Z	compressibility factor
Z_M	maximum coordination number

Greek Symbols

α	BWR EOS parameter
α_o	PRG EOS parameter
κ_i	PRG EOS parameters
γ	BWR EOS parameter

ρ	density
$\tilde{\rho}$	reduced density (v^*/v)
μ_i	chemical potential of species i
Ω_a, Ω_b	PR EOS parameters
π	spreading pressure
τ	geometrical constant (0.74048)
θ	fraction of monolayer coverage
ω	accentric factor, amount adsorbed per unit of adsorbent

Subscripts

A	attractive term
c	critical state
R	repulsive term
r	reduced parameter
calc	calculated
expt	experimental
inj	injected gas or injection side of the experiment
cell	cell side of the experiment
unads	unadsorbed
solu	solubility

Superscripts

*	characteristic parameter
att	attractive term
rep	repulsive term
gas	gas phase
ads	adsorbed phase

SECTION 1 - EXPERIMENTAL WORK

CHAPTER I

INTRODUCTION

The United State's coalbeds contain two to four times the amount of natural gas contained in traditional reservoirs [1]. In conventional gas reservoirs, natural gas exists in a gaseous state and can be easily recovered as an energy supply. In coalbeds, methane is adsorbed on the coal surface, where it exists at liquid-like densities. The adsorbed layer holds more methane than an equal volume of conventional reservoir due to the higher density of the adsorbed gas [2].

Current coalbed methane recovery technology uses primary depletion methods. Using such methods, the cleat (cleavage planes in a coal seam) pressure is reduced by pumping out water. Due to the reduced pressure, methane desorbs from the coal matrix and diffuses to the cleats. Methane and water flow to the well bore, thus increasing the recovery of methane. The enhanced recovery method uses nitrogen or carbon dioxide, which is injected into the cleats. Injected gases result in increasing the total cleat pressure and concurrently reducing the partial pressure of methane. Methane desorbs from the coal matrix and diffuses to the cleats then flows out with water and nitrogen or carbon dioxide gas [3].

The effect of the adsorption behavior of methane and the injected gases on the mechanism of enhanced recovery is not well understood. Preliminary investigations were

conducted by Amoco Production Company in Tulsa on wet Fruitland coal at 115°F and pressures to 1800 psia to study the adsorption phase behavior of methane, nitrogen, carbon dioxide and their mixtures [4]. The investigation performed by Amoco involved few data points covering limited compositions. The experimental measurements were carried out to provide engineers with detailed phase behavior information required to optimize the production and recovery of coalbed methane. The conditions of the experimental pressures and temperature were chosen to be representative of the Fruitland wet coal found in the Colorado portion of the San Juan Basin [3].

The specific objectives of the present work were as follows:

1) Measure the adsorption of methane, nitrogen, carbon dioxide mixtures on Fruitland wet coal at 115°F and to pressures of 1800 psia.

2) Develop and evaluate mathematical models to represent the adsorption behaviors of these gases.

The experimental facility for the present work has been designed, constructed and tested by Hall [3]. Hall has reported experimental measurements for pure carbon dioxide, nitrogen, and methane and their mixtures. The binary gas adsorption data were measured in a joint effort undertaken by Hall and me. Concurrently, mathematical models were developed by Zhou [5] to adequately represent the adsorption data for the pure gases and mixtures.

The following chapters briefly outline the theory and the experimental procedures and present the mixture adsorption data in a format suitable for use in modeling the depletion behavior of coalbed methane reserves. Section 2 deals with the prediction of compressibility factors using various equations of state (EOS). Knowledge gained from this project can be used to design optimum strategies for coalbed methane production.

CHAPTER II

LITERATURE REVIEW

This chapter briefly reviews the theory and experimental work related to the measurement of mixture adsorption data. Specifically, the topics reviewed are (1) the theory of adsorption, (2) experimental techniques, and (3) previous experimental work. All these topics have been described in detail by my co-workers [3, 5].

Theory

Adsorption occurs when the intermolecular attractive forces between a solid and a gas are greater than those existing between molecules of the gas itself, resulting in the accumulation of the gas on the surface of the solid, even though the pressure may be lower than the vapor pressure at the prevailing temperature [6]. Adsorption can be classified as physical adsorption or chemical adsorption, based on the type of interaction between the solid and gas. Physical adsorption involves molecular interaction forces and is accompanied by evolution of heat which is of the order of the heat of sublimation of the gas. Physical adsorption may be a multilayer reversible phenomenon. Chemical adsorption or activated adsorption is the result of chemical interactions between the solid and the adsorbed substance. The heat liberated is of the order of the heat of chemical reaction. The process is irreversible, and on desorption the original substance will often be found to have undergone a chemical change [6]. The present work deals with physical adsorption, and the term adsorption refers to physical adsorption.

Desorption of the adsorbed gas can be achieved in different ways [6], e.g., by lowering the pressure of the gas phase or by raising the temperature of the adsorbed gas.

Many theories and models have been developed to explain the different types of adsorption isotherms. The resulting equations are then used to predict the amounts adsorbed based on a limited number of experiments. The various isotherm models [6] follow three different approaches: (a) the Langmuir approach, (b) the Gibbs or thermodynamic approach, and (c) the Potential theory.

The Langmuir Approach

The Langmuir model is a simple two-parameter model which is widely used in industry. The Langmuir isotherm utilizes the concept of dynamic equilibrium between the rates of condensation (adsorption) and evaporation (desorption) and relies on the following assumptions [7-8]:

1) Each adsorption site can accommodate one and only one molecule or atom.

2) The adsorbed molecule or atom is held at definite, localized sites.

3) The energy of adsorption is constant over all sites, and there is no interaction between neighboring adsorbates.

The Langmuir equation [7] is written as:

$$\theta = \frac{\omega}{L} = \frac{BP}{1 + BP} \tag{1}$$

where θ is the fraction of monolayer coverage, ω is the amount adsorbed per unit of adsorbent, L is the amount adsorbed per unit of adsorbent upon the completion of a hypothetical monolayer, and B is the Langmuir adsorption constant. Assuming ideal localized monolayer adsorption, the Langmuir isotherm can be extended to gas mixtures. The extended Langmuir model [6] is defined as:

4

$$\omega_i = \frac{L_i B_i P y_i}{1 + \sum_j B_j P y_i} \qquad (2)$$

where L_i and B_i are the Langmuir model constants for pure i.

The Gibbs Approach

The fundamental property relation for a three-dimensional open system can be written as [8]:

$$(ndU) = Td(nS) - Pd(nV) + \sum \left(\mu_i \, dn_i \right) \qquad (3)$$

where U, S, and V are the molar internal energy, entropy, and volume, respectively. The chemical potential of component i is denoted by μ_i, and n_i denotes the number of moles of component i. According to Hill [9], the interfacial region between a bulk gas and a solid surface may be treated as a two-dimensional phase with its own thermodynamic properties. Therefore, for a two-dimensional phase an analogous expression results in [8]

$$d(nU) = Td(nS) - \pi d(na) + \sum \left(\mu_i \, dn_i \right) \qquad (4)$$

where π is the spreading pressure and 'a' is the molar area. The Gibbs function is defined as [8]

$$G = U + \pi a - TS \qquad (5)$$

Equations (4) and (5) result in the following general expression:

$$d(nG) = (na)d\pi - (nS)dT + \sum \left(\mu_i \, dn_i \right) \qquad (6)$$

Equations for d(nH) and d(nA) can be derived in a similar way from the enthalpy H and Helmholtz function A defined as [8]

$$H = U + \pi a \tag{7}$$

$$A = U - TS \tag{8}$$

From Equation (6) it is clear that [8]

$$\mu_i = \left[\frac{\partial(nG)}{\partial n_i}\right]_{T,\pi,n_j} = \tilde{G}_i \tag{9}$$

where $\tilde{G}_i$ is the partial molar Gibbs function and is equal to the partial derivative by definition. The Gibbs function G is also related to the chemical potentials as [8]:

$$G = \sum(\mu_i x_i) \quad \text{or} \quad nG = \sum(\mu_i n_i) \tag{10}$$

The equilibrium criterion for the heterogeneous gas phase and the adsorbed phases for i components can be expressed as [10]:

$$T^{gas} = T^{ads} \tag{11}$$

$$p^{gas} = p^{ads} \tag{12}$$

$$\mu_i^{gas} = \mu_i^{ads} \tag{13}$$

These equilibrium relations are helpful in determining the adsorption properties.

Differentiating Equation (10) and comparing with Equation (6) yields the Gibbs-Duhem equation for the two-dimensional phase [8], i.e.,

$$(nS)dT - (na)d\pi + \sum\left(n_i d\mu_i\right) = 0 \tag{14}$$

or

$$SdT - ad\pi + \sum\left(x_i d\mu_i\right) = 0 \tag{15}$$

Therefore at constant temperature, Equation (15) will reduce to the Gibbs adsorption isotherm [8]:

$$-a d\pi + \sum (x_i d\mu_i) = 0 \qquad (16)$$

At equilibrium $d\mu_i^{gas} = d\mu_i^{ads}$ and the Gibbs adsorption isotherm can be written as [8],

$$-a d\pi + \sum (x_i d\mu_i^{gas}) = 0 \quad \text{(const T)} \qquad (17)$$

Assuming ideal gas behavior, it can be shown that

$$d\mu_i^{gas} = RT d\ln y_i P \qquad (18)$$

where P is the pressure and y_i is the gas mole fraction. In this case, the Gibbs adsorption isotherm becomes [8]

$$-a d\pi + RT \sum (x_i d\ln y_i P) = 0 \quad \text{(const T)} \qquad (19)$$

rewriting Equation (19) we have

$$-\left(\frac{a}{RT}\right) d\pi + d\ln P + \sum (x_i d\ln y_i) = 0 \quad \text{(const T)} \qquad (20)$$

where $a = A/n_t$ and $d\ln P = dP/P$

Increasing the gas pressure from zero to P and the spreading pressure from zero to π, but keeping the gas phase composition constant, the Gibbs isotherm upon integration gives

$$\frac{\pi}{RT} = \int_0^P \frac{(n_t / A)}{P} dP \quad \text{(const T and y)} \qquad (21)$$

Equation (21) can be used for both pure fluids and mixtures to evaluate π from experimental data. Upon evaluation of π/RT from Equation (21) for various values of compositions (y_i) for the same temperature and pressure, $d\ln P$ in Equation (20) can be set equal to zero and solved for x_i.

$$-ad\pi + \sum(x_i d\mu_i) = 0 \qquad (16)$$

At equilibrium $d\mu_i^{gas} = d\mu_i^{ads}$ and the Gibbs adsorption isotherm can be written as [8],

$$-ad\pi + \sum(x_i d\mu_i^{gas}) = 0 \quad \text{(const T)} \qquad (17)$$

Assuming ideal gas behavior, it can be shown that

$$d\mu_i^{gas} = RTd\ln y_i P \qquad (18)$$

where P is the pressure and y_i is the gas mole fraction. In this case, the Gibbs adsorption isotherm becomes [8]

$$-ad\pi + RT\sum(x_i d\ln y_i P) = 0 \quad \text{(const T)} \qquad (19)$$

rewriting Equation (19) we have

$$-\left(\frac{a}{RT}\right)d\pi + d\ln P + \sum(x_i d\ln y_i) = 0 \quad \text{(const T)} \qquad (20)$$

where $a = A/n_t$ and $d\ln P = dP/P$

Increasing the gas pressure from zero to P and the spreading pressure from zero to π, but keeping the gas phase composition constant, the Gibbs isotherm upon integration gives

$$\frac{\pi}{RT} = \int_0^P \frac{(n_t/A)}{P} dP \quad \text{(const T and y)} \qquad (21)$$

Equation (21) can be used for both pure fluids and mixtures to evaluate π from experimental data. Upon evaluation of π/RT from Equation (21) for various values of compositions (y_i) for the same temperature and pressure, $d\ln P$ in Equation (20) can be set equal to zero and solved for x_i.

$$\frac{A}{n_t}\left(\frac{\partial \frac{\pi}{RT}}{\partial y_1}\right)_{T,P} = \frac{x_1 - y_1}{y_1(1-y_1)} \tag{22}$$

The composition of the adsorbate can be calculated from Equations (21) and (22).

The isotherms derived from the Potential theory have found utility in interpreting adsorption by capillary condensation, or pore filling, and will not be discussed here. Equations (19) to (22) indicate that the required experimental data are the total amount adsorbed, n_t in gmoles/g sorbent, at constant gas compositions while varying the total pressure. Compressibility factors should be used when the gas phase is not ideal.

Experimental Techniques

The amount adsorbed at equilibrium can be determined by (a) volumetric (b) gravimetric, or (c) chromatographic methods [6]. Using the volumetric method, the pressures before and after adsorption in a closed system are measured, whereas using the gravimetric method, the amount adsorbed is determined by the weight gain in the flow system. Adsorption measurements by the chromatographic method require highly idealized conditions, including: dilute mixtures, plug flow, instantaneous equilibrium between fluid and solid phases for both concentration and temperature, and no pressure drop. Such stringent conditions often result in large errors [6]. Adsorption for mixtures can be calculated from breakthrough curves, by frontal chromatography, or by elution chromatography. In this work, a constant volume (volumetric) method is used to determine the amount adsorbed for mixtures.

Previous Experimental Data

Previous experimental data at high pressures for binary mixtures on coal are very scarce. At the time of this writing, only one source [11] was available with the adsorption

data on coal at 86 °F and 750 psia for the gases of interest. Only low pressure adsorption data using activated carbon, molecular sieve and charcoal as adsorbents were available. Preliminary studies by Amoco Production Company [4] in Tulsa, resulted in adsorption data for pure fluids and binary mixtures as well. The adsorption data were not extensive and were measured only at limited compositions. In the present work at Oklahoma State University (OSU), adsorption measurements were conducted at uniform intervals of gas-phase mole fractions: 0.0, 0.2, 0.4, 0.6, 0.8 and 1.0.

CHAPTER III

EXPERIMENTAL APPARATUS AND PROCEDURES

The experimental apparatus and procedures used in this work for measuring the adsorption of pure and mixed gases on Fruitland wet coal are discussed in detail by Hall [3]. Following is a brief description of the experimental procedures and the calculations associated with them.

Figure 1 illustrates the schematic diagram for the experimental setup [3]. The experimental apparatus consists of two sections, the pump section and the cell section. The cell section contains Fruitland wet coal which acts as an adsorbent. The equilibrium moisture content of the coal sample was found to be 2.2% by weight [3]. The experiments were conducted with the moisture content kept between 4% and 14%, thus reducing the possibility of obtaining varying degree of adsorption. The amount of gas injected from the pump section is calculated from the pvT properties on the pump side. Similarly, the amount of gas remaining in the cell section is calculated after equilibrium has been reached on the cell side. The difference in the amounts gives us the amount of gas adsorbed on the adsorbent.

A Ruska positive displacement injecting pump is used on the pump side to inject the gas with known composition. Air bath temperature controllers were used for both the pump and cell sections to maintain steady-state environment within the control volumes. The temperature of the contents of the pump was controlled by using a water bath and
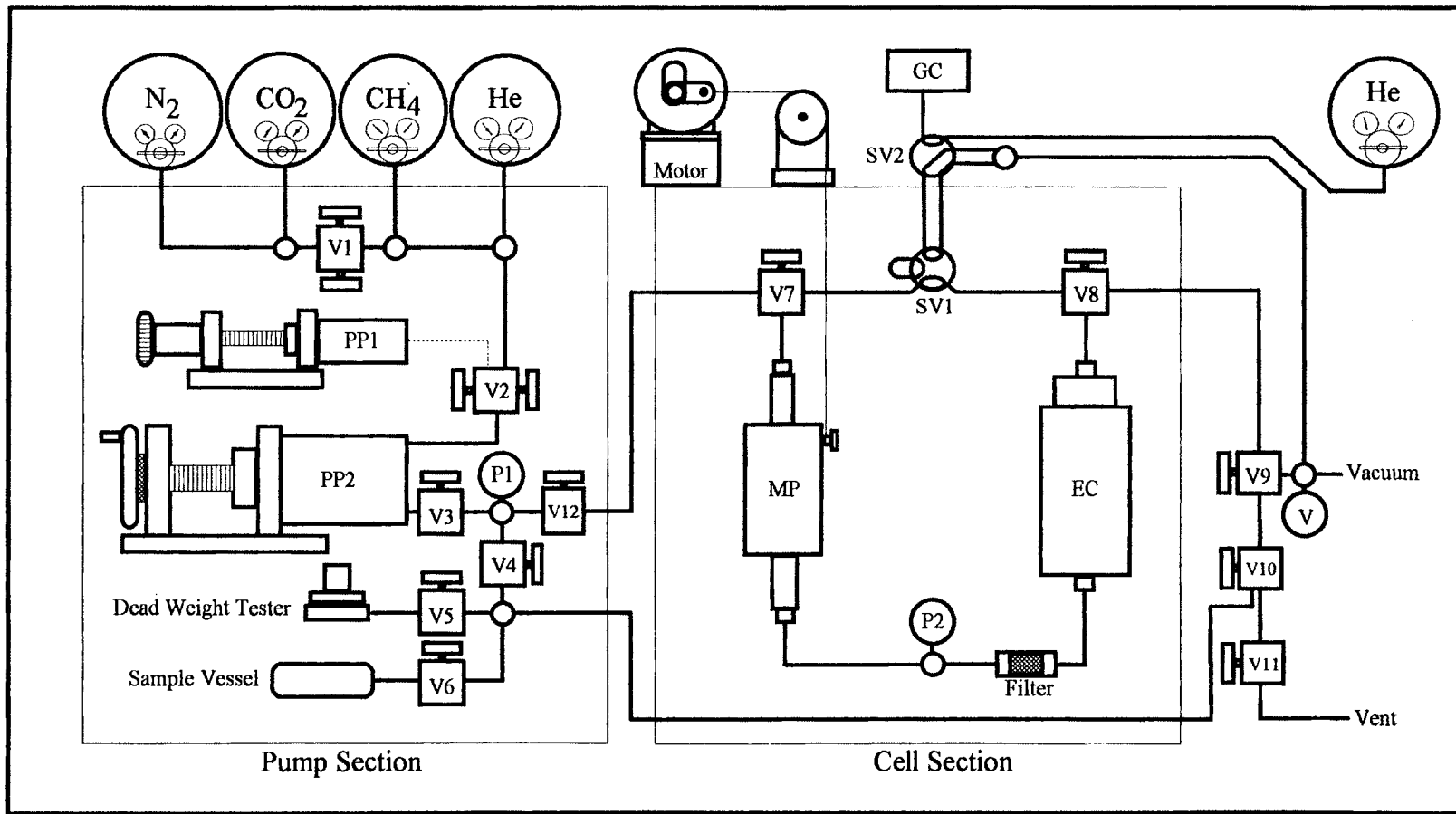
Figure 1. Schematic Diagram for the Adsorption Experimental Apparatus

circulator (Haake Model NB3). The cell side consists of a high-pressure vessel which holds the adsorbent. Pressure transducers [Sensotech Model 450] are used to measure the pressures. Temperatures are monitored by Hart Scientific A1011 RTD Thermometers. The pressure transducers were calibrated against a Ruska dead-weight pressure gauge [Model No. 2465] available in the laboratory.

In the case of mixtures, the equilibrium gas compositions were analyzed using a Perkin Elmer Sigma 2 gas chromatograph. A Spherocarb column is used to analyze the mixtures under study. The gas chromatograph is calibrated prior to the mixture adsorption measurements. Details on the gas chromatograph operating conditions and the calibration procedure are given elsewhere [3].

<div align="center">Governing Equations</div>

The amount adsorbed for component k in a binary mixture is determined by the difference in the amount of gas injected from the positive displacement pump $(n_{inj})_k$ and the amount unadsorbed $(n_{unads})_k$. In addition, the amount of component dissolved in the moisture present in the coal is accounted for. Accordingly,

$$(n_{ads})_k = (n_{inj})_k - (n_{unads})_k - (n_{solu})_k \qquad (23)$$

where the amount of component k injected is given by [3]

$$(n_{inj})_k = z_k \sum_j \left[\rho_{p_i} V_{p_i} - \rho_{p_f} V_{p_f} \right]_j \qquad (24)$$

where j is equal to number of injections. The amount of component k unadsorbed in the free gas in the equilibrium cell is given by

$$(n_{unads})_k = y_k \, \rho_c \, V_{void} \qquad (25)$$

where ρ_c is the gas density within the cell, and y_k is the mole fraction of component k in the equilibrium gas mixture. The cell section void volume is obtained by injecting known amounts of helium from the positive displacement pump into the cell section at

<div align="center">12</div>

sequentially higher pressures. Helium is assumed to be inert and does not adsorb on to the coal. The void volume in the cell section is calculated by [3]

$$n_{He_{inj}} = n_{He_{cell}} \tag{26}$$

and

$$\left[\frac{PV_{inj}}{Z_{He}RT} \right]_{pump} = \left[\frac{PV_{void}}{Z_{He}RT} \right]_{cell} \tag{27}$$

so

$$V_{void} = \left[\frac{PV_{inj}}{Z_{He}RT} \right]_{pump} / \left[\frac{P}{Z_{He}RT} \right]_{cell} \tag{28}$$

The solubility of each component in water is estimated at its partial pressure using a proprietary program [26]. Thus, the amount of each component adsorbed at a given pressure is corrected to account for its solubility in water. Therefore, knowing the amount of gas injected, the amount of unadsorbed gas and the amount of gas dissolved in water, the amount of gas adsorbed on Fruitland wet coal can be determined.

Relation between Gibbs and Absolute Adsorption

In Gibbs adsorption, the volume of the gas phase is assumed to be equal to the void volume and therefore the volume of the adsorbed phase is assumed to be negligible. Thus, the adsorption data determined from the constant volume method is based on the Gibbs adsorption. Absolute adsorption is defined by Young [12] as the total number of moles of an adsorbate held by the surface molecular forces between the adsorbate and adsorbent. Hence, Gibbs adsorption is corrected using the density of the adsorbed phase. The relationship between Gibbs adsorption and absolute adsorption can be expressed as [4, 13]:

$$\left[\omega^a\right]_{abs} = \frac{\left[\omega^a\right]_{Gibbs}}{\left[1 - \dfrac{v^a P}{ZRT}\right]} \qquad (29)$$

or

$$\omega^a_{Gibbs} = \omega^a_{abs}\left[1 - \left(\frac{\rho_{gas}}{\rho_{ads}}\right)\right] \qquad (30)$$

There are two approximations commonly used in estimating molar adsorbate volume. One approximation, suggested by Yee [2], is to use liquid density at the atmospheric boiling point pressure. The methane and nitrogen adsorbed phase density estimates are 0.421 and 0.808 gm/cc, respectively. Carbon dioxide is a solid at atmospheric boiling point pressure. Therefore, the density for a saturated liquid at the triple point (1.18 gm/cc) is used. The second approximation calls for the use of temperature-dependent van der Waals covolumes [13] as the molar adsorbate volumes. The following expression is used to estimate the molar adsorbate volume above the critical temperature

$$v^a = \frac{RT_c}{8P_c}, \quad T \geq T_c \qquad (31)$$

The van der Waals covolumes calculated using the above equation are 43.10 cc/mole for methane, 38.64 cc/mole for nitrogen and 42.82 cc/mole for carbon dioxide, respectively.

Experimental Errors

Theory of multivariate error propagation was used to estimate the errors in the adsorption experiments. The uncertainty associated with each quantity is estimated by expressing the desired quantity as a function of measured variables. The uncertainty in each measured variable is expressed in terms of its standard deviation, σ. Therefore for a

14

quantity R, calculated from a set of input variables $(x_1, x_2, ...x_N)$, the uncertainty in R is expressed as [14]:

$$\sigma_R^2 = \sum_{i=1}^{N} \left[\left(\frac{\partial R}{\partial x_i} \right)^2 \sigma_{x_i}^2 \right] \qquad (32)$$

where the summation is carried out over all input variables, x_i. The error analysis for the present experimental work has been discussed in detail by Robinson et al. [14] in a report to Amoco. The major contributors for the uncertainty in the adsorbed amount are adsorbed phase molar volume, void volume, injection pump dead volume and compositional terms. Additional discussion and examples are documented by Hall, in the Supplementary Material [15] related to his thesis.

Experimental Difficulties

Many problems have been encountered during the course of the experiment. Synthesizing a mixture of required composition was found to be very time consuming. The time can be reduced drastically if a pre-synthesized mixture is used. Also, minute leaks in the experimental setup are difficult to detect with a helium detector. This problem can be overcome either by using a more sensitive helium detector or by designing the experimental setup with a minimum number of fittings'. The magnetic circulation pump was a constant source of maintenance problems during the experiments. Better means of shielding the pump from coal particles should be devised to reduce the amount of maintenance required.

Gas Compressibility Factors

Accurate compressibility factors for pure components and mixtures are necessary in processing the adsorption experimental data. The importance of the compressibility

factors can be gauged from the fact that a 1% error in the value for the compressibility factor can propagate into a 10% error in adsorption values [3]. This is because compressibility factors are used in the calculation of the void volume, the moles injected or moles unadsorbed for both pure and mixture components. The three-dimensional Redlich-Kwong equation of state (3-D RK EOS) was used to calculate the compressibility factors. The optimization of the EOS constants and interaction parameters is discussed in detail by my co-workers [3, 5]. The data published by the International Union of Pure and Applied Chemistry (IUPAC) [16-17] were used to regress the EOS constants for the pure components. Binary experimental data at the temperature and pressure ranges of interest were selected from the literature [18-22] to determine the interaction parameters. For helium, the compressibility factor data were obtained from the National Bureau of Standards Technical Note 631 [23].

On regressing the EOS constants and the interaction parameters, the residuals in compressibility factors are on the order of 0.04% for helium (100-1000 psia), 0.01% for methane, 0.004% for nitrogen and 0.004% for carbon dioxide throughout the operating pressure range [3]. For binary mixtures, the optimum interaction parameters (C_{ij}) are 0.0859 for the methane-nitrogen mixtures, 0.1032 for the methane-carbon dioxide mixtures and -0.0537 for the nitrogen-carbon dioxide mixture [3]. The maximum deviation for the compositions considered is 0.5% for the methane-nitrogen mixtures, 1.2% for the methane-carbon dioxide mixtures and 0.1% for the nitrogen-carbon dioxide mixtures in the range of interest [3].

CHAPTER IV

EXPERIMENTAL RESULTS AND DISCUSSION

Experimental adsorption data for methane, nitrogen and carbon dioxide binary mixtures were measured at 115°F and to pressures of 1800 psia and are well documented by Hall [3]. The experimentally determined absolute adsorbed values of methane, nitrogen and carbon dioxide and their mixtures were plotted against the cell side pressure and feed mole gas fraction by Hall [3]. The equilibrium phase-rule variables include temperature, pressure and phase compositions [10]. The feed gas mole fraction variable is not a phase-rule variable, therefore, it cannot be used to fix the state of a system. Hence to present the data in a more suitable format, the absolute adsorbed values for the binary mixtures are plotted against the equilibrium adsorbate mole fraction and equilibrium gas mole fraction. Also, the equilibrium phase compositions are represented graphically at fixed intervals in pressure.

For the methane-nitrogen mixtures, the adsorption information is shown as the total absolute adsorption as a function of methane adsorbate mole fraction and, similarly, as function of methane equilibrium gas mole fraction up to pressures of 1800 psia. For the methane-carbon dioxide mixtures and the nitrogen-carbon dioxide mixtures, similar figures are generated in addition to plots which present the experimental data to a pressure range of 1000 psia. This is due to the observed multilayer adsorption for carbon dioxide above 1200 psia [3, 5]. The sharp increase in sorption capacity for carbon dioxide was also

exhibited by the pure gas [3]. Combination of cubic spline and polynomial fits [25] are used to obtain a smooth representation for the data wherever possible.

The error analysis for the present measurements has been performed and presented in detail by Hall [3]. From the results presented by Hall, the individual component errors in the adsorbed amount range from one to seven percent in the case of binary mixtures.

Methane-Nitrogen Adsorption

Experimental data for the methane-nitrogen binary mixture are presented in Figures 2 to 8. Measurements are made for methane feed gas molar compositions of 20/80, 40/60, 60/40 and 80/20. Figure 2 illustrates the total absolute adsorption as a function of methane adsorbate mole fraction. The total adsorption varies from a minimum value corresponding to pure nitrogen to a maximum value for pure methane. The 80/20 mixture at high pressures closely approaches the pure methane isotherm. This indicates that methane and nitrogen are competing for the same adsorption sites at high pressures, and methane is preferentially adsorbed. It is also seen that the methane adsorbate mole fraction is almost constant irrespective of the pressure for the same methane feed gas mole fraction. This indicates that irrespective of the pressure, the system tries to maintain a relatively constant adsorbate composition of methane, although the individual adsorbed amounts may vary; variations within 0.02 in mole fraction are observed for pressures extending from 100-1800 psia. This is also illustrated in Figures 5 to 8, where the adsorbed amount is a function of the equilibrium gas mole fraction. Another indication that methane is preferentially adsorbed is that, for a 20/80 feed gas mole fraction, the adsorbate mole fraction of methane is around 45/55, which indicate that more methane is adsorbed relative to nitrogen even at low methane concentrations.

Figure 2. Effect of Adsorbate Composition on Total Absolute Adsorption for Methane-Nitrogen Mixtures

61

Figure 3. Effect of Adsorbate Composition on Absolute Adsorption for Methane from Methane-Nitrogen Mixtures

Figure 4. Effect of Adsorbate Composition on Absolute Adsorption for Nitrogen from
Methane-Nitrogen Mixtures

Figure 5. Effect of Equilibrium Gas Composition on Total Absolute Adsorption for Methane-Nitrogen Mixtures

Figure 6. Effect of Equilibrium Gas Composition on Absolute Adsorption for Methane from Methane-Nitrogen Mixtures
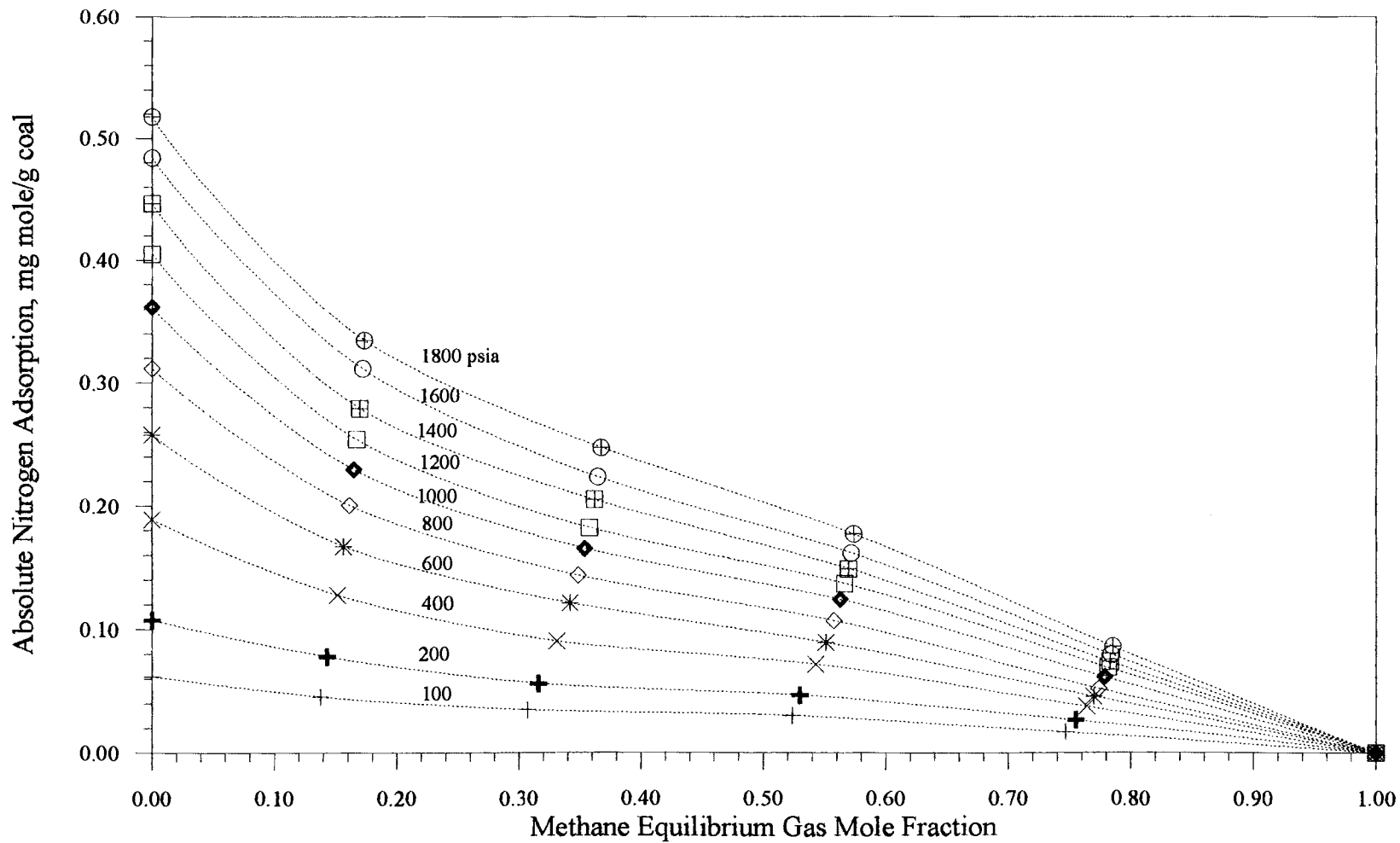
Figure 7. Effect of Equilibrium Gas Composition on Absolute Adsorption for Nitrogen from Methane-Nitrogen Mixtures
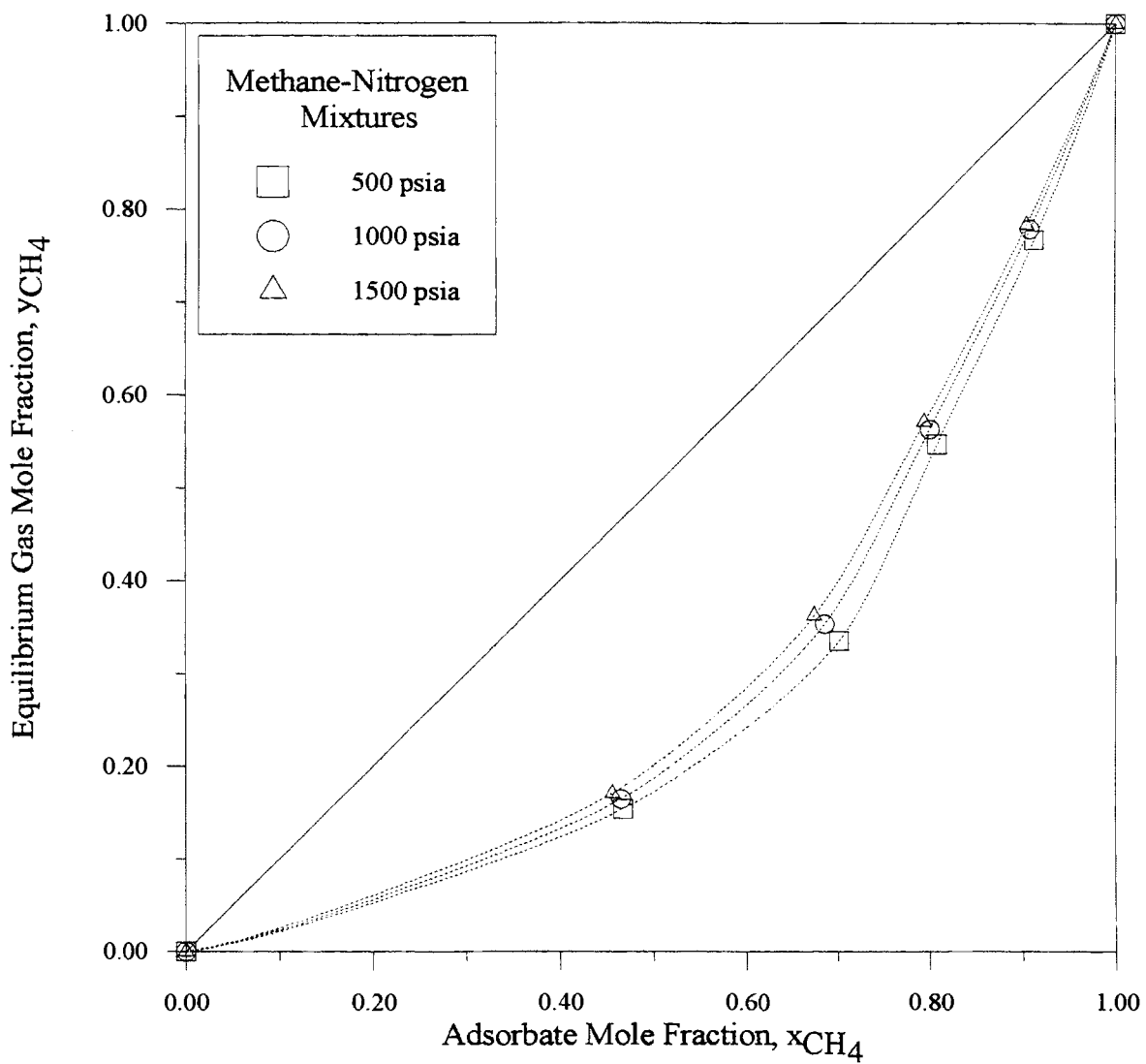
Figure 8. Phase Compositions for Adsorption of Methane-Nitrogen Mixtures on Wet Fruitland Coal

Figures 3 and 4 show the absolute adsorption for methane and nitrogen as a function of methane adsorbate mole fraction. As the methane adsorbate mole fraction increases, as expected the absolute amount of methane adsorbed increases. Similar trends are observed when the total absolute adsorption is plotted as a function of methane equilibrium gas mole fraction, as given in Figures 6 and 7. Figure 8 illustrates the effect of pressure on the adsorbate and gas compositions. In addition, Figure 8 indicates that the composition of the adsorbate phase is significantly different from that of the equilibrium gas phase. Similar behavior is observed for the methane-nitrogen mixture adsorption data presented by Stevenson [11] at 86°F and pressures to 750 psia.

Methane-Carbon Dioxide Adsorption

Measurements for the methane-carbon dioxide binary mixtures are made at injection feed gas mole fractions of 20/80, 40/60, 60/40 and 80/20. The adsorption data are illustrated in Figures 9 to 22. Figures 15 to 20 present the adsorption data only up to 1000 psia. Thus, the increased adsorption exhibited by carbon dioxide above pressures of 1200 psia is not shown in these figures. As the methane adsorbate mole fraction decreases, the total adsorption increases for a given pressure. This shows that as the methane in the feed gas mole fraction decreases, carbon dioxide is preferentially adsorbed, resulting in the increase in total adsorbed amount at a given pressure. Figure 16 illustrates that up to pressures of 1000 psia, as the pressure increases, for a given feed gas mole fraction, the adsorbate composition remains almost constant. The behavior is similar to that of methane-nitrogen adsorption. The variation in the adsorbate mole fraction for a given feed mole fraction is due to high sorption capacity of carbon dioxide relative to methane. Figures 10 and 11 illustrate the adsorbed amount of methane and carbon dioxide as a function of methane adsorbate mole fraction. The behavior is similar to that of methane-nitrogen adsorption. Similar figures present the adsorbed amount as a
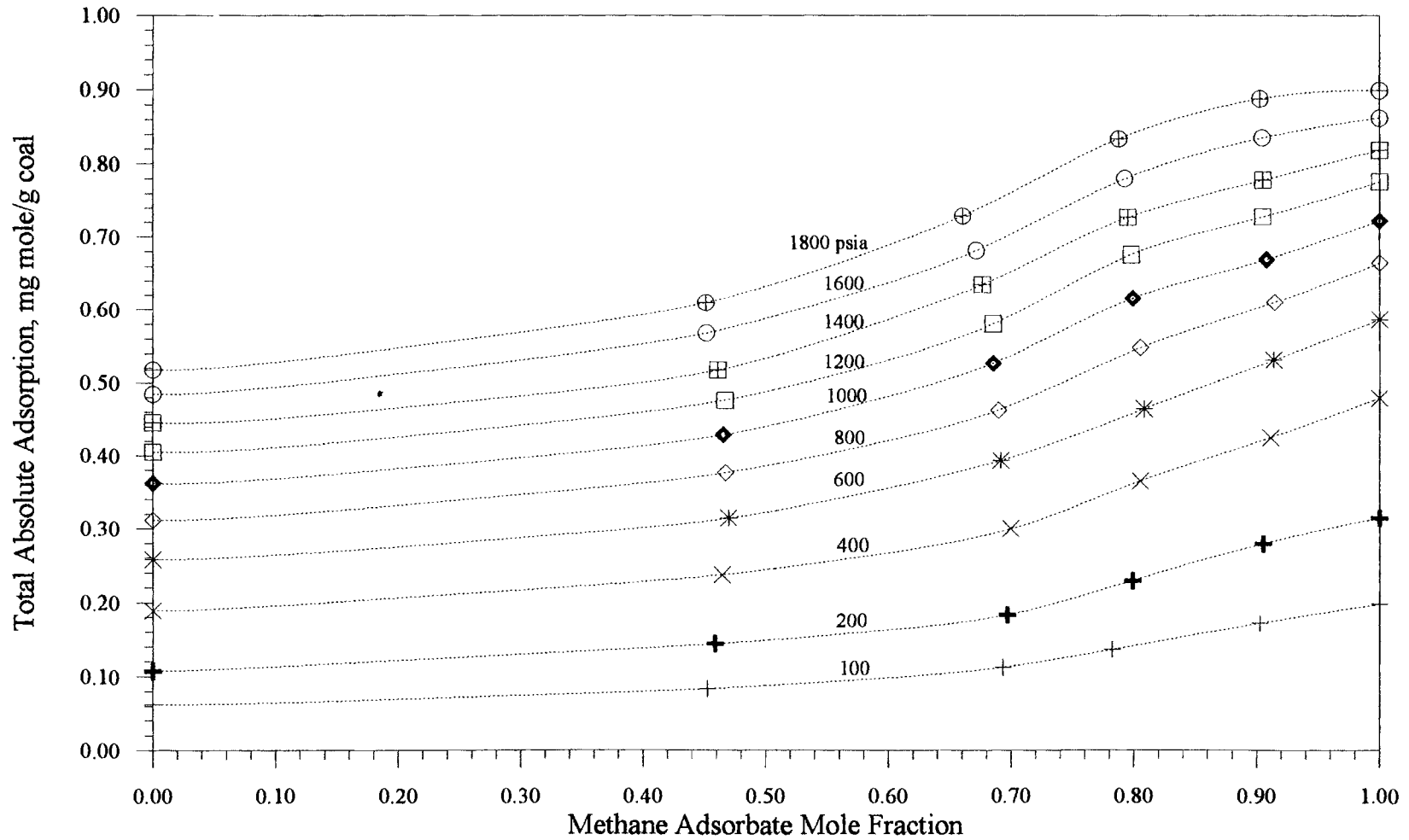
Figure 9. Effect of Adsorbate Composition on Total Absolute Adsorption for Methane-Carbon Dioxide Mixtures
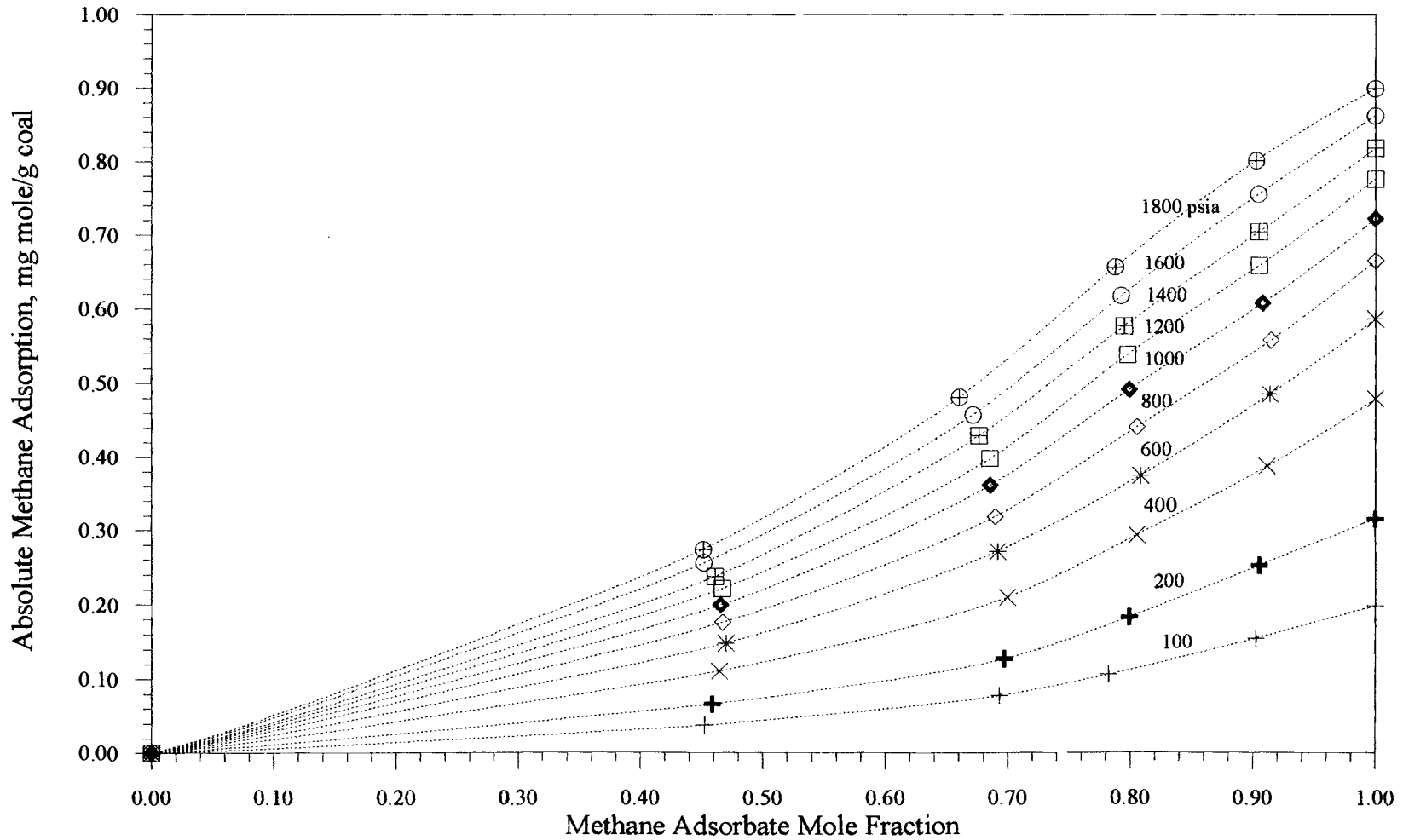
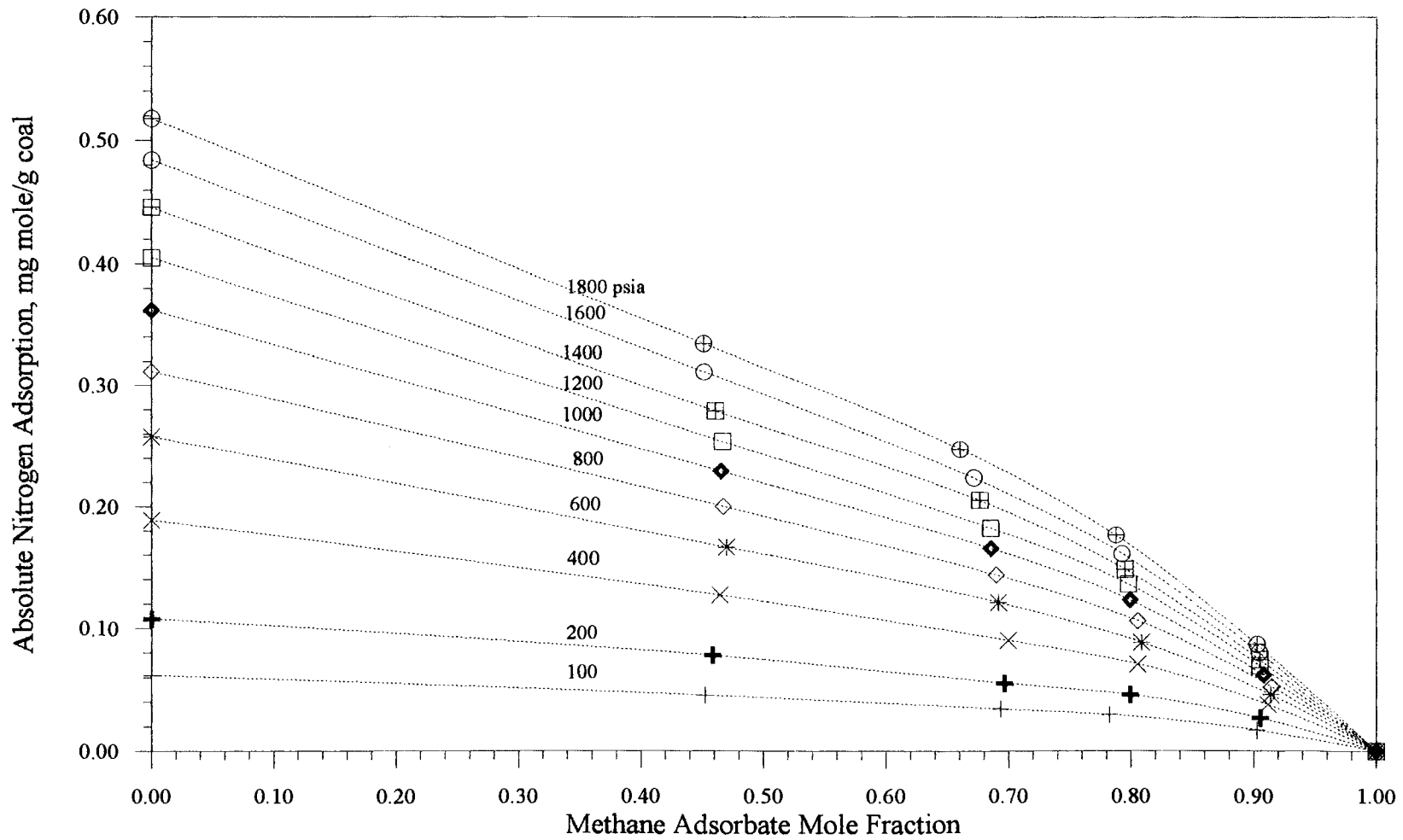Figure 10. Effect of Adsorbate Composition on Absolute Adsorption for Methane from
Methane-Carbon Dioxide Mixtures

Figure 11. Effect of Adsorbate Composition on Absolute Adsorption for Carbon Dioxide
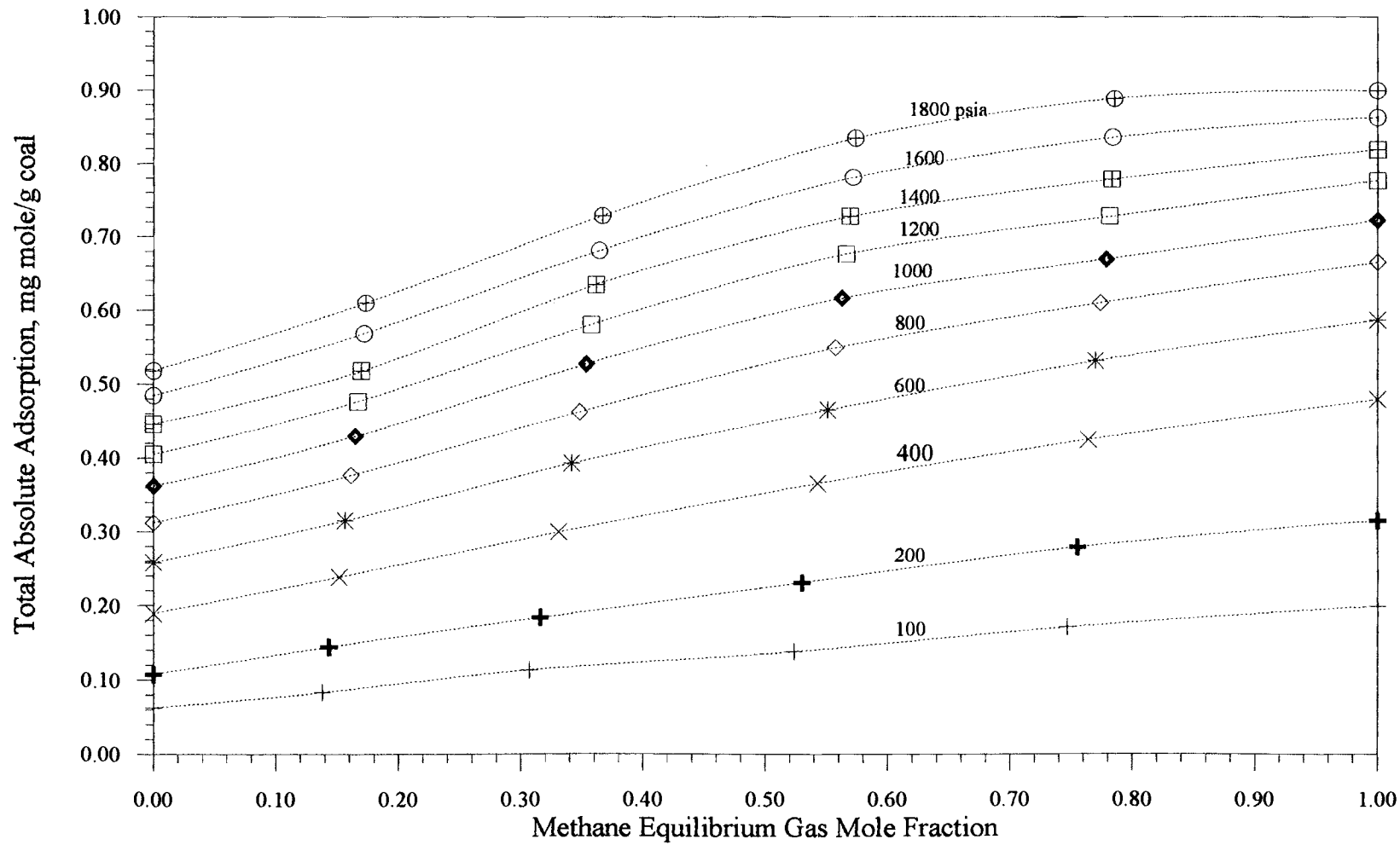from Methane-Carbon Dioxide Mixtures

29

Figure 12. Effect of Equilibrium Gas Composition on Total Absolute Adsorption for
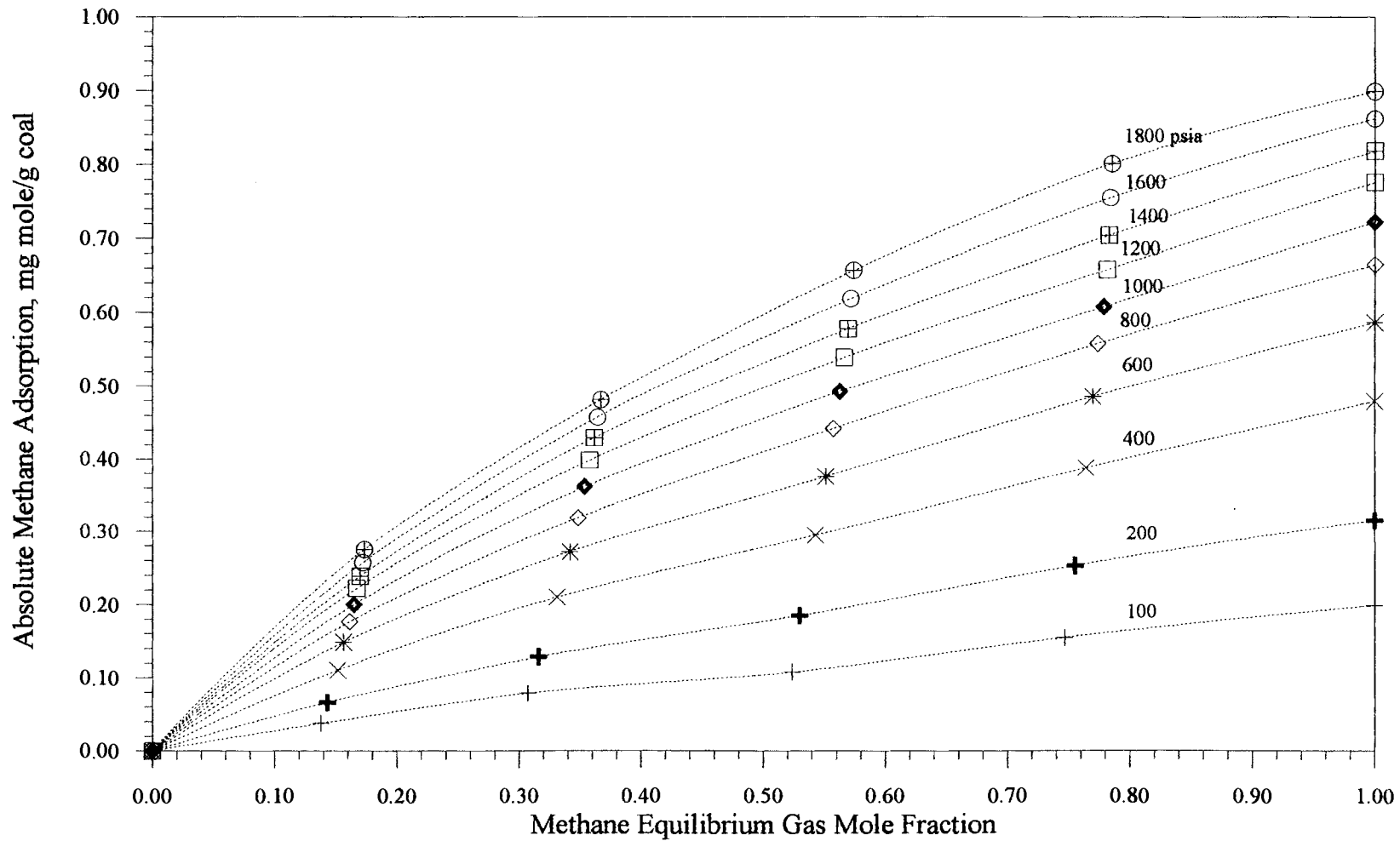Methane-Carbon Dioxide Mixtures

30

Figure 13. Effect of Equilibrium Gas Composition on Absolute Adsorption for Methane from Methane-Carbon Dioxide Mixtures

Figure 14. Effect of Equilibrium Gas Composition on Absolute Adsorption for Carbon Dioxide
from Methane-Carbon Dioxide Mixtures

Figure 15. Effect of Adsorbate Composition on Total Absolute Adsorption for
Methane-Carbon Dioxide Mixtures to Pressures of 1000 psia

Figure 16. Effect of Adsorbate Composition on Absolute Adsorption for Methane from
Methane-Carbon Dioxide Mixtures to Pressures of 1000 psia

Figure 17. Effect of Adsorbate Composition on Absolute Adsorption for Carbon Dioxide
from Methane-Carbon Dioxide Mixtures to Pressures of 1000 psia

Figure 18. Effect of Equilibrium Gas Composition on Total Absolute Adsorption for
Methane-Carbon Dioxide Mixtures to Pressures of 1000 psia

36

Figure 19. Effect of Equilibrium Gas Composition on Absolute Adsorption for Methane from Methane-Carbon Dioxide Mixtures to Pressures of 1000 psia

Figure 20. Effect of Equilibrium Gas Composition on Absolute Adsorption for Carbon Dioxide
from Methane-Carbon Dioxide Mixtures to Pressures of 1000 psia
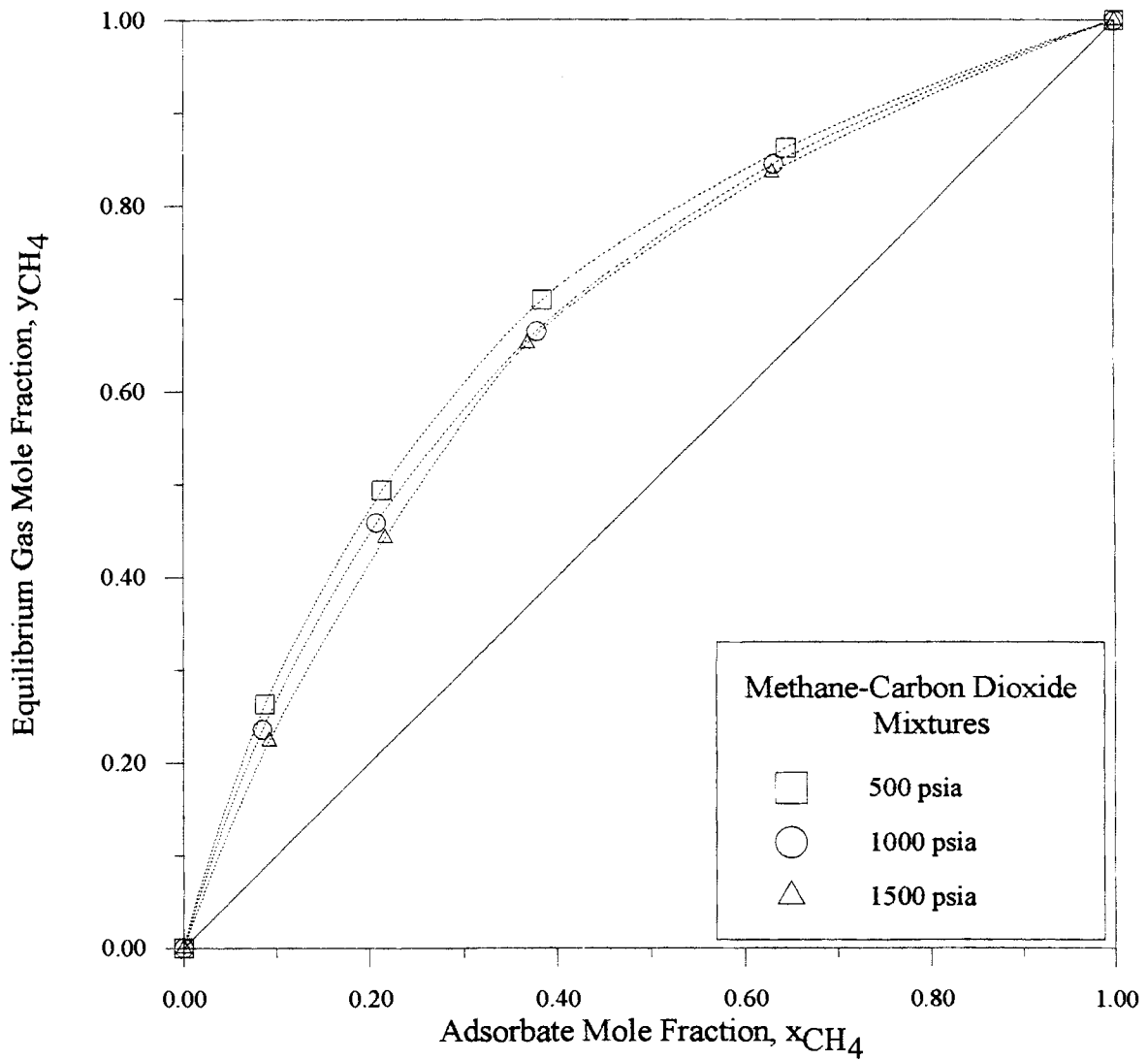
Figure 21. Phase Compositions for Adsorption of Methane-Carbon dioxide
Mixtures on Wet Fruitland Coal to Pressures of 1500 psia
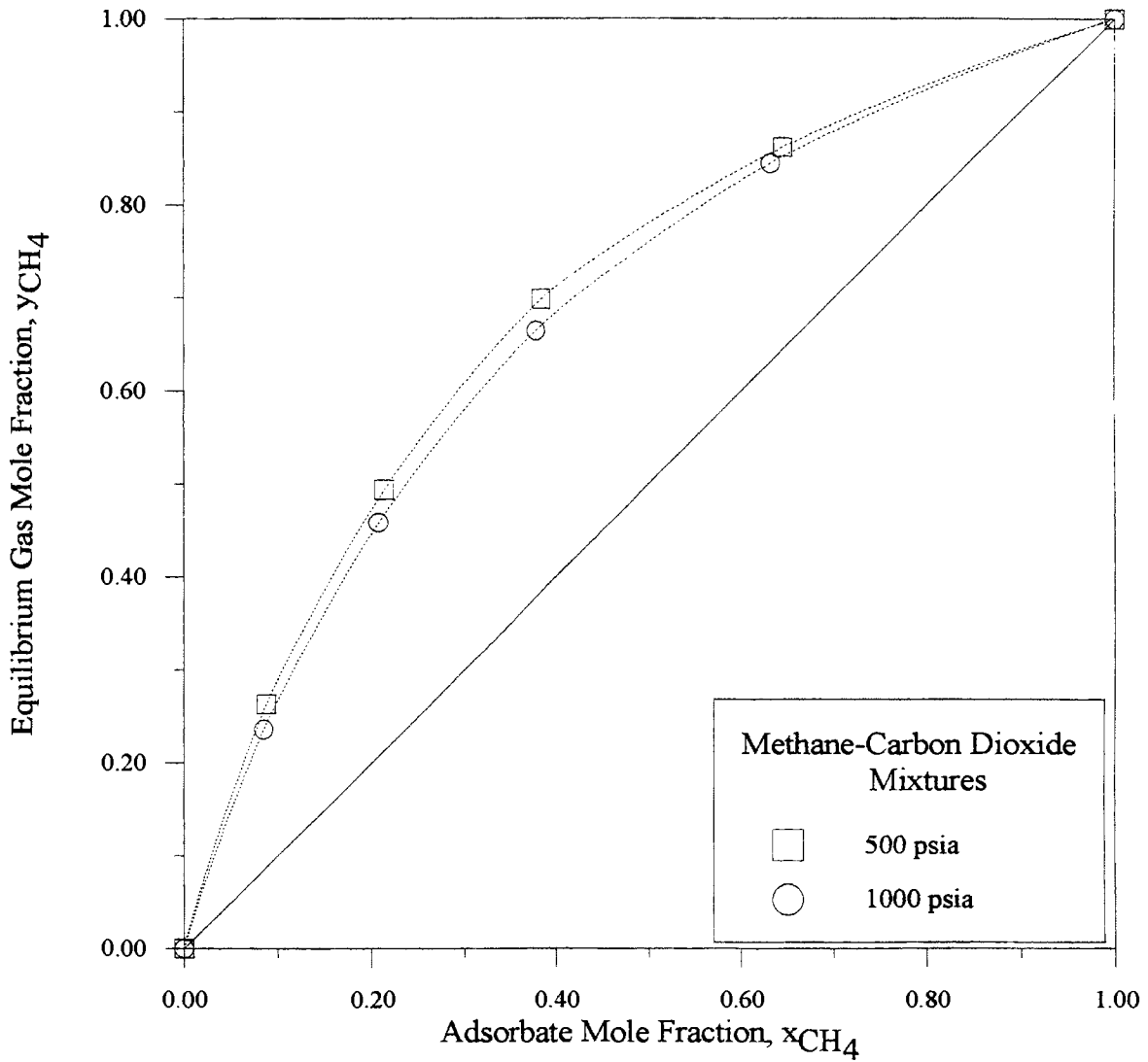
Figure 22. Phase Compositions for Adsorption of Methane-Carbon dioxide
Mixtures on Wet Fruitland Coal to Pressures of 1000 psia

function of equilibrium gas mole fraction. Figures 21 and 22 illustrate the effect of pressure on the methane-carbon dioxide x-y plot. It is evident that the phase compositions differ considerably. Stevenson and co-workers [11] performed the adsorption measurements at 86°F and pressures to 750 psia. They have reported a cross over in the x-y plots due to variations in pressure. The phase behavior of the present compositions, however, is different from that observed by Stevenson et al. [11], since the cross over behavior does not occur even at pressures of 1500 psia.

Nitrogen-Carbon Dioxide Adsorption

Adsorption measurements were made for the nitrogen-carbon dioxide binary mixture at feed gas compositions of 20/80, 40/60, 60/40, 70/30 and 80/20. Figures 23 to 25 illustrate the amount adsorbed as a function of nitrogen adsorbate mole fraction. Figures 29 to 34 present the mixture data up to 1000 psia, and thus excludes multilayer adsorption exhibited by carbon dioxide above 1200 psia. The data exhibit behavior similar to that of methane-nitrogen mixture adsorption discussed earlier. As the nitrogen mole fraction in the feed gas drops, there is a sharp drop in the nitrogen adsorbate mole fraction and concurrently in the amount of nitrogen adsorbed. This shows that carbon dioxide efficiently displaces nitrogen, i.e., carbon dioxide adsorbs preferentially with respect to nitrogen. Figures 26 to 28 present the amount adsorbed as a function of nitrogen equilibrium gas mole fraction. The behavior is similar to that of the methane-carbon dioxide mixture adsorption. As in the case of the methane-carbon dioxide system, the phase composition behavior of the nitrogen-carbon dioxide mixtures as illustrated in Figures 35 and 36, is non-ideal [5] at higher pressures.

The experimental data presented by my co-workers for the binary systems differed significantly [3, 5]. On recalculation [24] of the adsorbed amounts for the pure components, it was determined that two different methods were used to compute the
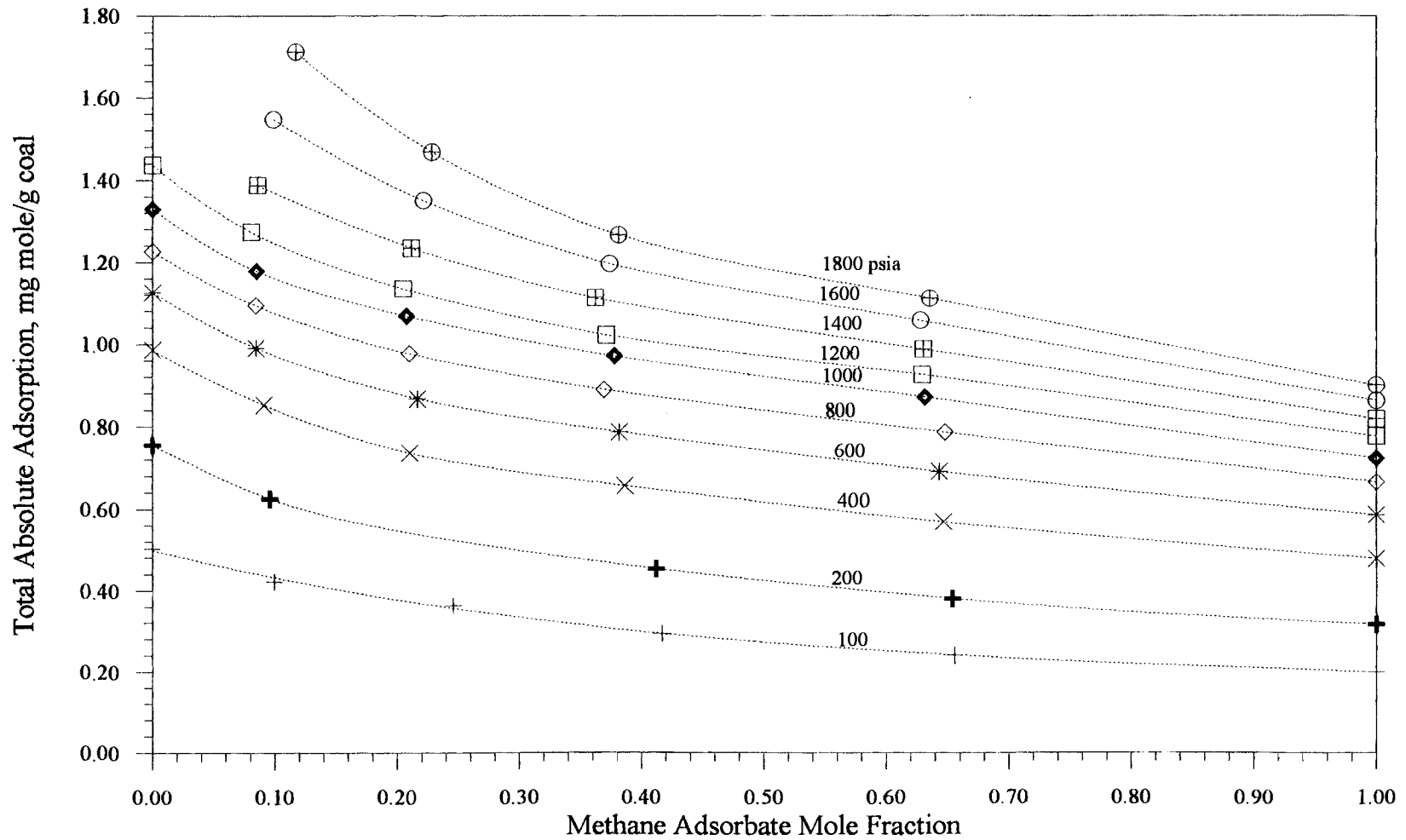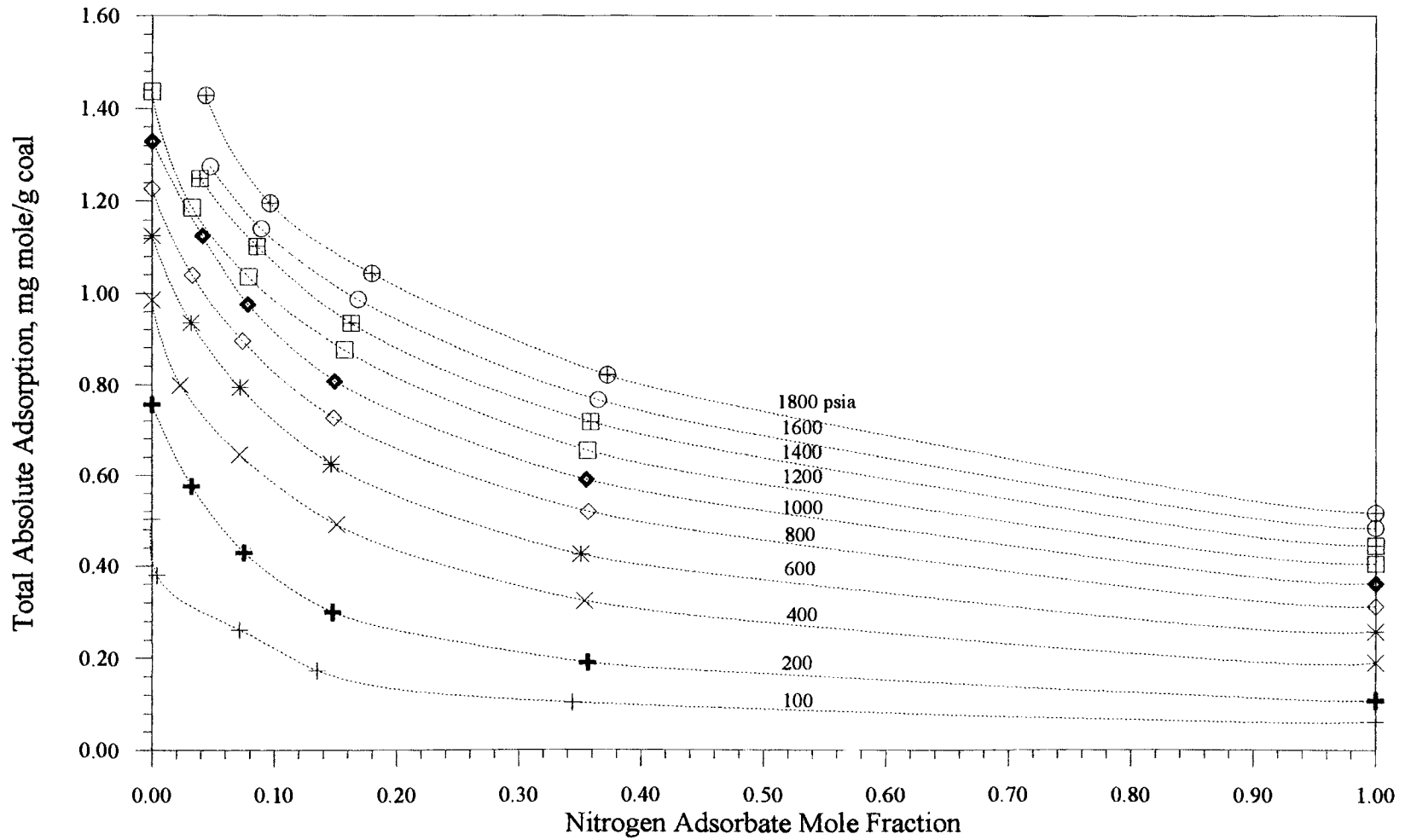
Figure 23. Effect of Adsorbate Composition on Total Absolute Adsorption for Nitrogen-Carbon Dioxide Mixtures
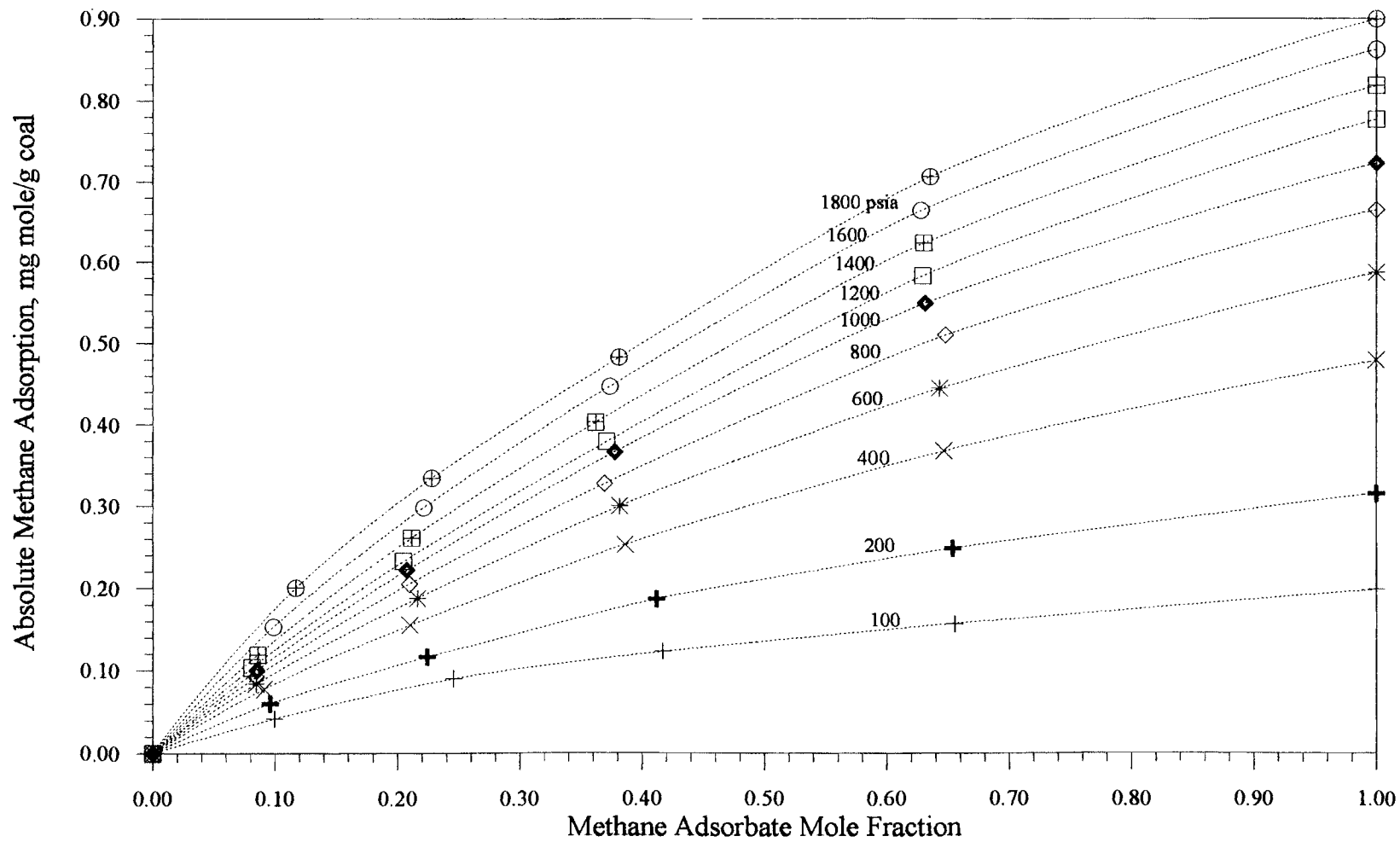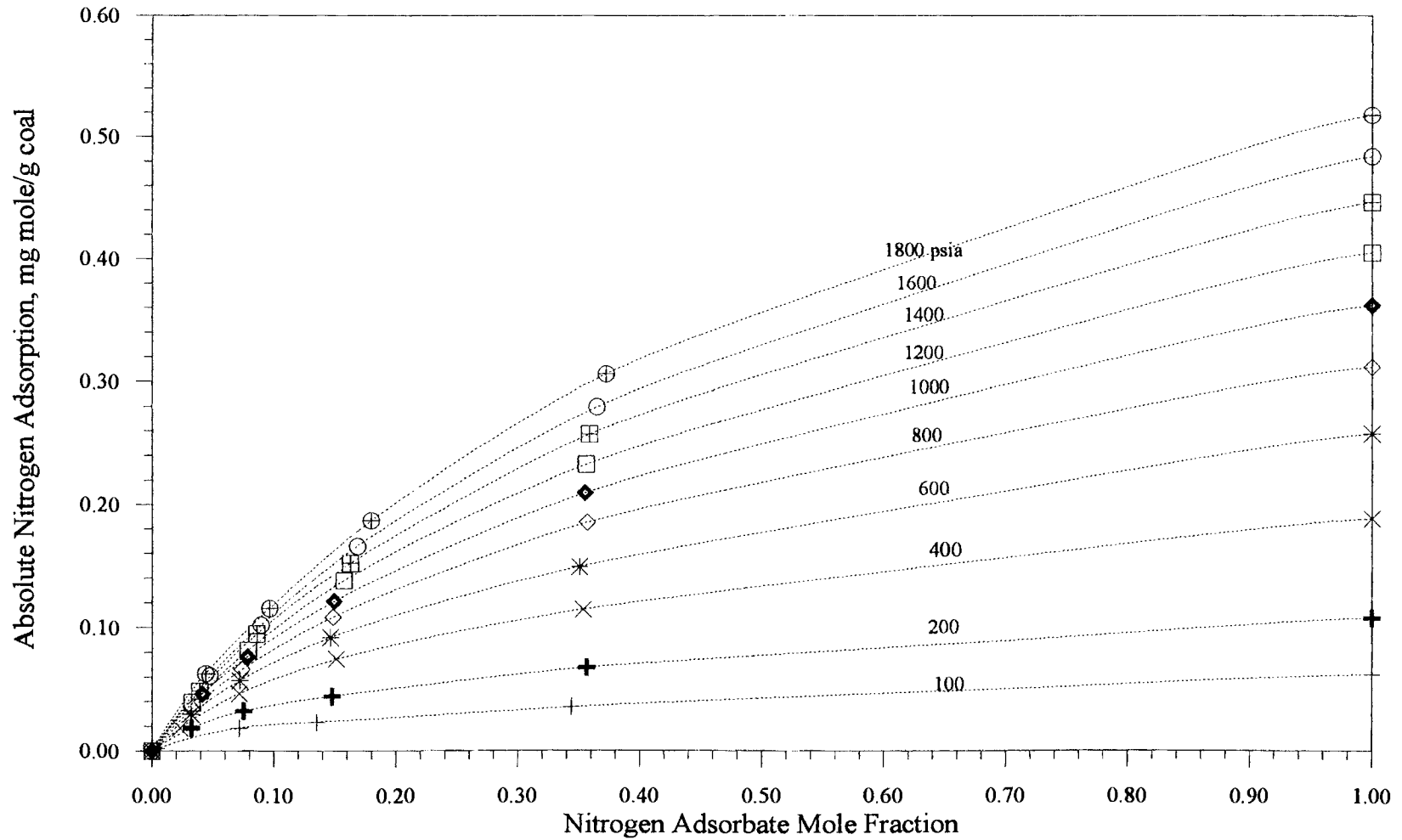
Figure 24. Effect of Adsorbate Composition on Absolute Adsorption for Nitrogen from Nitrogen-Carbon Dioxide Mixtures
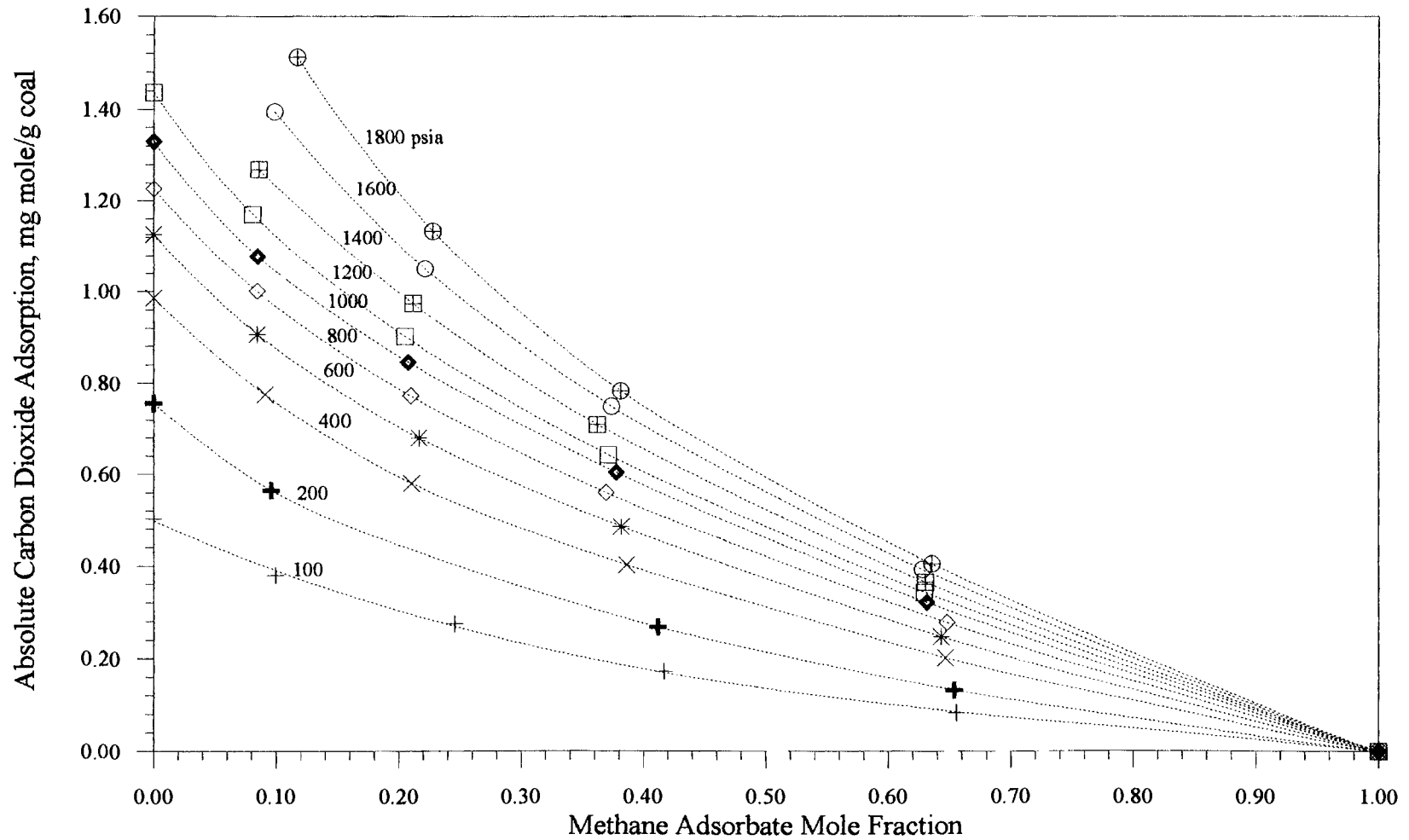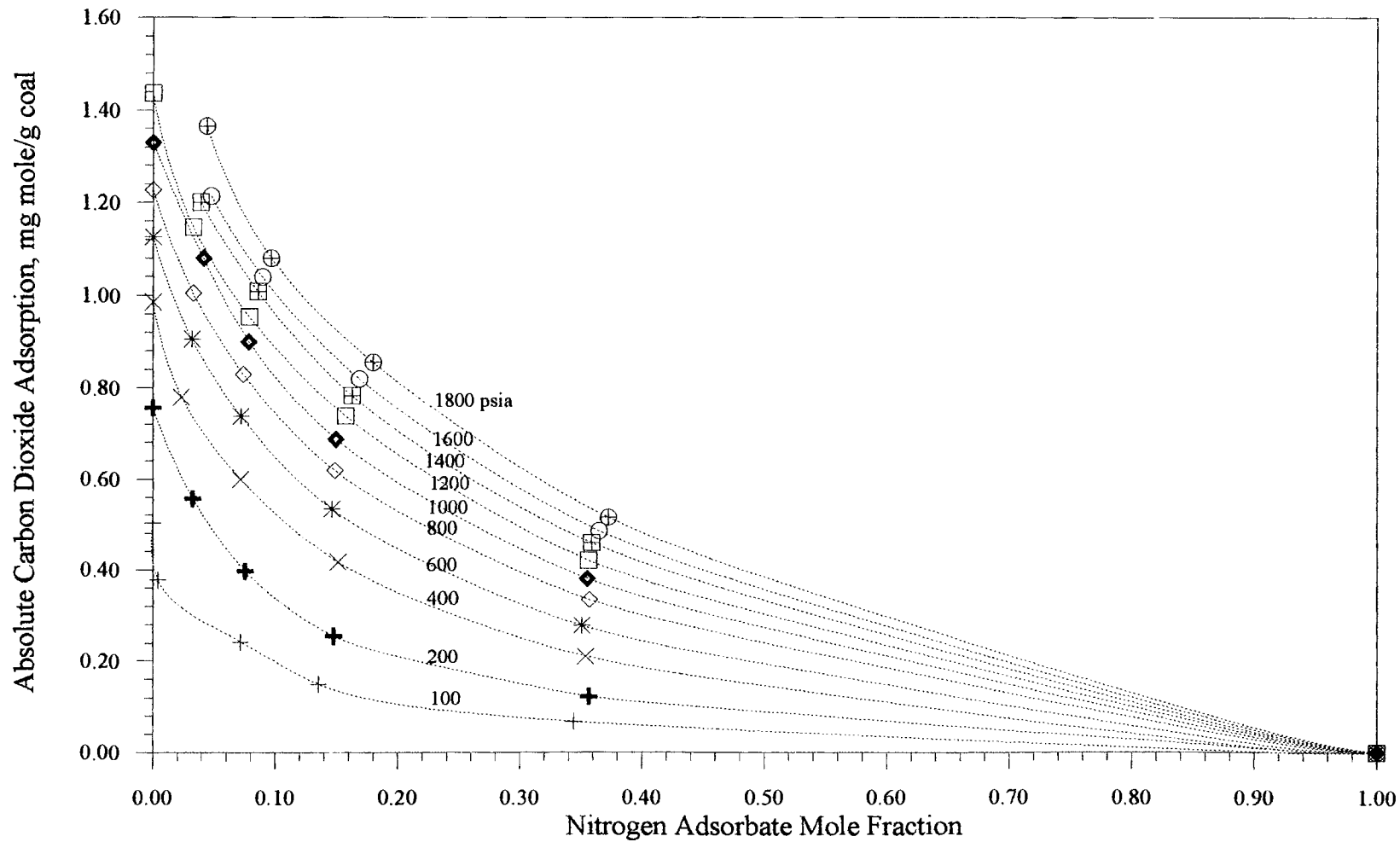
Figure 25. Effect of Adsorbate Composition on Absolute Adsorption for Carbon Dioxide from Nitrogen-Carbon Dioxide Mixtures
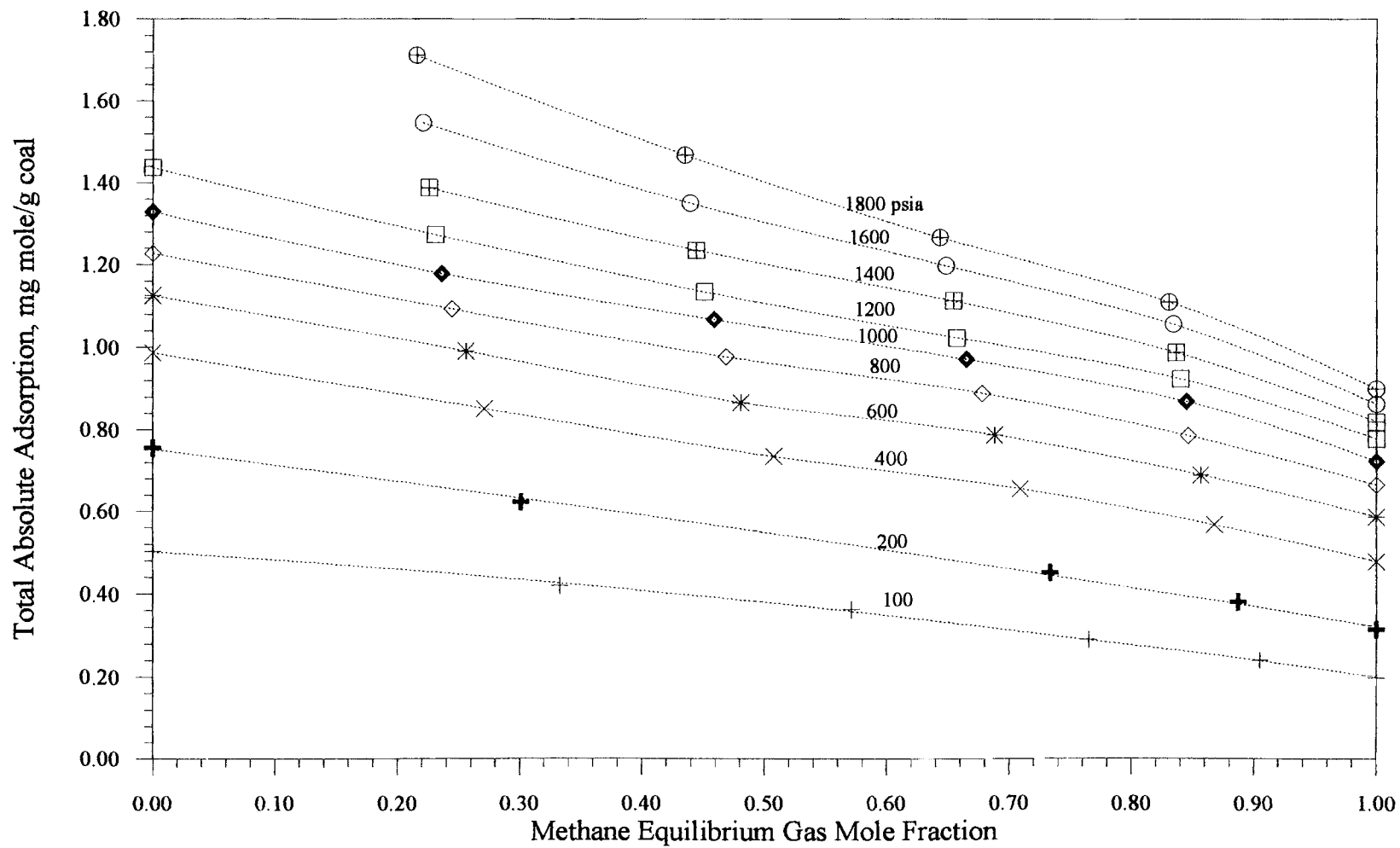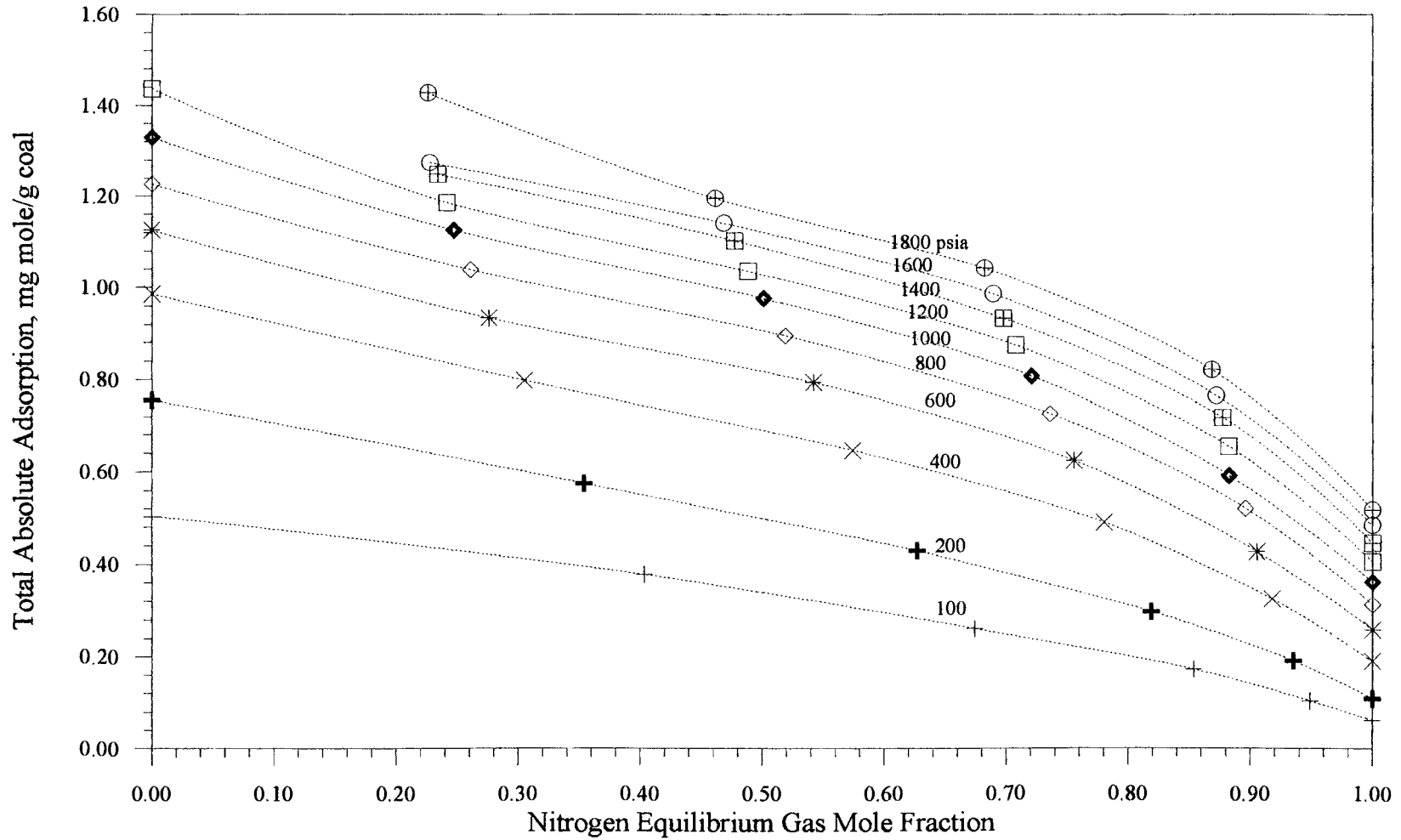
Figure 26. Effect of Equilibrium Gas Composition on Total Absolute Adsorption for
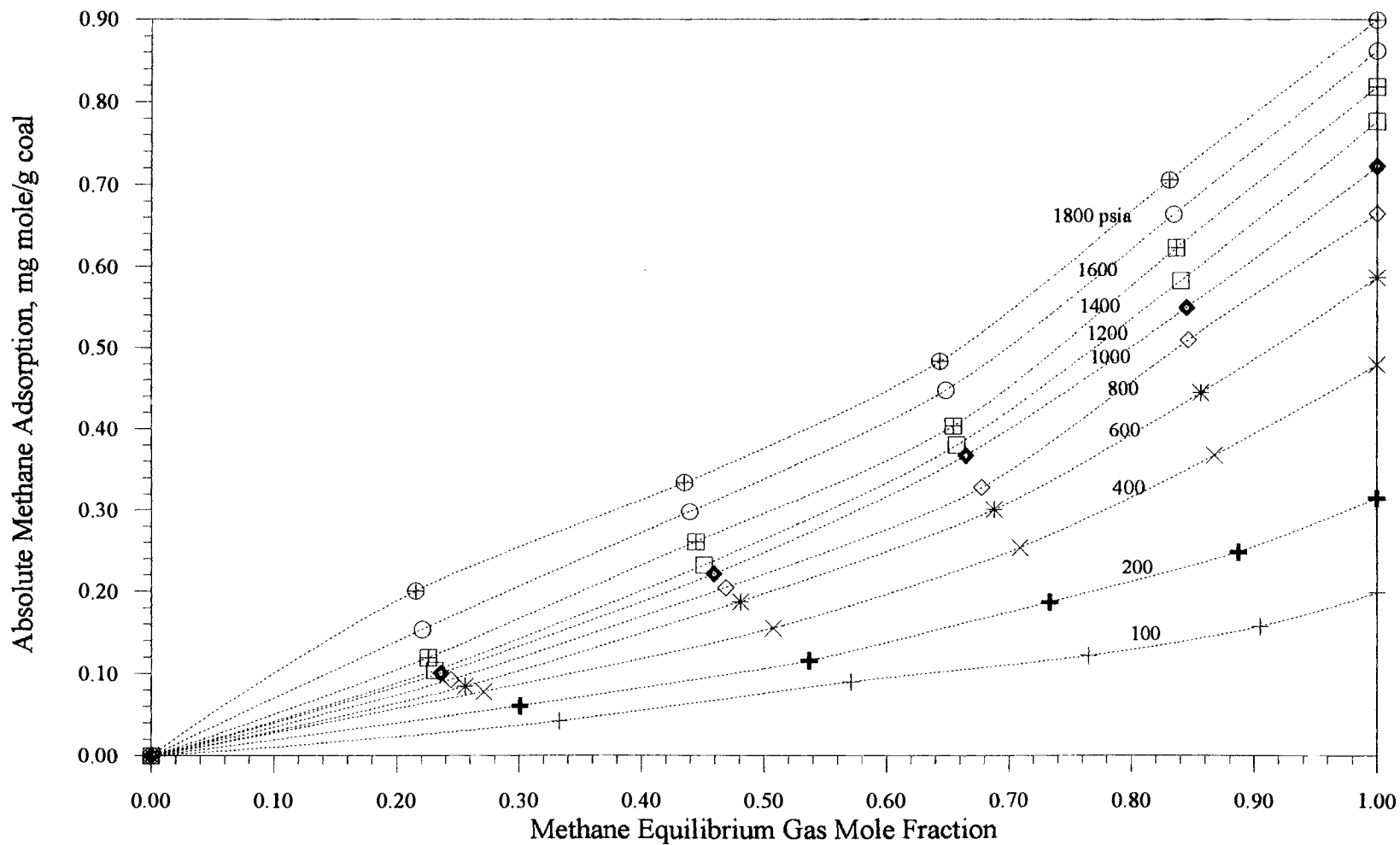Nitrogen-Carbon Dioxide Mixtures
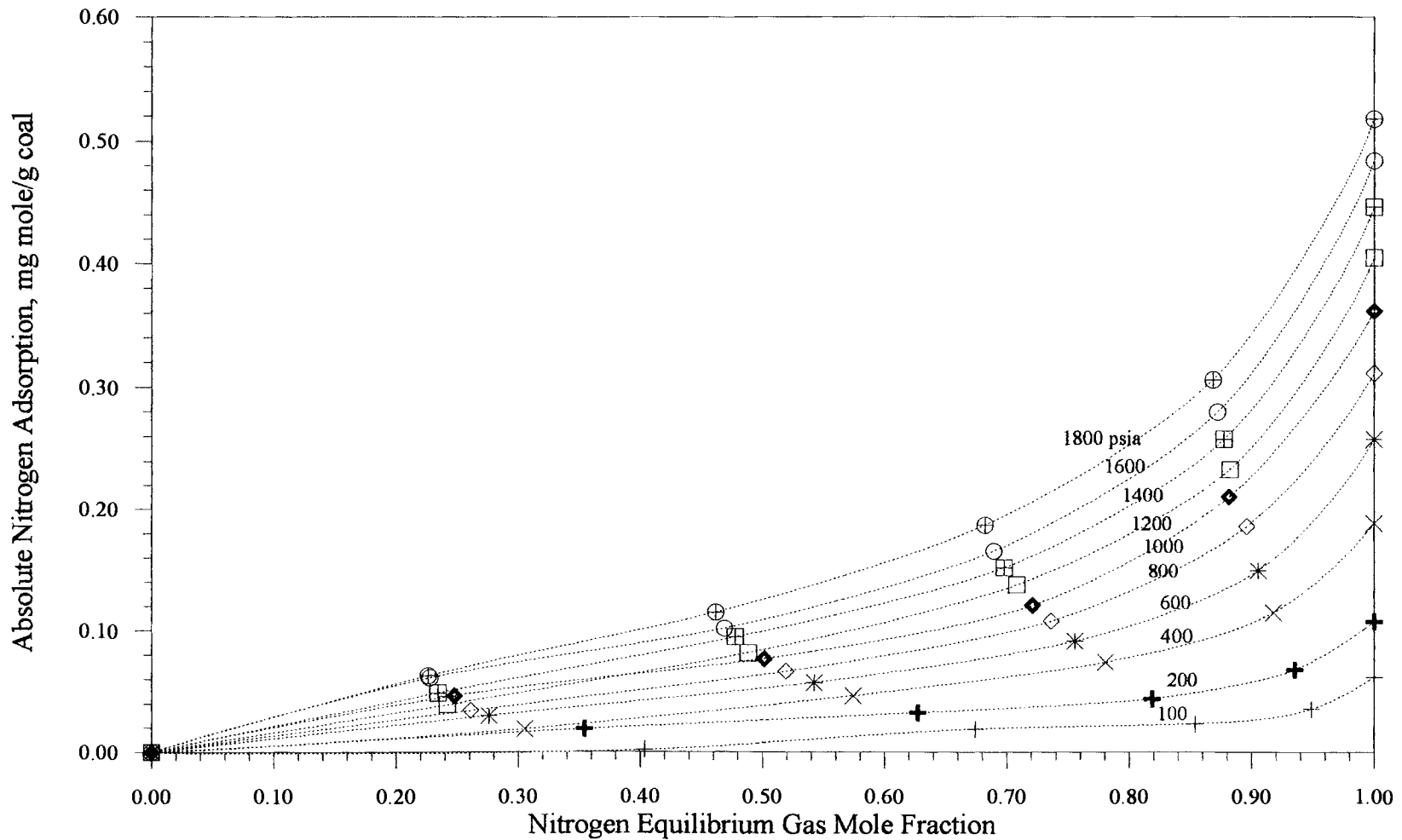
Figure 27. Effect of Equilibrium Gas Composition on Absolute Adsorption for Nitrogen from Nitrogen-Carbon Dioxide Mixtures
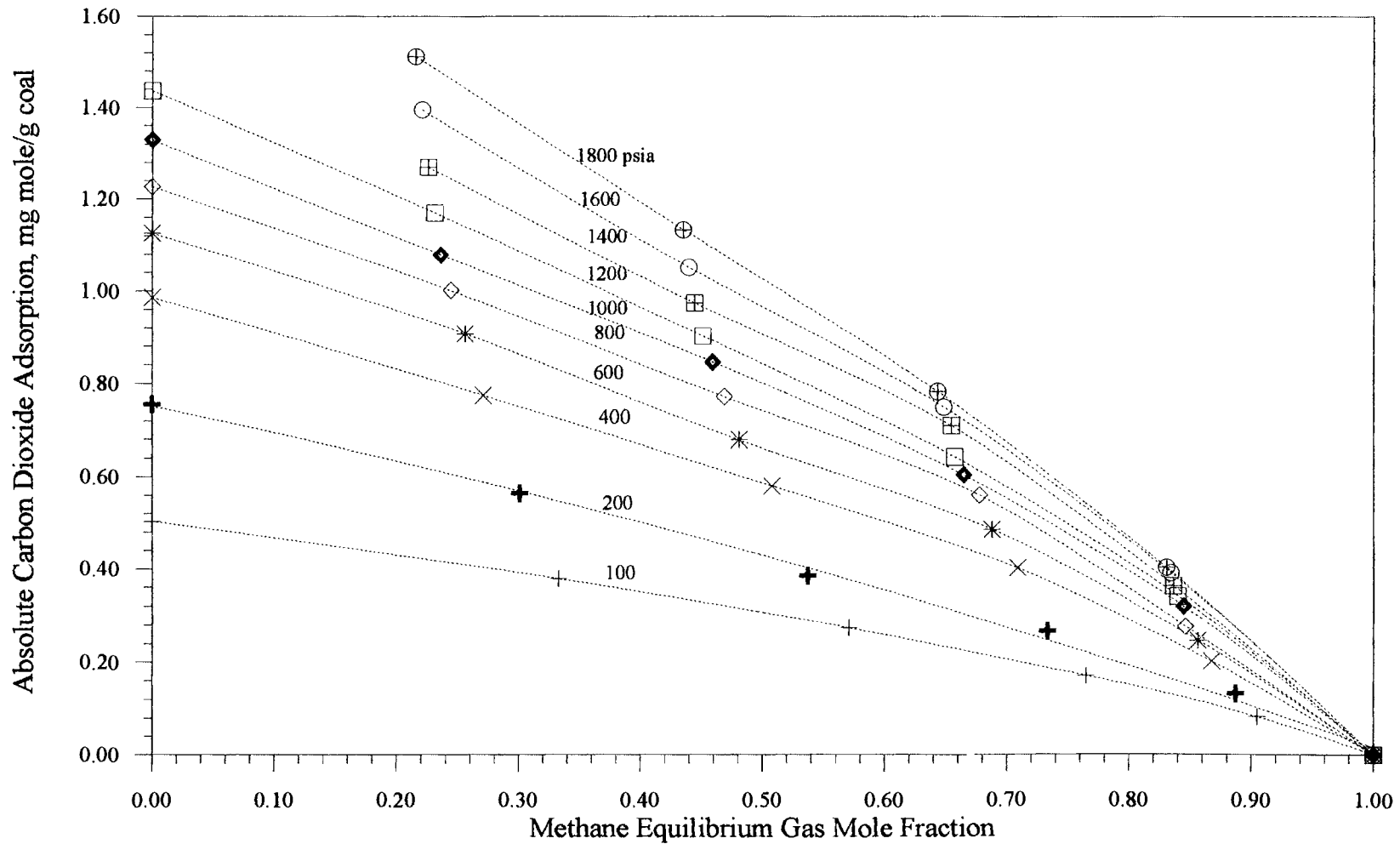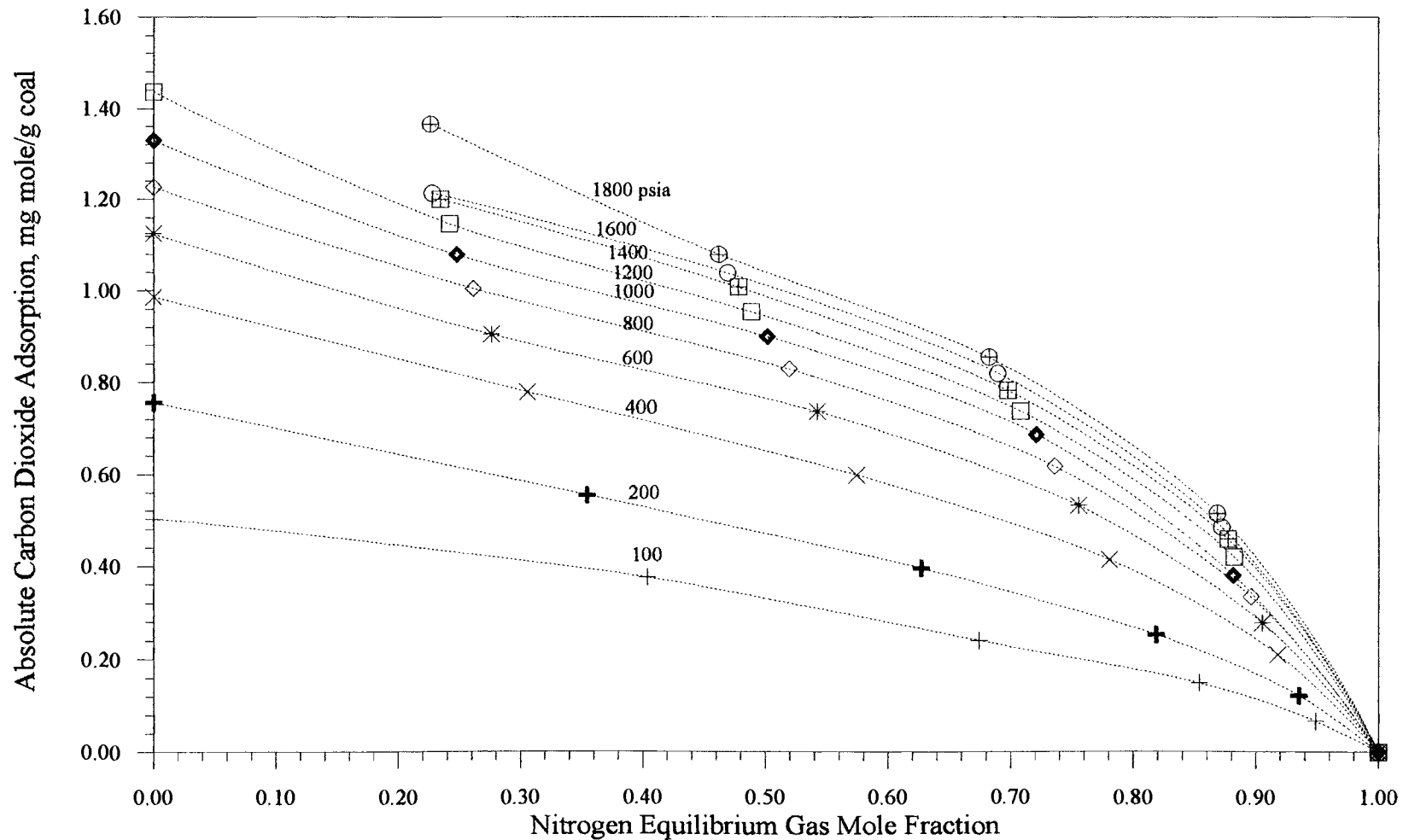
Figure 28. Effect of Equilibrium Gas Composition on Absolute Adsorption for Carbon Dioxide from Nitrogen-Carbon Dioxide Mixtures
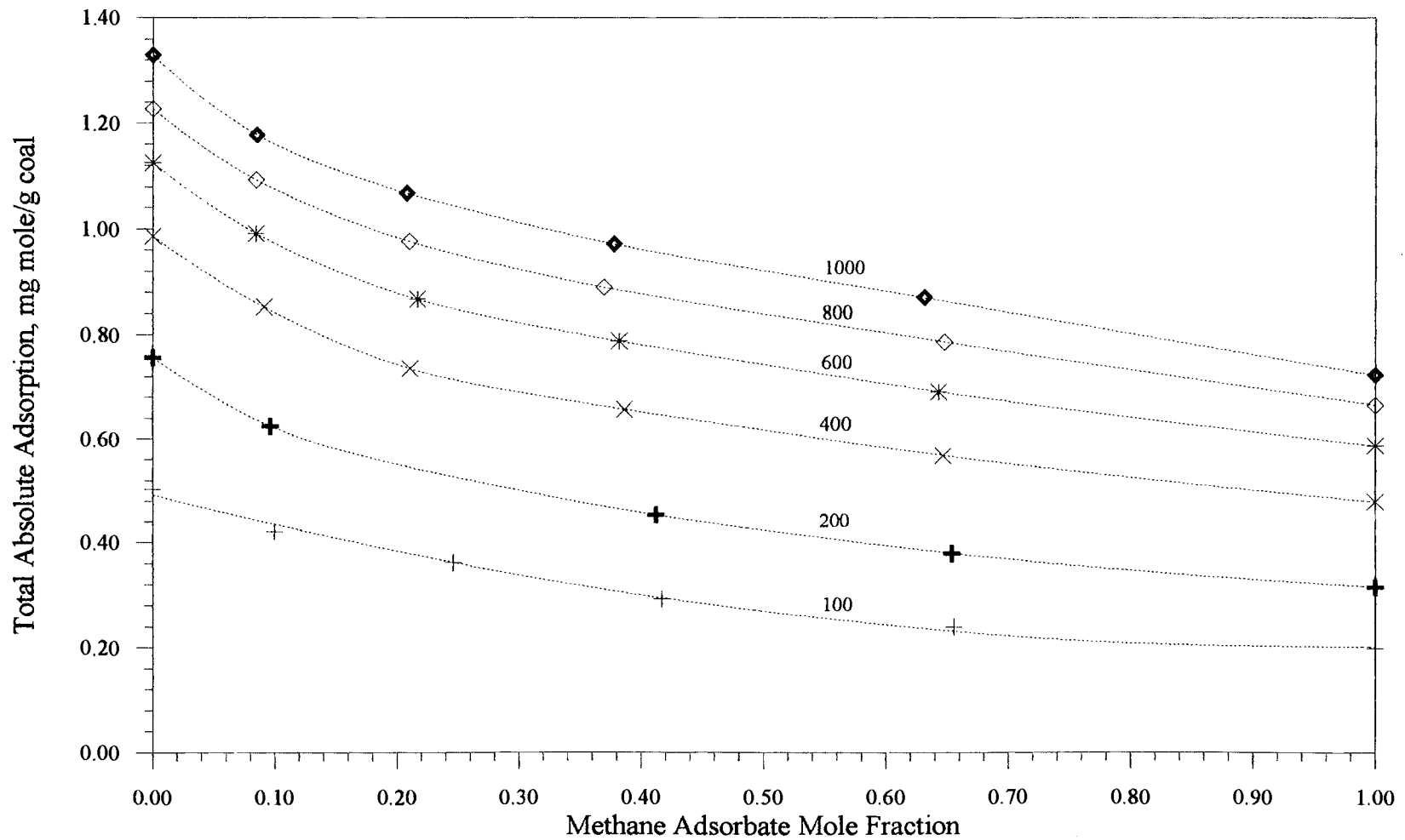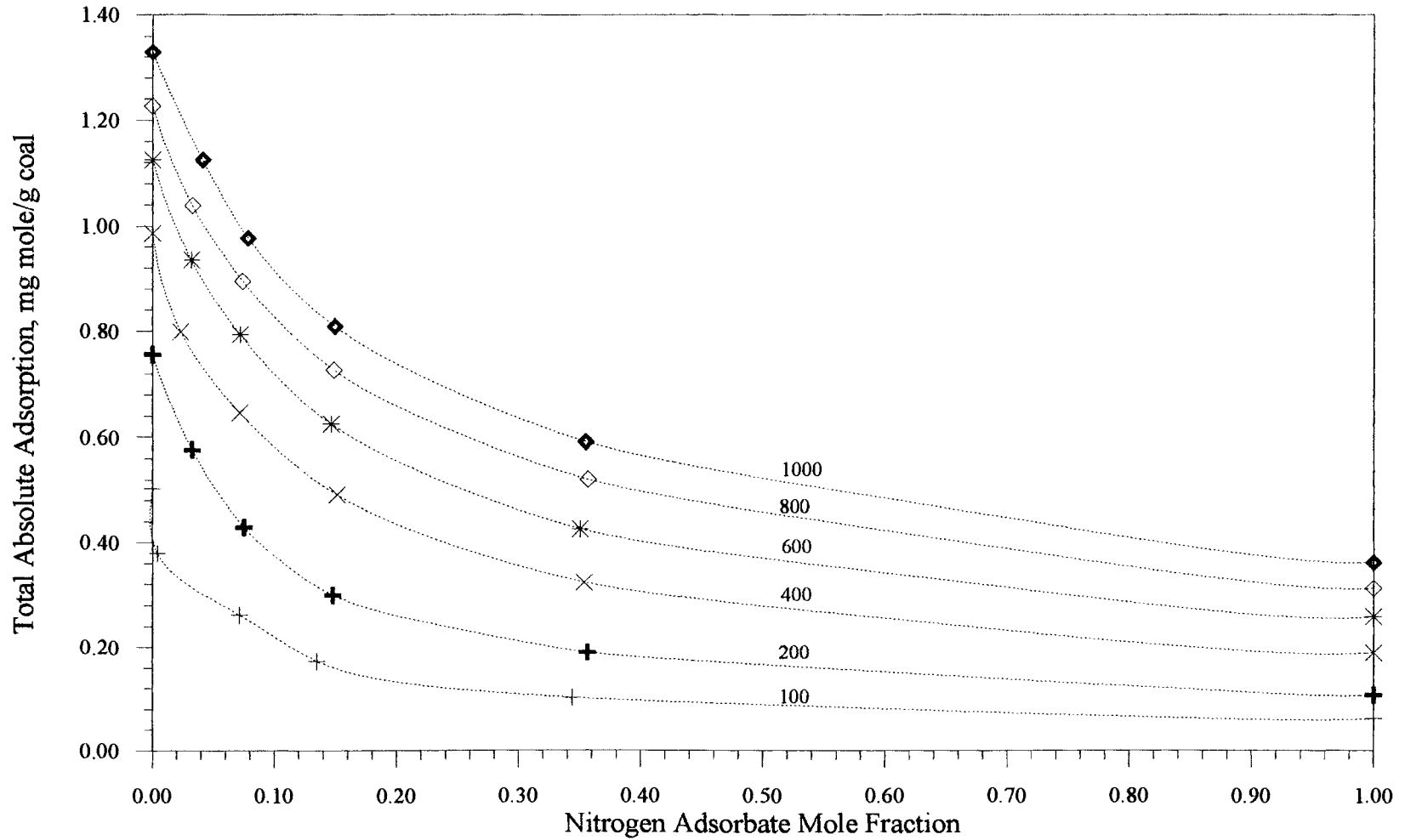
Figure 29. Effect of Adsorbate Composition on Total Absolute Adsorption for
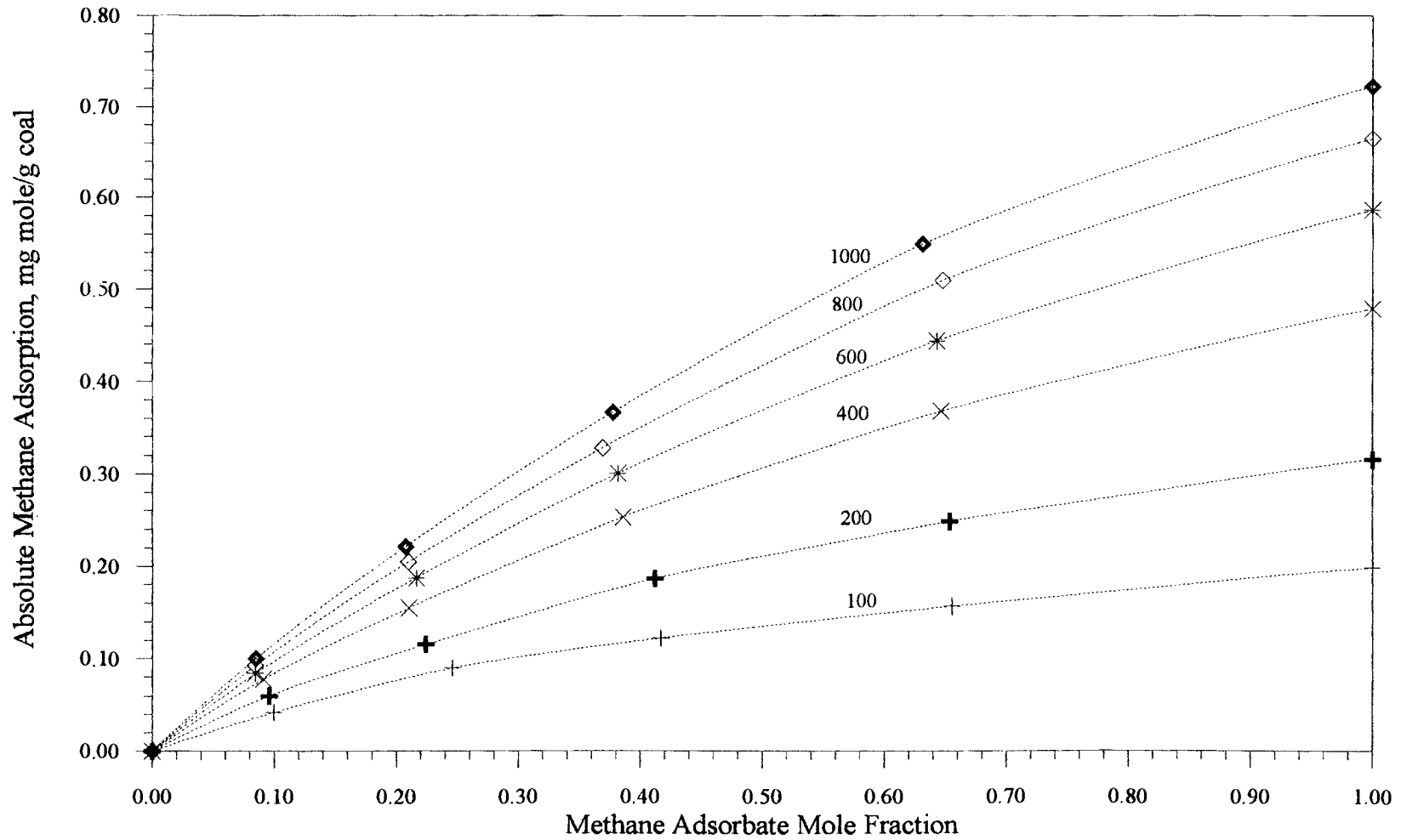Nitrogen-Carbon Dioxide Mixtures to Pressures of 1000 psia
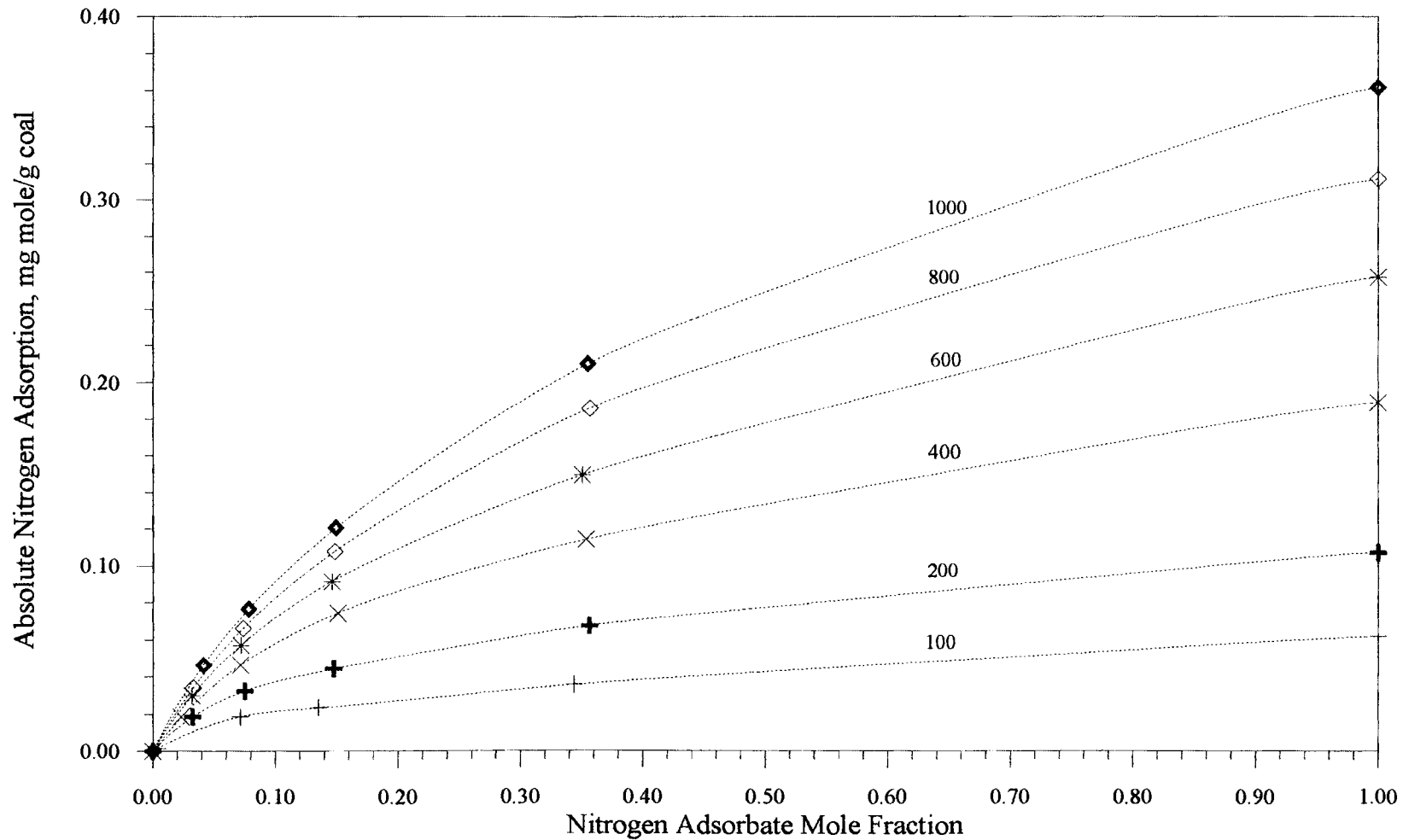
Figure 30. Effect of Adsorbate Composition on Absolute Adsorption for Nitrogen from Nitrogen-Carbon Dioxide Mixtures to Pressures of 1000 psia
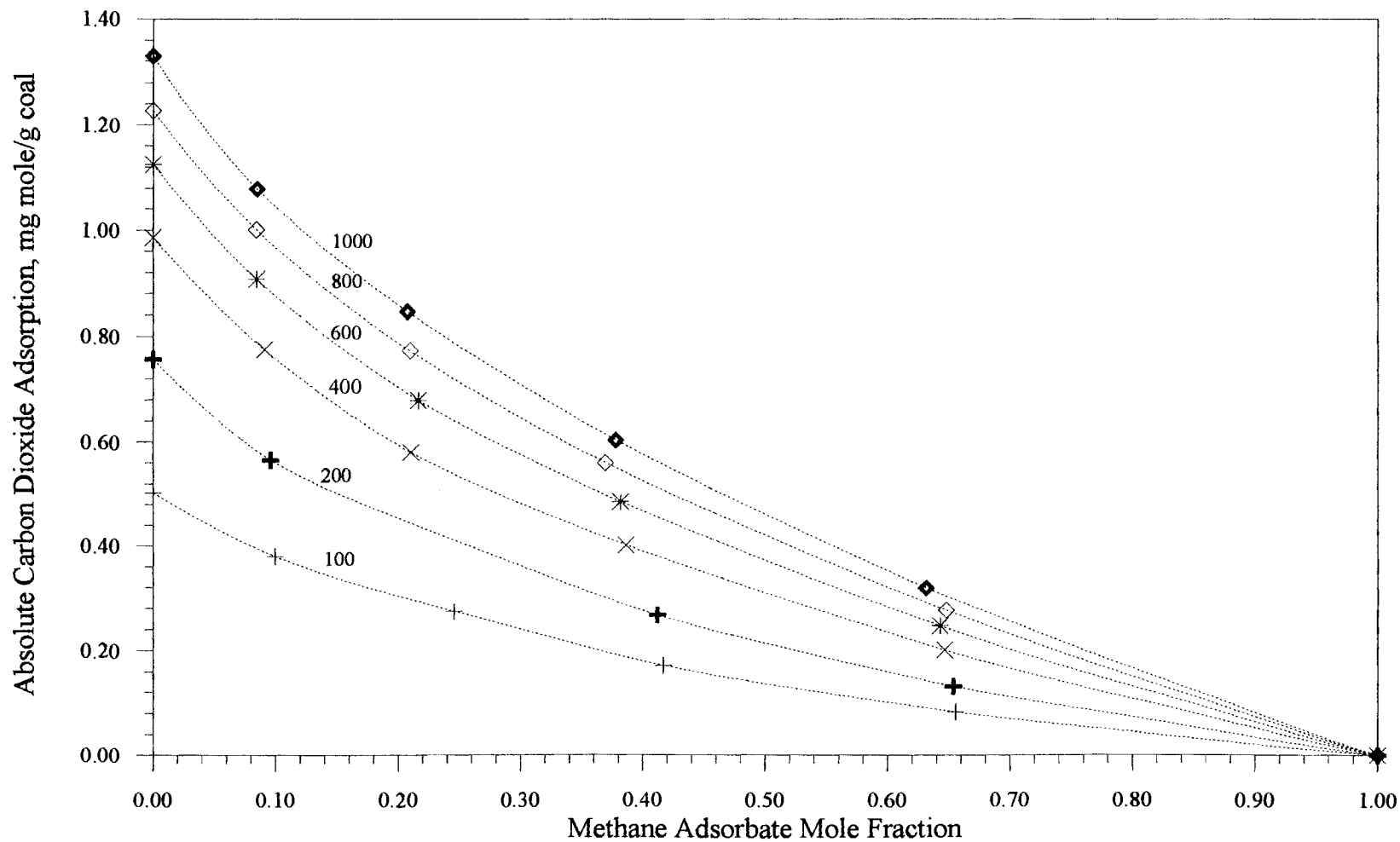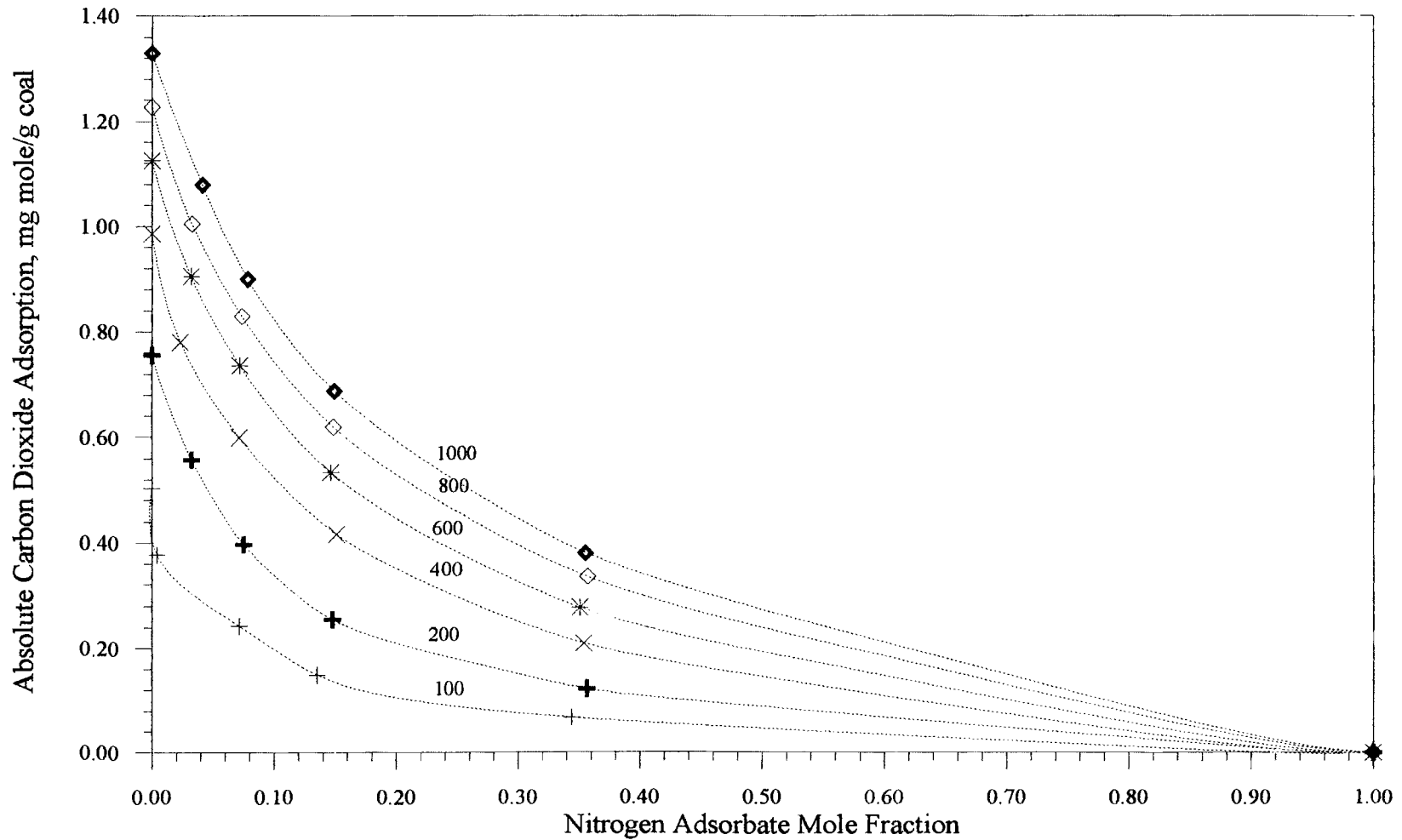
Figure 31. Effect of Adsorbate Composition on Absolute Adsorption for Carbon Dioxide from Nitrogen-Carbon Dioxide Mixtures to Pressures of 1000 psia
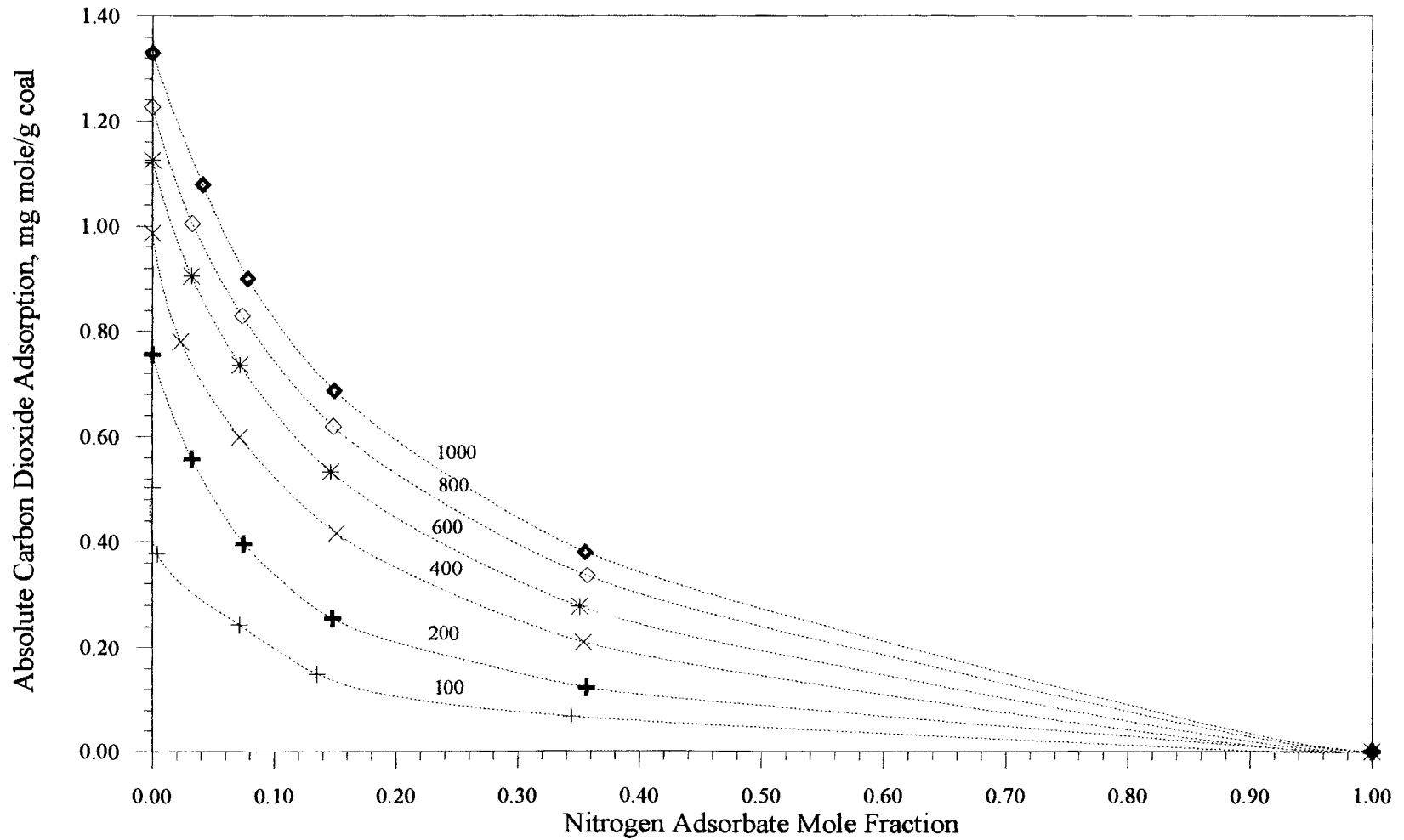
Figure 31. Effect of Adsorbate Composition on Absolute Adsorption for Carbon Dioxide from
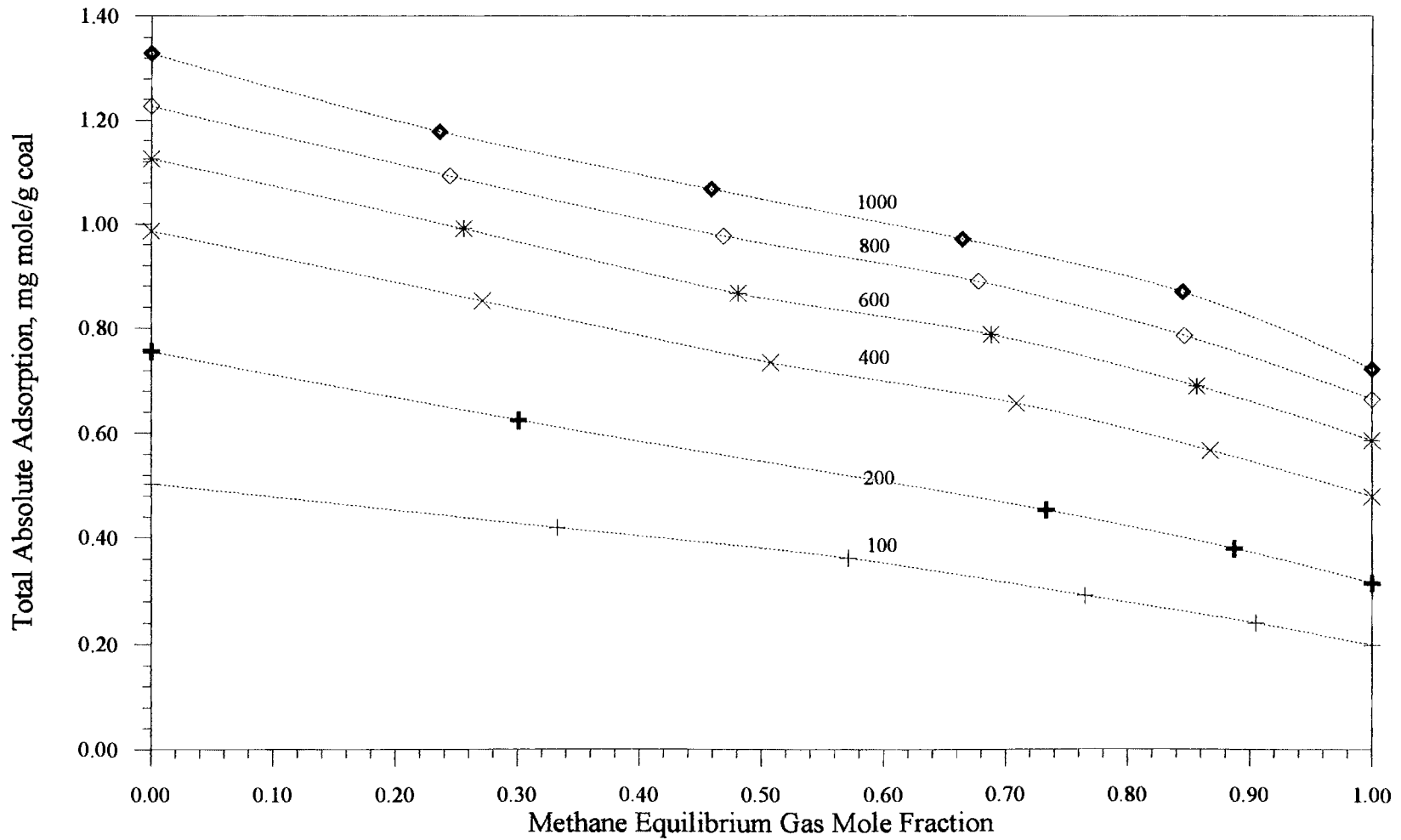Nitrogen-Carbon Dioxide Mixtures to Pressures of 1000 psia
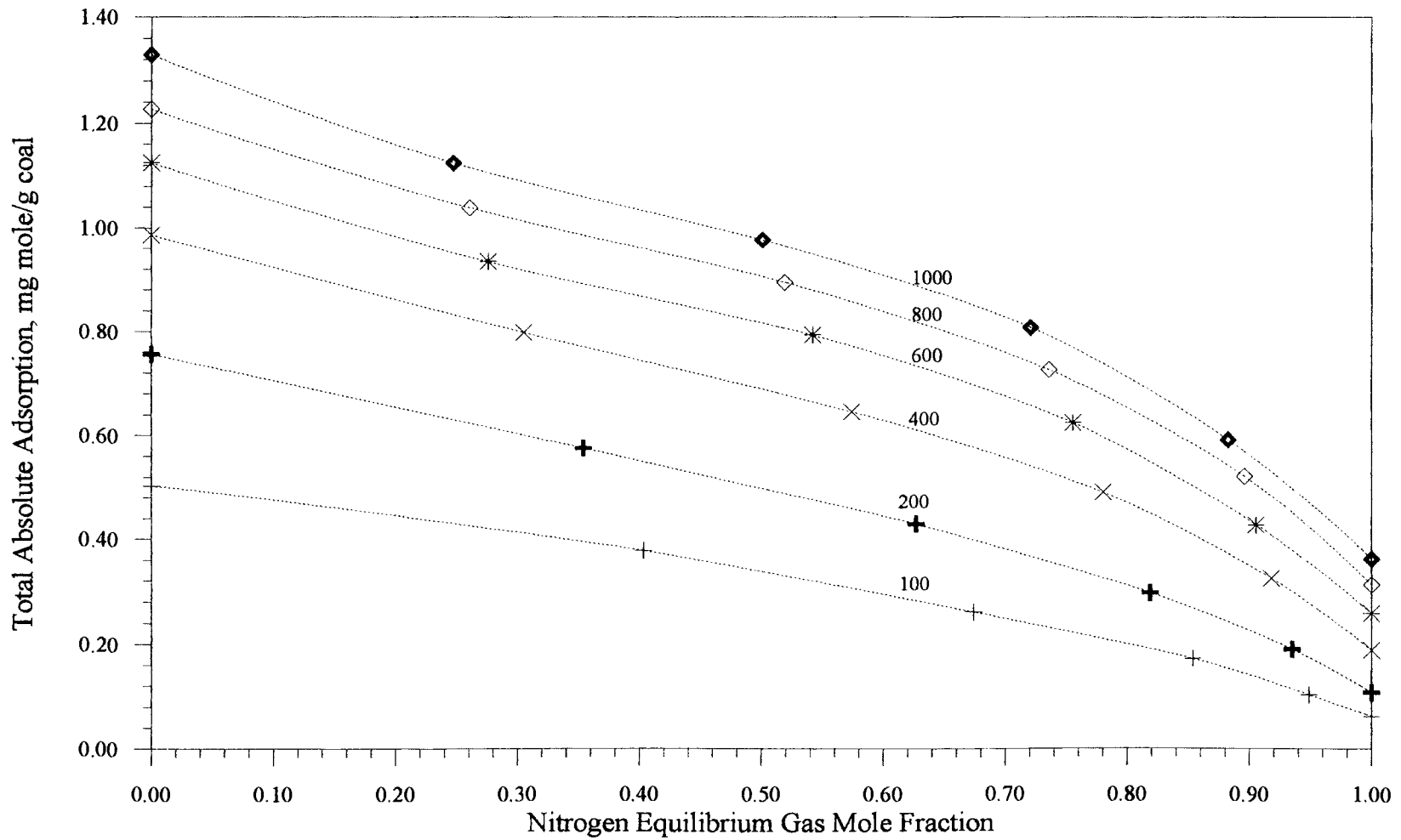
Figure 32. Effect of Equilibrium Gas Composition on Total Absolute Adsorption for
Nitrogen-Carbon Dioxide Mixtures to Pressures of 1000 psia
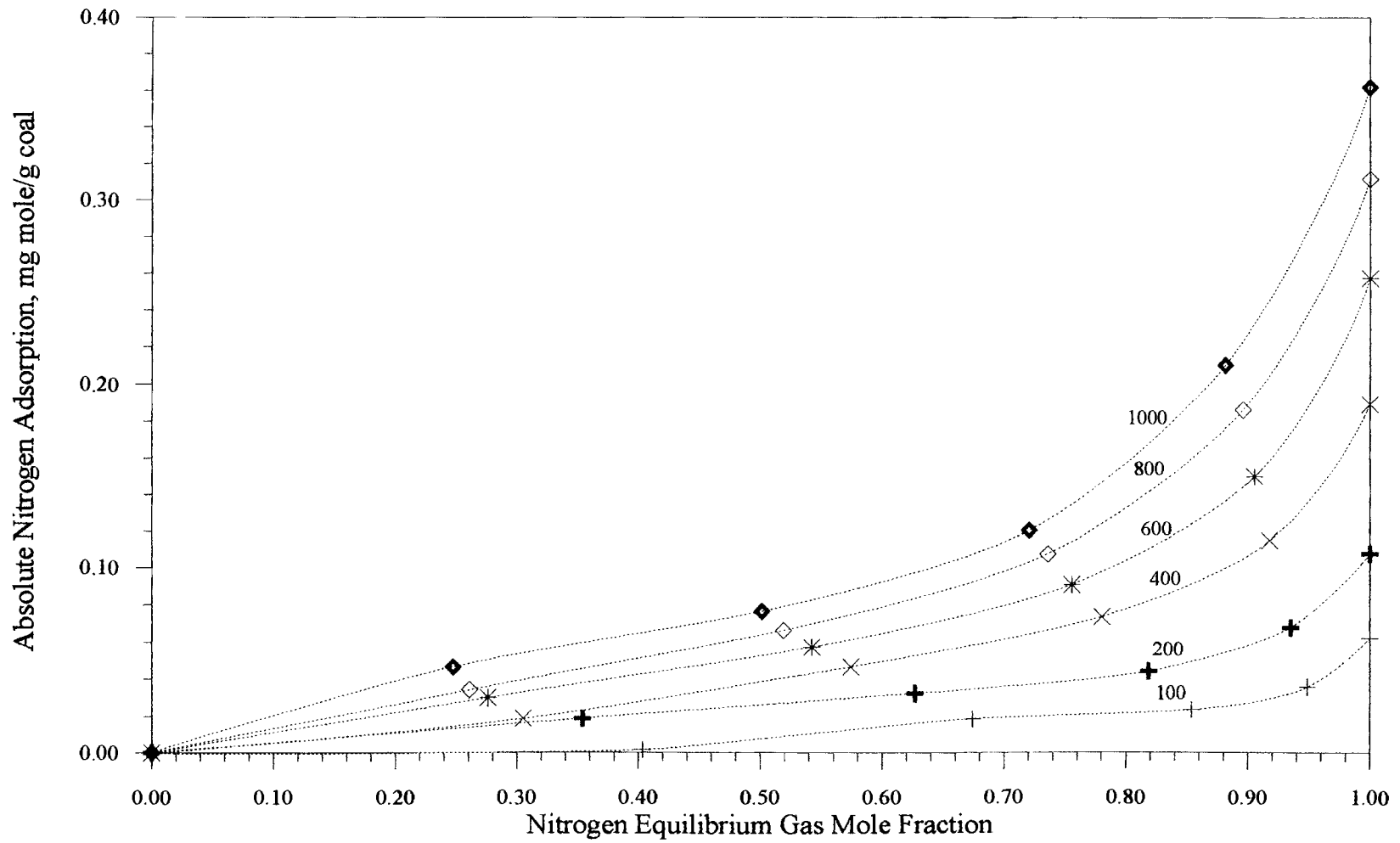
Figure 33. Effect of Equilibrium Gas Composition on Absolute Adsorption for Nitrogen from
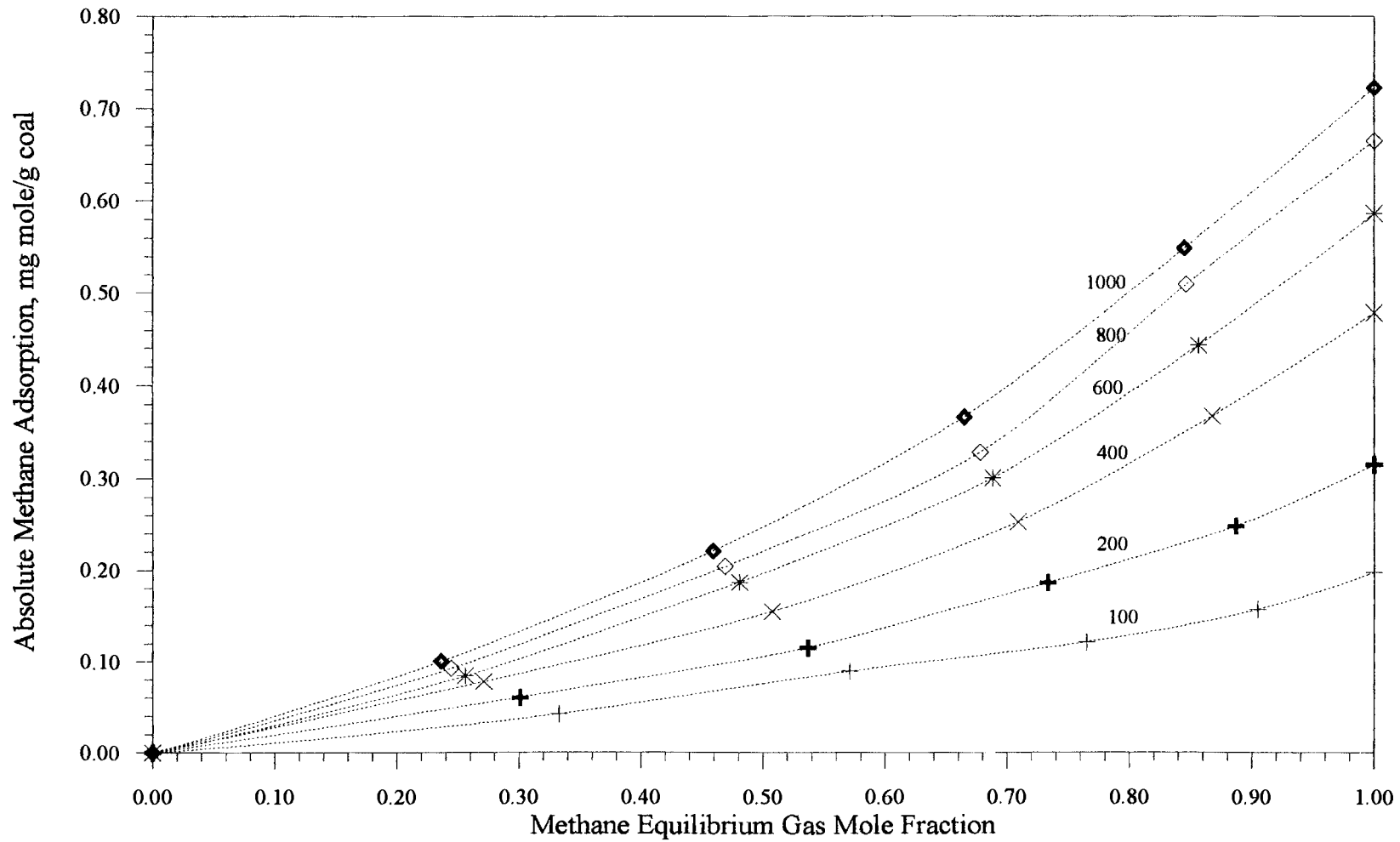Nitrogen-Carbon Dioxide Mixtures to Pressures of 1000 psia

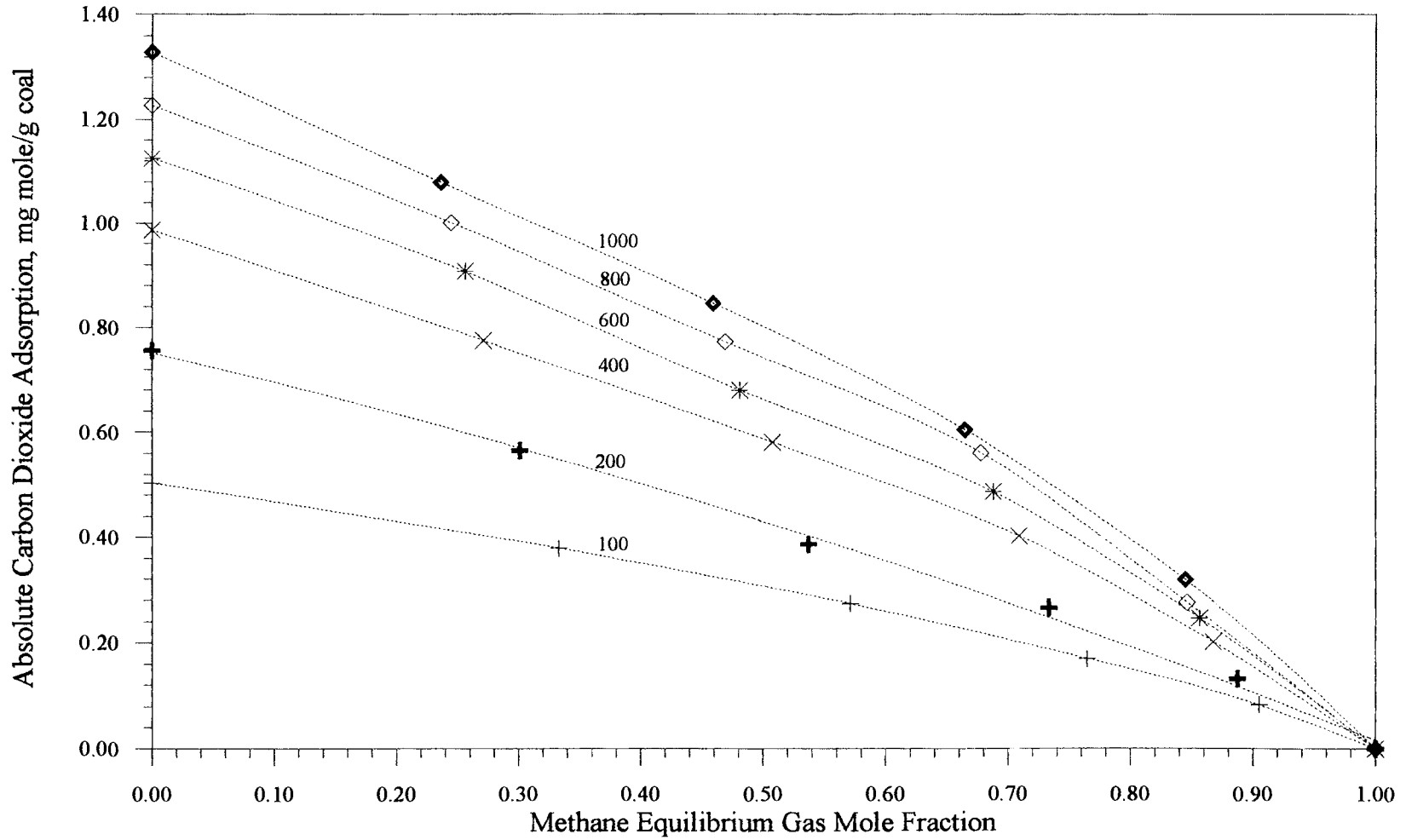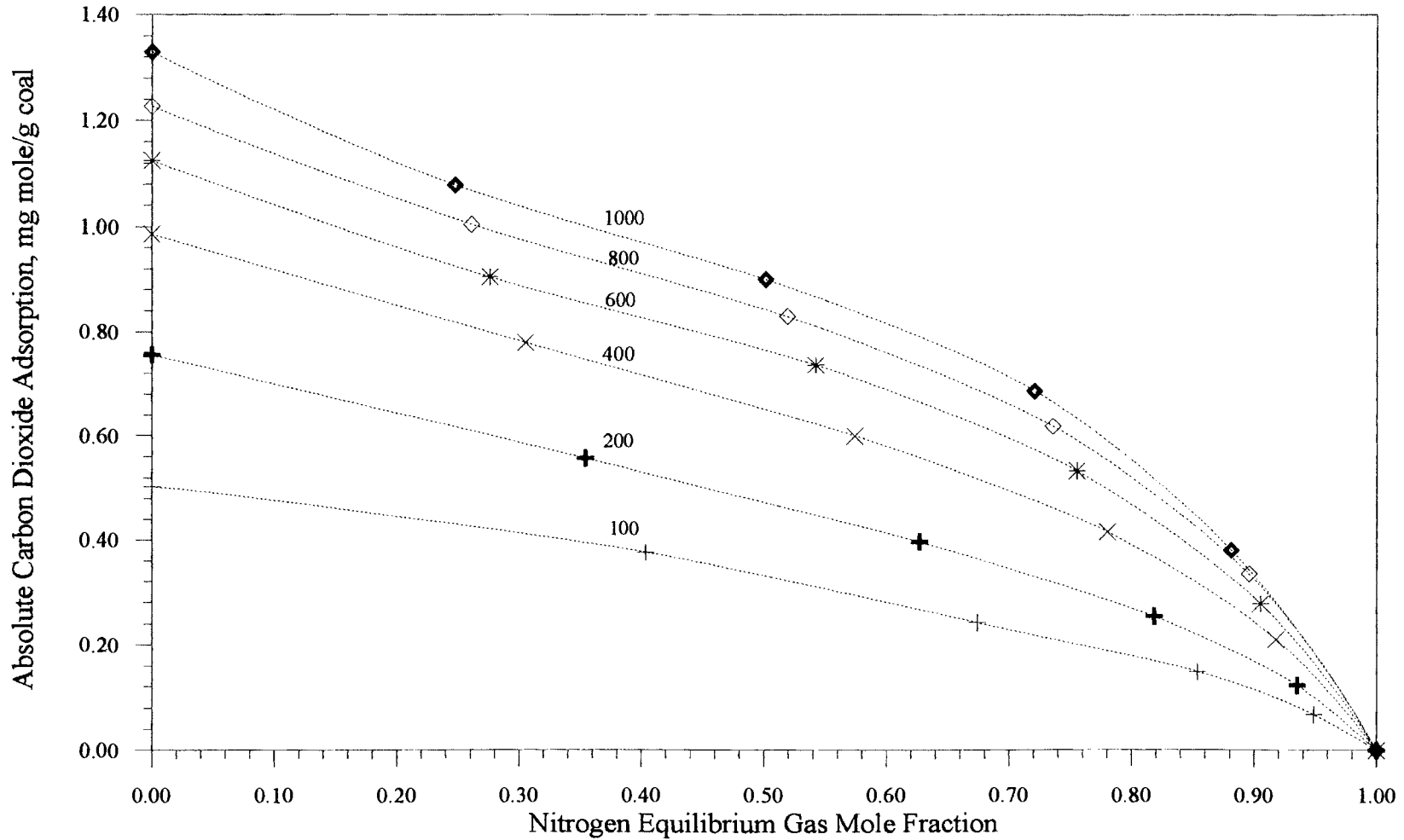Figure 34. Effect of Equilibrium Gas Composition on Absolute Adsorption for Carbon Dioxide from Nitrogen-Carbon Dioxide Mixtures to Pressures of 1000 psia
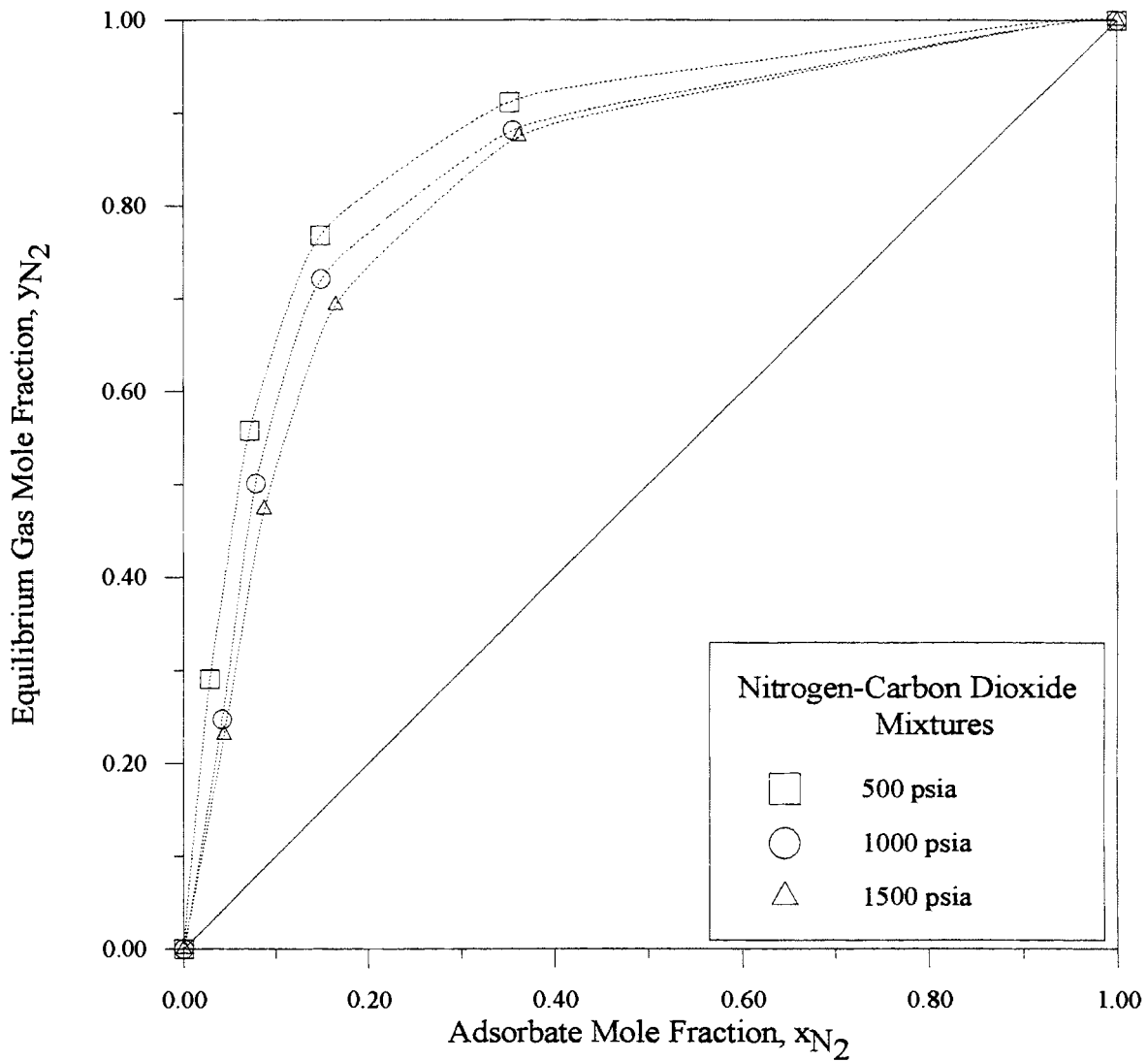
Figure 35. Phase Compositions for Adsorption of Nitrogen-Carbon Dioxide
Mixtures on Wet Fruitland Coal to Pressures of 1500 psia
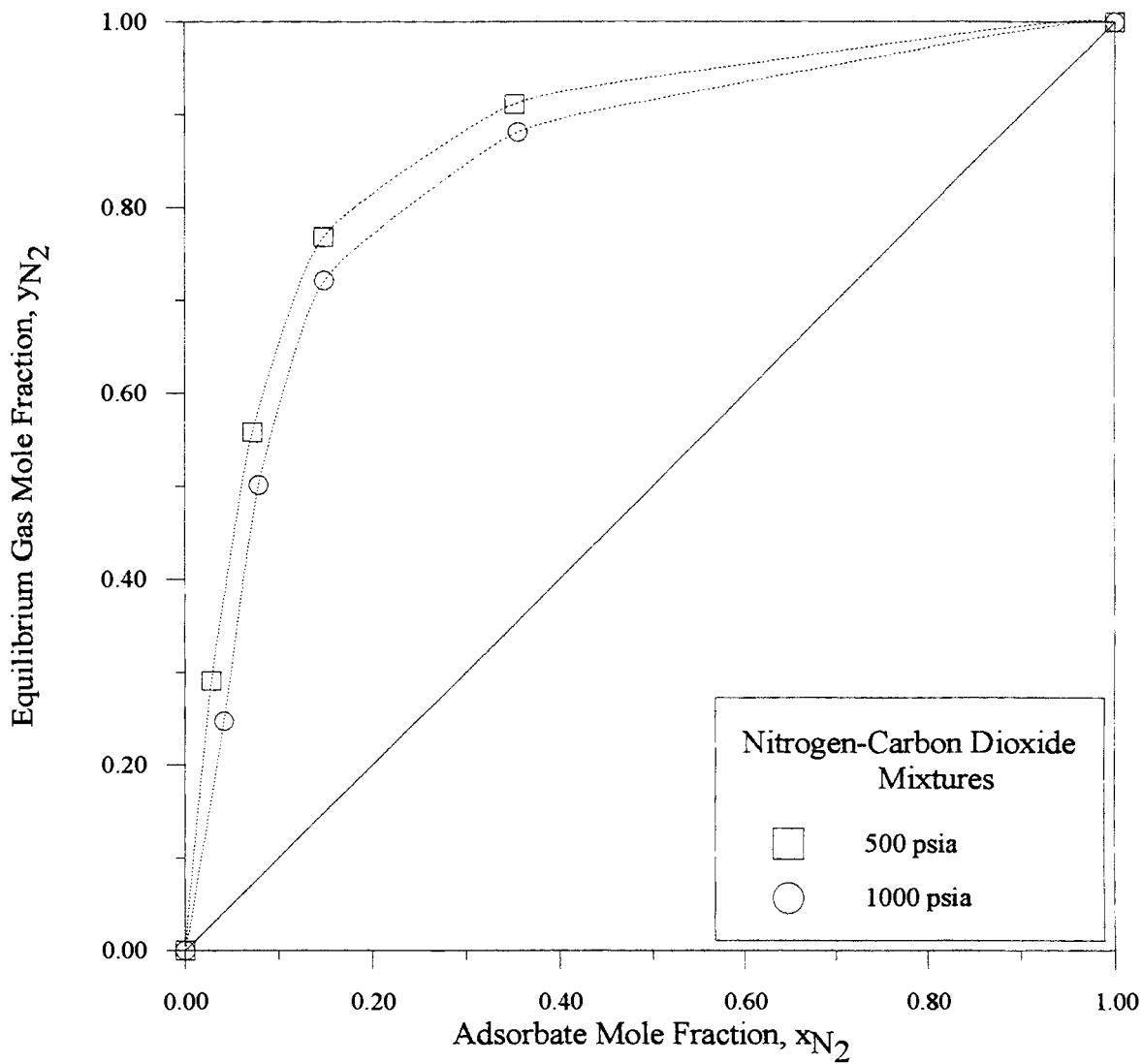
Figure 36. Phase Compositions for Adsorption of Nitrogen-Carbon Dioxide Mixtures on Wet Fruitland Coal to Pressures of 1000 psia

adsorbed phase molar volume. Also, correlations presented by the two authors have utilized different units for the Langmuir constant B. Hall [3] used units of psia^{-1}, whereas Zhou [5] presented B in units of bar^{-1}, therefore the discrepancies in the results should not be misinterpreted.

CHAPTER V

CORRELATION OF BINARY EXPERIMENTAL DATA

Measurement of mixed gas adsorption is a tedious process. Therefore any empirical correlation which caters to design purposes is a welcome substitute for gas adsorption measurements. Adsorption measurements for pure methane, nitrogen and carbon dioxide and their mixtures were performed on wet Fruitland coal at a temperature of 115 °F and pressures to 1800 psia at OSU. There are two replicate isotherms for methane, three for nitrogen, and three for carbon dioxide. For mixtures, the adsorption data were collected at uniform intervals of 0.2, 0.4, 0.6 and 0.8 in feed gas mole fractions.

A mathematical model which describes the adsorption behavior of binary gases on coal at conditions of interest has been developed and tested. The pure component adsorption data were fit to a simple Langmuir model and the constants thus obtained were used to test and compare the new model with the extended Langmuir model.

The Langmuir isotherm is the simplest and the most commonly used model in the industry. The specific form of the Langmuir isotherm was presented earlier in the Literature Review. The following objective function was used in the regression of model constants:

$$S_M = \sum_{j=1}^{N_p} \left| \frac{\omega^c(j) - \omega^e(j)}{\omega^e(j)} \right|^2 \qquad (33)$$

where ω^c is the calculated value of the amount adsorbed and ω^e is the experimental value.

Optimum values for the two parameters in the Langmuir model were determined for each

pure component and are tabulated in Table I. Carbon dioxide exhibits multilayer

adsorption above 1010 psia [3]. Therefore, the regressions for the pure carbon dioxide

data were limited to a pressure of 1010 psia.

The Langmuir equation represents the selected data satisfactorily to give %AAD

ranging from 2.3 to 2.9. The model constants and the resultant statistics are given in

Table I.

TABLE I. Simple Langmuir Model for Pure Adsorption Isotherms

Component	Points	L, mg mole/ gm coal	B, psia^{-1}	RMSE	%AAD	WRMS
CH_4	20	1.084	0.001989	0.0119	2.3	1.5
N_2	30	0.8976	0.0006566	0.0081	2.9	1.7
CO_2	24	1.481	0.004838	0.0281	2.6	1.6

The extended Langmuir equation described earlier in the Literature Review section

is used to predict the adsorption of mixtures. To obtain a better description of the binary

data, the simple Langmuir model is modified to include the following mixing rules for the

LB term in the numerator and B in the denominator:

$$LB = \sum_j \sum_k M_{jk} y_j^{0.5} y_k^{0.5}$$

$$B = \sum_j \sum_k B_{jk} y_j y_k$$

Thus, the modified model used in correlating the present experimental data is given

as:

$$\omega = \frac{\left(\sum_j \sum_k M_{jk} y_j^{0.5} y_k^{0.5}\right) P}{1 + \left(\sum_j \sum_k B_{jk} y_j y_k\right) P} \tag{34}$$

for the total amount adsorbed and

$$\omega_i = \frac{y_i^{0.5} \left(\sum_k M_{ik} y_k^{0.5}\right) P}{1 + \left(\sum_j \sum_k B_{jk} y_j y_k\right) P} \tag{35}$$

for the individual component adsorption, where $M_{ii} = L_i B_i$ and M_{ij} and B_{ij} are the regressed parameters. This model collapses to a simple Langmuir model when M_{ij} and B_{ij} equal to zero, for a pure fluid. Therefore, only the pure parameters L_i and B_i are used in the extended Langmuir model predictions. In contrast, for the modified model, in addition to the pure parameters obtained from the simple Langmuir model, the cross coefficients are regressed separately for ω_1, ω_2 and ω, for the whole feed gas composition range.

Comparisons between the predictions obtained by extended Langmuir model, referred to here as Case I, and by the new correlative model, referred to as Case II are presented in terms of %AAD (average absolute percentage deviation) and AAD (average absolute deviation) in Table II. The regressed values for the cross coefficients for different mixtures are presented in Table III.

For methane-nitrogen mixtures a total of 39 experimental data points were used in the correlation work. The predictions are illustrated in Figures 37 to 39. The extended Langmuir model results in good predictions for the total amount of gas adsorbed. It also

TABLE II. Comparison of Predictions for Binary Adsorption Data

%AAD (AAD)					
Case	No. of Parameters	Points	ω_1	ω_2	ω
Methane(1) + Nitrogen(2)					
I	4	39	4.9 (0.011)	13.8 (0.016)	3.5 (0.015)
II	6	39	3.2 (0.011)	10.5 (0.013)	3.5 (0.015)
Methane(1) + Carbon Dioxide(2)					
I	4	24	10.1 (0.015)	6.2 (0.019)	4.2 (0.026)
II	6	24	4.6 (0.009)	5.5 (0.019)	2.9 (0.019)
Nitrogen(1) + Carbon Dioxide(2)					
I	4	24	51.2 (0.025)	11.3 (0.037)	7.0 (0.038)
II	6	24	25.1 (0.011)	6.1 (0.021)	3.5 (0.016)

Case I - extended Langmuir
Case II - Modified version of extended Langmuir

TABLE III. Model Constants for the New Model

Co-efficient	ω_1	ω_2	ω
Methane(1) + Nitrogen(2)			
M_{12}	0.0001694	0.0000962	0.0000019
B_{12}	0.0017712	0.0021225	0.0013494
Methane(1) + Carbon Dioxide(2)			
M_{12}	-0.0001965	0.00048403	0.0003327
B_{12}	0.0034598	0.0046531	0.0047119
Nitrogen(1) + Carbon Dioxide(2)			
M_{12}	-0.0001769	0.0010441	0.0002887
B_{12}	0.0046966	0.0049988	0.0042890
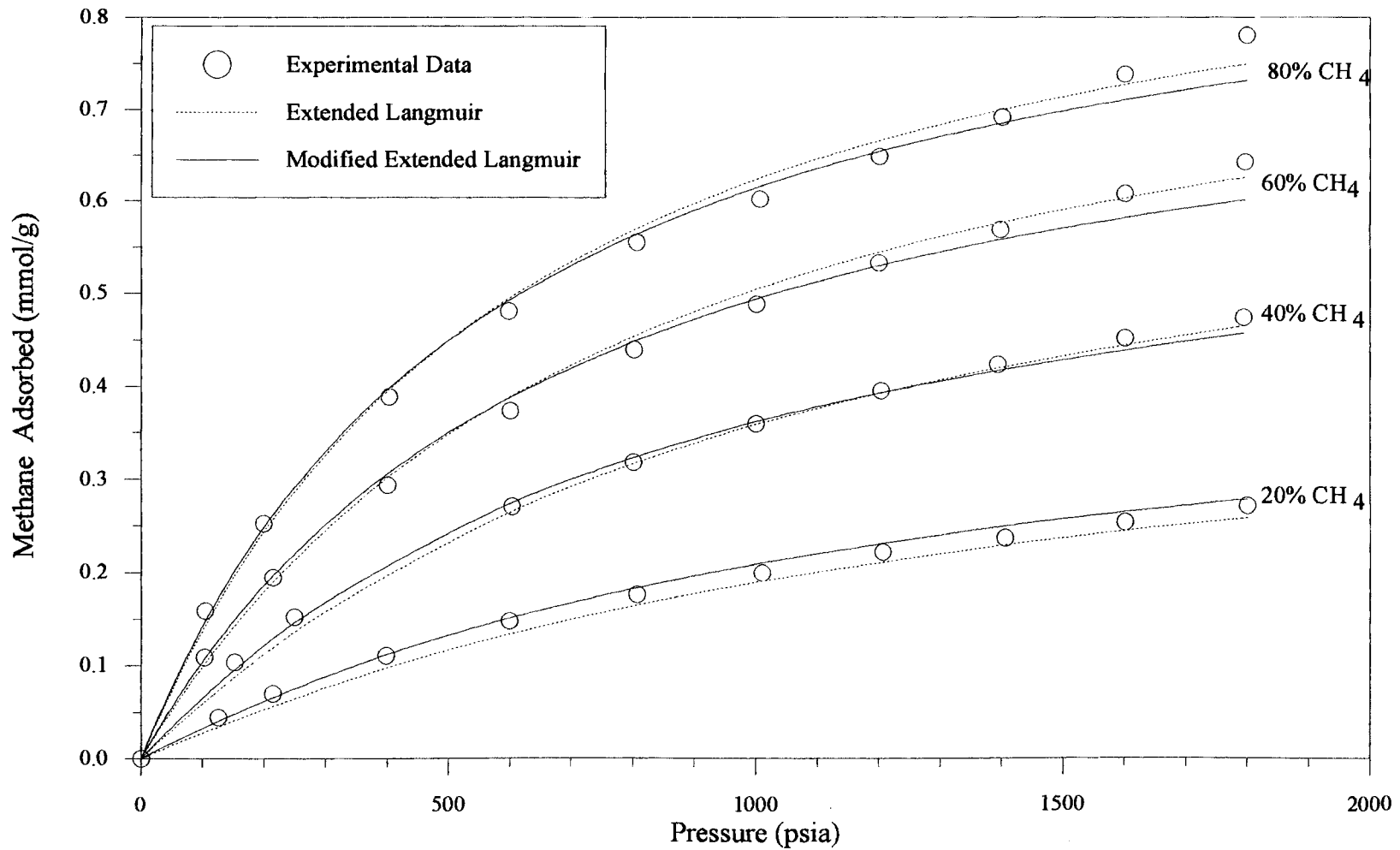
Figure 37. Prediction of the Amount of Methane Adsorbed for Methane-Nitrogen Mixtures
on Wet Fruitland Coal
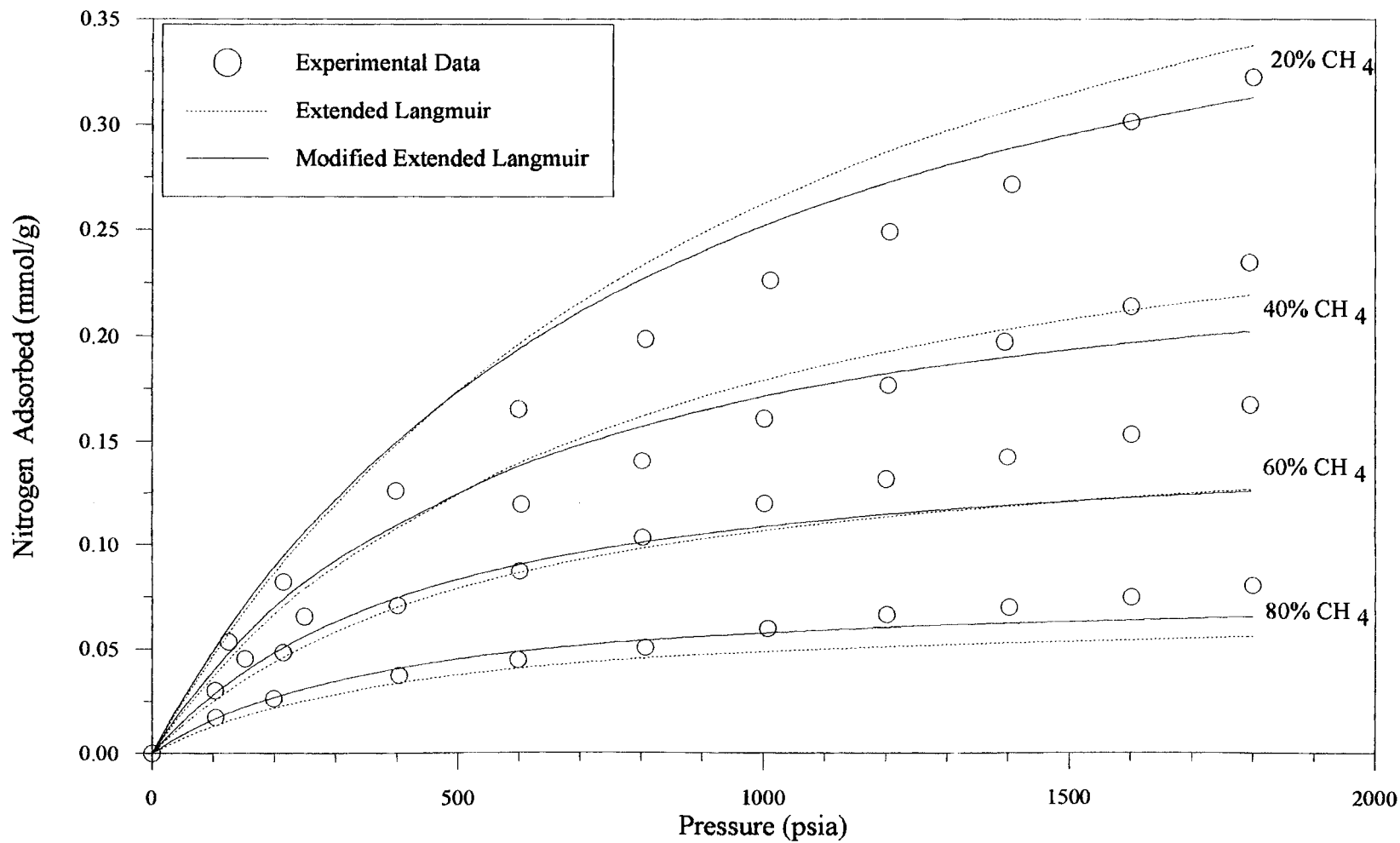
Figure 38. Prediction of the Amount of Nitrogen Adsorbed for Methane-Nitrogen Mixtures
on Wet Fruitland Coal
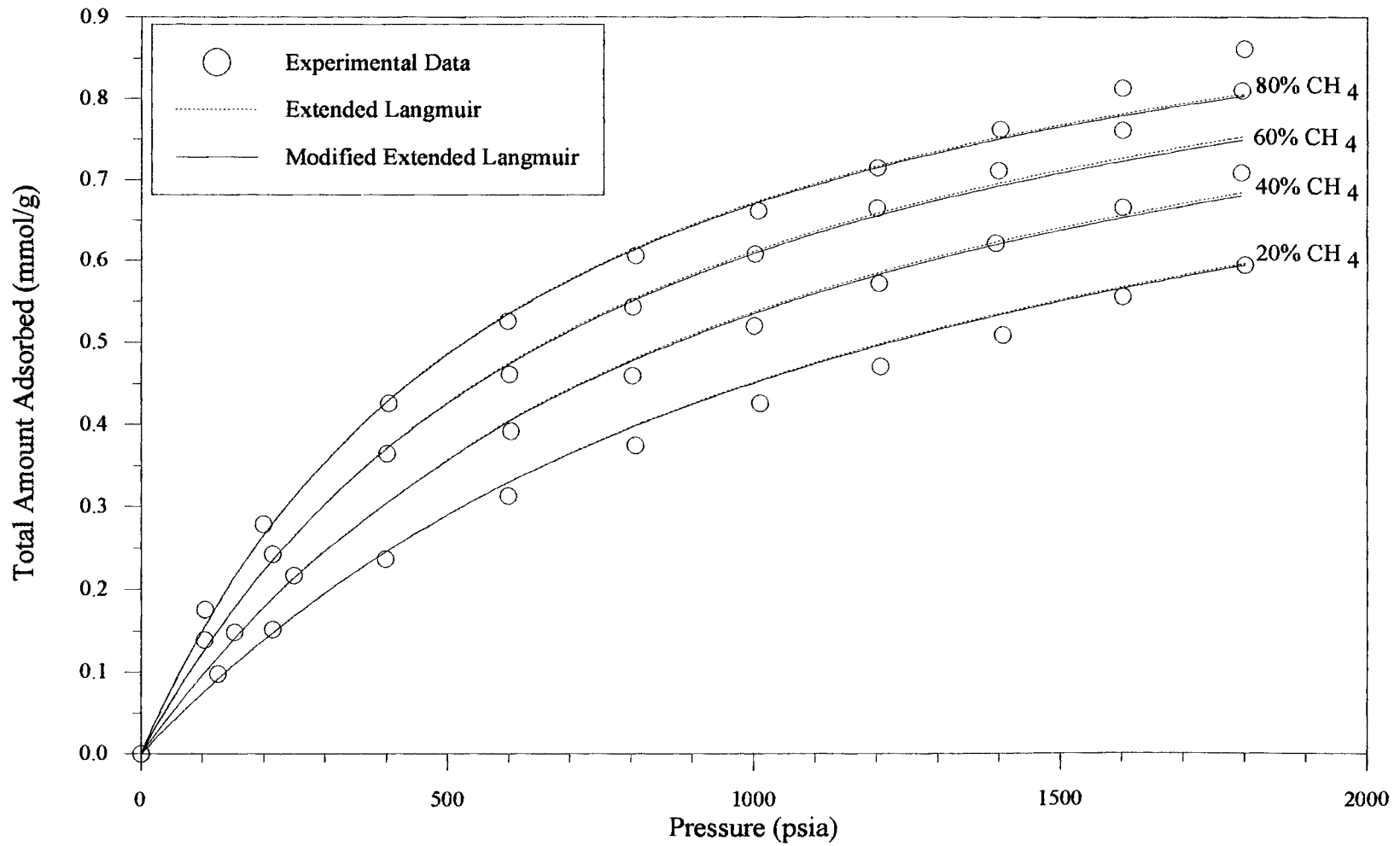
Figure 39. Prediction of the Total Amount Adsorbed for Methane-Nitrogen Mixtures
on Wet Fruitland Coal
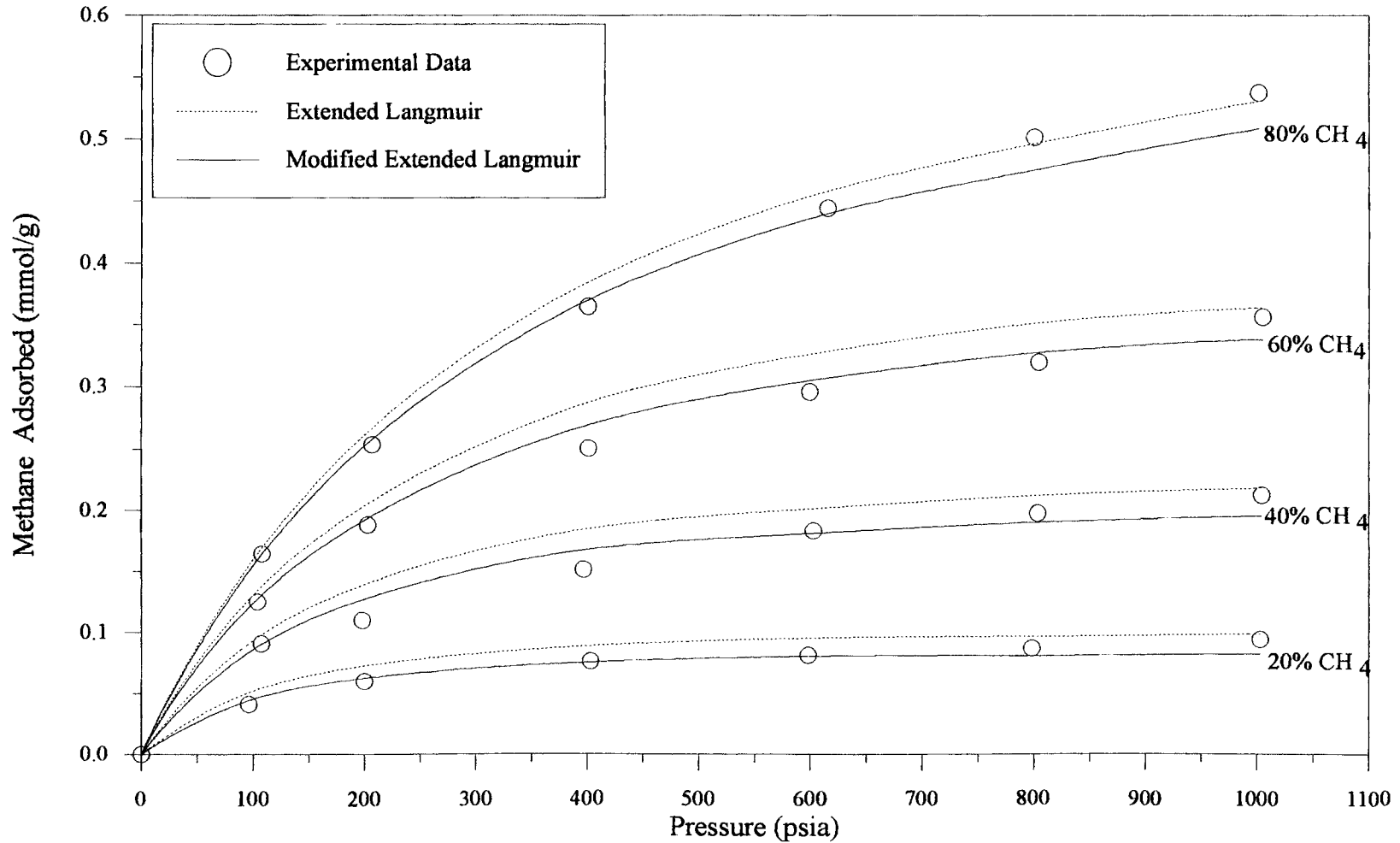
Figure 40. Prediction of the Amount of Methane Adsorbed for Methane-Carbon Dioxide Mixtures on Wet Fruitland Coal
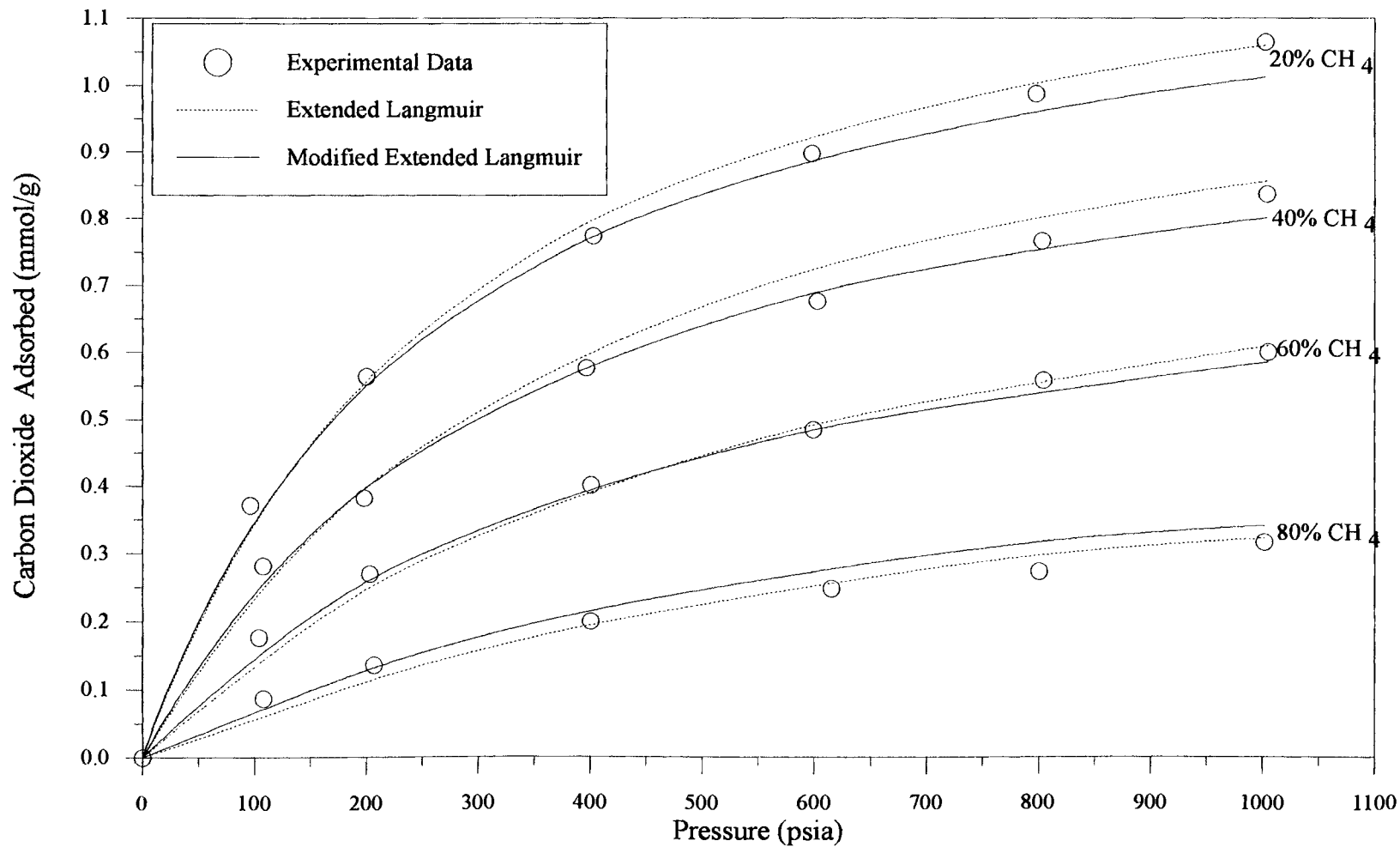
Figure 41. Prediction of the Amount of Carbon Dioxide Adsorbed for Methane-Carbon Dioxide Mixtures on Wet Fruitland Coal
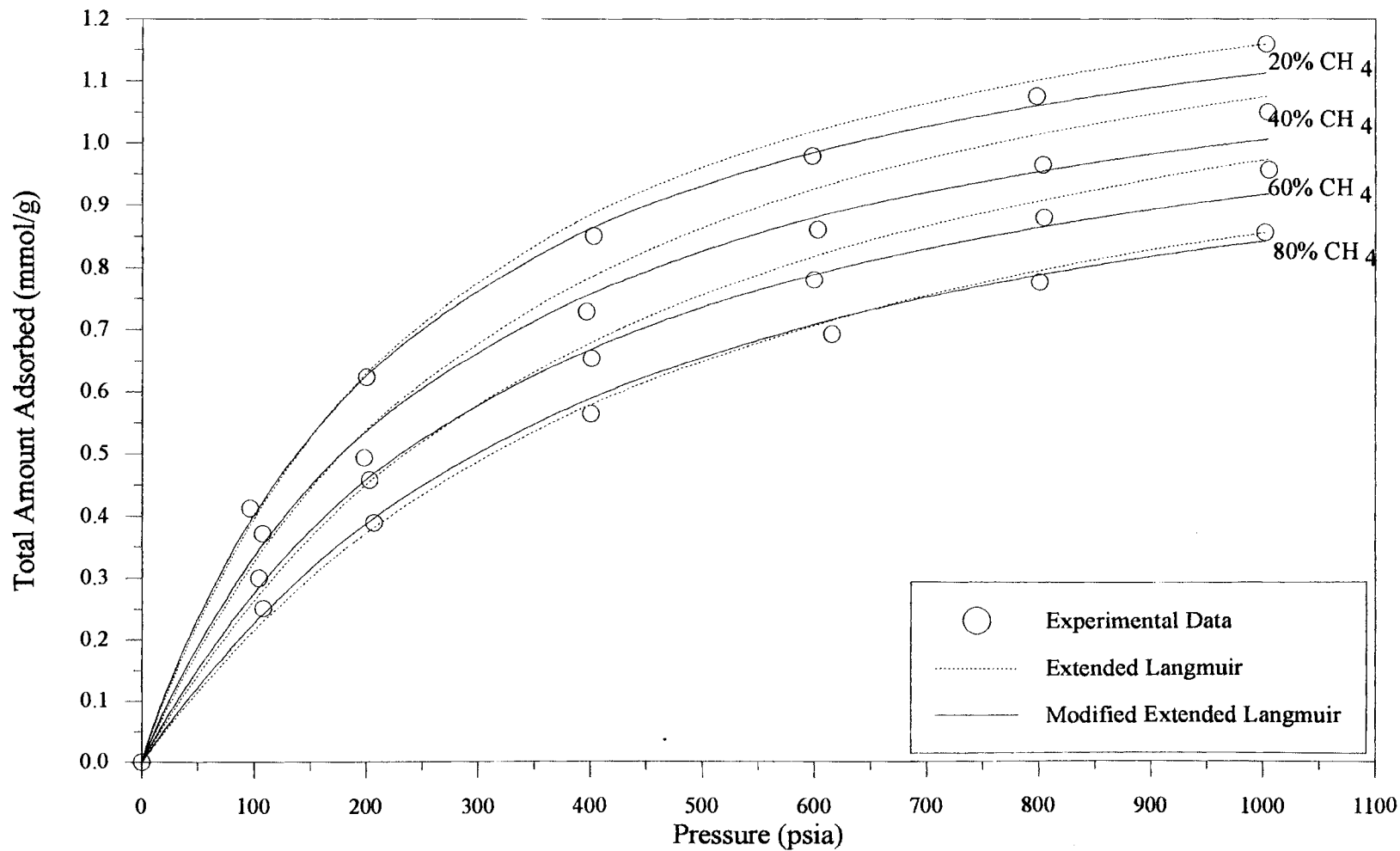
Figure 42. Prediction of the Total Amount Adsorbed for Methane-Carbon Dioxide Mixtures
on Wet Fruitland Coal
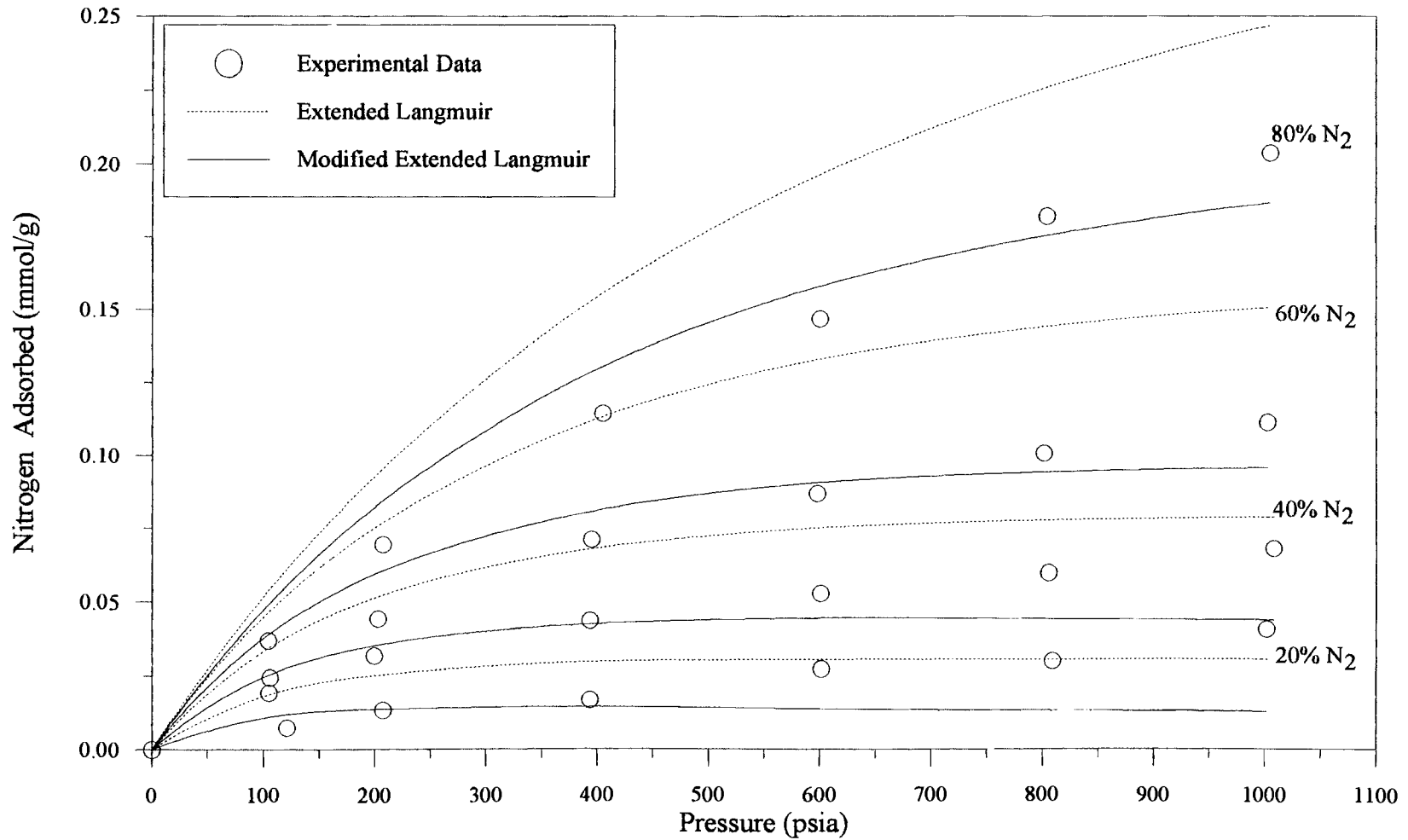
Figure 43. Prediction of the Amount of Nitrogen Adsorbed for Nitrogen-Carbon Dioxide Mixtures on Wet Fruitland Coal
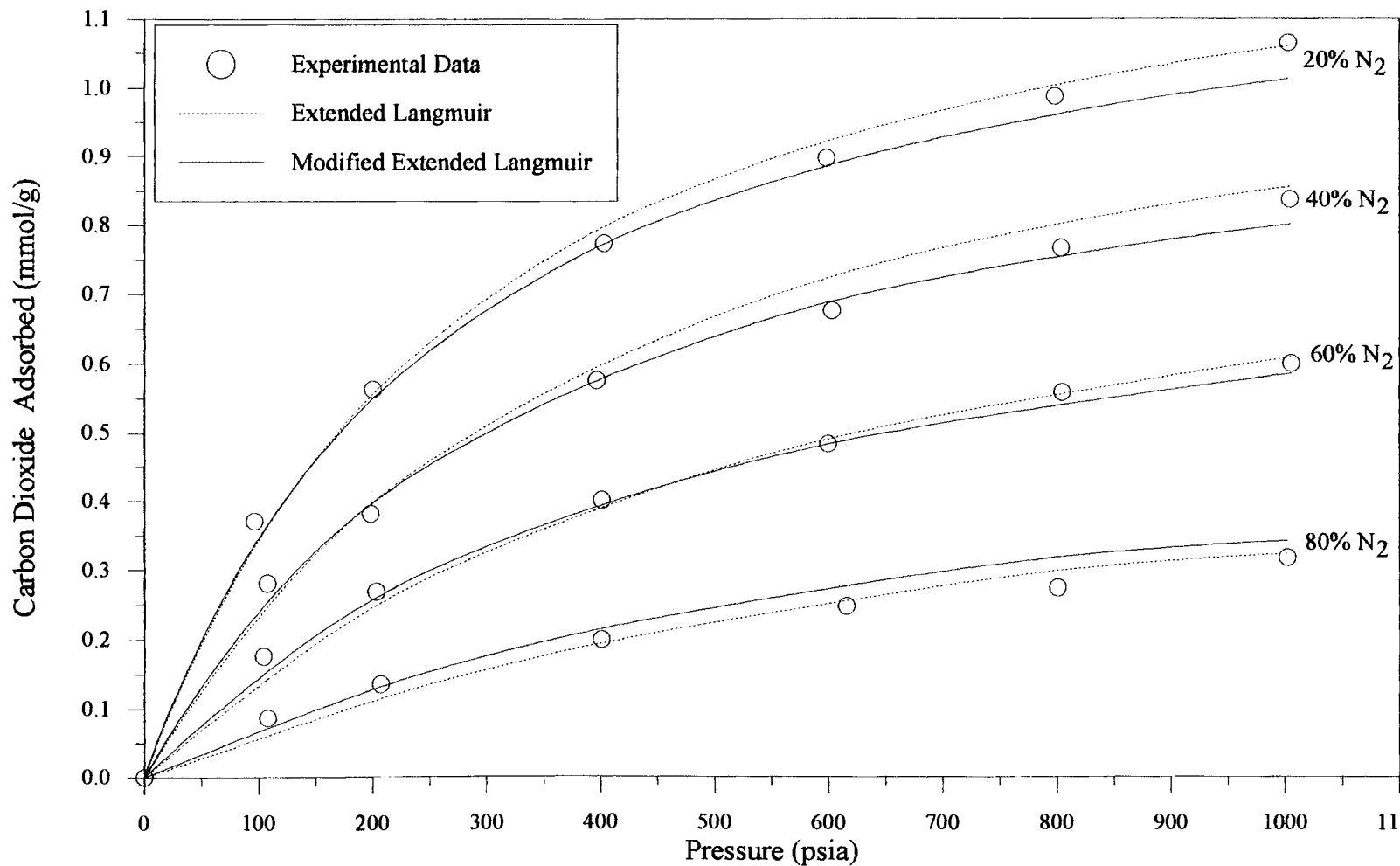
Figure 44. Prediction of the Amount of Carbon Dioxide Adsorbed for Nitrogen-Carbon Dioxide Mixtures on Wet Fruitland Coal
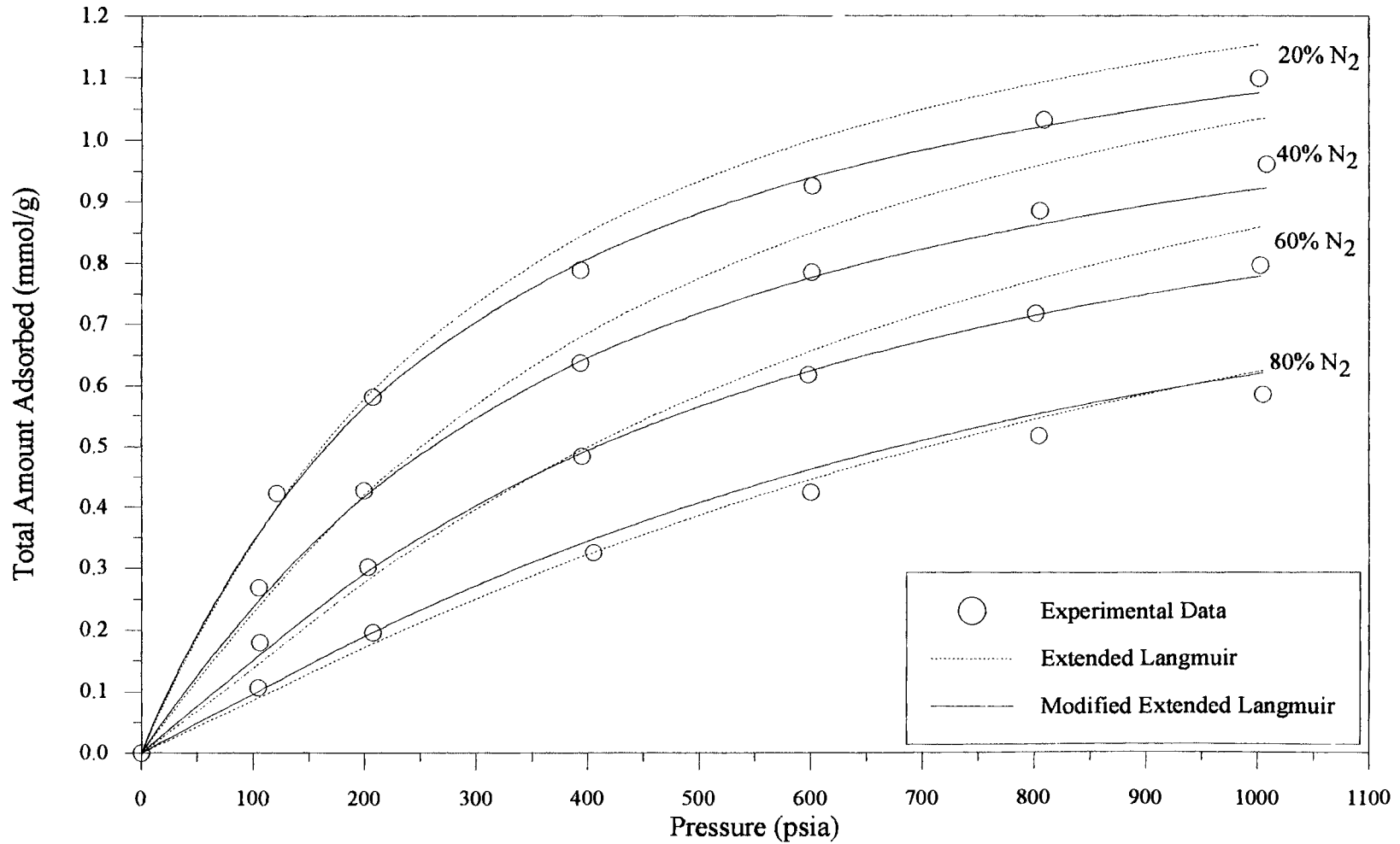
Figure 45. Prediction of the Total Amount Adsorbed for Nitrogen-Carbon Dioxide Mixtures on Wet Fruitland Coal

yields predictions for the amount of methane adsorbed with a %AAD of 4.9. In comparison, the quality of predictions for nitrogen (on a relative basis) is less favorable, as indicated by an average deviation of 13.8%. No significant changes were observed for the individual component adsorption amounts. For Case II, there is not much improvement in the average percentage deviation for the total amount adsorbed. The minor improvement in the fits is signified by near-zero values obtained for the cross coefficient B_{12} and M_{12}.

For the methane-carbon dioxide mixtures, the evaluations were restricted to the low pressure region (pressures to 1010 psia) due to the nature of the multilayer adsorption of carbon dioxide at high pressures [3]. The predictions are illustrated in Figures 40 to 42 to a pressure of 1010 psia only. Similar to the methane-nitrogen mixtures, the least adsorbed gas, in this case methane, has higher deviations than carbon dioxide. Using the modified model and regressing the cross coefficients has reduced the observed deviations by 50% for the amount of methane adsorbed. However, no similar improvements are realized for the total amount adsorbed or in the amount of carbon dioxide adsorbed.

For the nitrogen-carbon dioxide mixtures, similar to the methane-carbon dioxide mixtures, the evaluations are also restricted to pressures of 1010 psia. The predictions are illustrated in Figures 43 to 45. The large deviations for nitrogen are due to the low adsorption capacity of nitrogen when compared to carbon dioxide. From Case II, the deviations are reduced by half for nitrogen, the least adsorbed gas. Significant reduction in deviations are observed for the total amount of gas adsorbed and the amount of carbon dioxide adsorbed. Moreover, in Case II, the AAD for the least adsorbed gas is reduced by half for the carbon dioxide mixtures.

The total amount of gas adsorbed for the three binary systems can be reasonably predicted using the two correlations mentioned above. The two models studied tend to give large relative deviations in the less adsorbed components, although the modified model reduces the deviations by half when compared to the extended Langmuir model. All predictions are applicable for mono-layer adsorption, worse predictions can be

expected at high pressures, as would be the case for carbon dioxide mixtures at 1010-1800 psia.

CHAPTER VI

CONCLUSIONS AND RECOMMENDATIONS

Adsorption measurements for methane-nitrogen, methane-carbon dioxide and nitrogen-carbon dioxide have been carried out in a joint effort with Hall [3]. In the present study, the experimental data have been presented in a more convenient format. The extended Langmuir model was employed to correlate the present data. In addition, new mixing rules were incorporated in the model to lend it greater flexibility. Following are the specific conclusions and recommendations which can be made based on this work.

Conclusions

1) For all the binary mixtures considered, the composition of the adsorbate phase is significantly different from that of the equilibrium gas phase.

2) The type of adsorption observed for carbon dioxide mixtures is similar to that of the pure component, with mono-layer adsorption occurring at lower pressures and multilayer adsorption occurring at higher pressures.

3) The non-ideal behavior exhibited in the adsorbate mole fraction as a function of gas phase mole fraction indicates that different gas species are competing for the same adsorption sites.

4) The absolute adsorption values differ considerably depending on the model used for calculating the adsorbed phase molar volume, with van der Waals covolume model giving larger values of the amount adsorbed.

5)   For the binary mixtures considered, the adsorbate composition of any component is almost constant for a given feed gas mole fraction at different pressures.

6)   Pure adsorption data are well represented by a simple Langmuir isotherm. The deviations are under three percent for the components considered.

7)   The extended Langmuir model yields the largest relative errors in the least adsorbed gas. For the carbon dioxide mixtures, the modified model reduces the deviations by 50% in the amount of gas adsorbed the least. Overall, the new model is slightly better than the extended Langmuir model for all the mixtures under study.

Recommendations

1)   The displacement pump dead volume should be reduced to minimize the associated experimental errors.

2)   The adsorption measurements are conducted at only one isotherm, and scarce information is available in the literature to compare the results at the conditions of interest. Thus, study of the adsorption phenomenon at different temperatures is recommended since coal reservoirs are found at different depths.

3)   Generalized models which can represent the compressibility factor data more accurately should be used to calculate the adsorbed amounts.

4)   New correlation techniques should be developed to predict the mixture adsorption data at high pressures.

LITERATURE CITED

1. Rightmire, C. T., G. E. Eddy, and J. N. Kerr, "Coalbed Methane Resources of the United States," American Association of Petroleum Geologists, Tulsa, Oklahoma, (1984).

2. Arri, L. E., D. Yee, W. D. Morgan, and M. W. Jeansome, Modeling Coalbed Methane production with Binary Gas Sorption, SPE Report, 243-263, (1992).

3. Hall, F. E., Adsorption of Pure and Multicomponent Gases on Wet Fruitland Coal, Masters Thesis, Oklahoma State University, (1993).

4. DeGance, A. E., Multicomponent High Pressure Adsorption Equilibria on Carbon Substrates, Amoco Production Company, Report 90319ART0008, November 1990.

5. Zhou, C., "Modeling and Prediction of Pure and Multicomponent Gas Adsorption," Ph.D. Dissertation, Oklahoma State University, (1994).

6. Yang, R. T., "Gas Separation by Adsorption Processes," Butterworths, Boston (1987).

7. Langmuir, I., J., "The Adsorption of Gases on Plane Surfaces of Glass, Mica and Platinum," J. Amer. Chem. Soc., Vol. 40, 1361, (1918).

8. Van Ness, H. C., Adsorption of Gases on Solids, Ind. Eng. Chem. Fund., Vol. 8, No. 3, 464-473, August 1969.

9. Hill, T. L., "Thermodynamic Transition from Adsorption to Solution," J. Chem. Phys., 14, 507, (1949).

10. Sandler, S. I., "Chemical and Engineering Thermodynamics," John Wiley and Sons, New York (1989).

11. Stevenson, M. D., W. V. Pinczewski, M. L. Somers, and S. E. Bagio, Adsorption/Desorption of Multicomponent Gas Mixtures at In-Seam Conditions, SPE Report 23026, (1991).

12. Young, D. M., and A. D., Crowell, "Physical Adsorption of Gases," Butterworths, Washington D. C. (1962).

13. Ricardo R., Waldemar T. Z. and Kenneth A. R., "Adsorption of Methane, Ethane, and Ethylene Gases and Their Binary and Ternary Mixtures and Carbon Dioxide on Activated Carbon at 212-301K and Pressures to 35 Atmospheres," Ind. Eng. Chem. Process Des. Dev., 19, 336-344, (1980).

14. Robinson, R. L. Jr., , Gasem K. A. M., Darwish N. A. and Freddie Hall, Jr., "Adsorption Studies for Optimum Production of Coalbed Methane," Progress Report to Amoco Production Company, (1992).

15. Hall, F. E., "Supplementary Material To: Adsorption of Pure and Multi-Component Gases on Wet Fruitland Coal," School of Chemical Engineering, Oklahoma State University, Stillwater, Oklahoma (1993).

16. Angus, S., K. M. de Reuck, and B. Armstrong, "International Thermodynamic Tables of the Fluid State-6 Nitrogen," International Union of Pure and Applied Chemistry, Pergamon Press, New York (1977).

17. Goodwin, R. D., "The Thermophysical Properties of Methane, from 90 to 500K at Pressures to 700 Bar," National Bureau of Standards Technical Note 653, Department of Commerce (1974).

18. Haney, R. D., and H. Bliss, Compressibilities of Nitrogen-Carbon Dioxide Mixtures, Ind. Eng. Chem. Fund., Vol. 36, No. 11, 989-993, November 1944.

19. Holste, J. C., "Properties of CO_2 Mixtures with N_2 and with CH_4," Gas Processors Association and Gas Research Institute, Research Report RR-122, Tulsa, Oklahoma (1989).

20. Keyes, F. G., and H. G. Burks, The Equation of State for Binary Mixtures of Methane and Nitrogen, Ind. Eng. Chem., Vol. 50, 1100-1106, April 1928.

21. Reamer, H. H., R. H. Olds, B. H. Sage, and W. N. Lacey, Phase Equilibria in Hydrocarbon Systems, Ind. Eng. Chem., Vol. 36, No. 2, January 1944.

22. Dymond, J. H., and E. B. Smith, "The Virial Coefficients of Pure Gases and Mixtures," Clarendon Press, Oxford (1980).

23. McCarty, R. D., "Thermophysical Properties of Helium-4 from 2 to 1500K with Pressures to 1000 Atmospheres," National Bureau of Standards Technical Note 631, Department of Commerce, (1972).

24. Gasem, K. A. M., Personal Communication, Oklahoma State University, Stillwater, Oklahoma, (1992-1994).

25. Grapher for Windows, Golden Software, Inc., (1993).

26. Electrochem, OLI Systems, Inc., Morris Plains, NY, (1991).

SECTION 2 - PREDICTING COMPRESSIBILITY FACTORS USING EQUATIONS OF STATE

CHAPTER I

INTRODUCTION

Understanding the fluid phase behavior of pure fluids and mixtures requires accurate thermodynamic tools. The most convenient form of representing phase behavior of fluids for process design and optimization calculations is by analytical equations of state (EOS). Numerous EOS exist in literature. The commonly used EOS include the modified Benedict Webb Rubin (BWR) equation [1] and the cubic van der Waal type equations such as the Peng-Robinson (PR) [2] and the Soave-Redlich-Kwong (SRK) [48] equations. To bridge the gap between conventional EOS and those used for representing polymeric fluids, more theoretically based equations such as the Perturbed-Hard-Chain Theory (PHCT), the Simplified-Perturbed-Hard-Chain Theory (SPHCT) [3-7], the modified SPHCT [8] and the Park-Robinson-Gasem (PRG) EOS [9] were developed. The cubic van der Waals EOS and the substance-specific form of the BWR EOS are well studied.

In the previous section, it was asserted that gas mixture adsorption calculations are extremely sensitive to the compressibility factors [10]. Pure component data were used to determine the pure substance RK EOS model constants [1]. Binary experimental data in the selected temperature and pressure range were used to determine the optimum interaction parameters in the RK EOS [1]. The RK EOS was used to determine the

compressibility factors for the mixtures, based on regressed model constants for binary interaction parameters.

Thus, the model constants obtained from the pure component experimental compressibility factor data play a key role in determining the amount adsorbed. Also, the components used in the adsorption experiments are in the supercritical region at the temperature and pressure ranges considered. The most common approach to obtain adequate EOS predictions is to regress the EOS constants using experimental pvTx data. Although this approach serves the immediate needs, it does not delineate the inconsistencies existing in the EOS itself.

The compressibility factor is comprised of two terms -- an attractive term and a repulsive term. Using a novel approach [11], experimental data can be used directly to compute these two terms separately, obtain the compressibility factors, and explore possible inconsistencies in an EOS model.

The specific objectives of the present work were as follows :

1)   Set up an extensive pvT literature database for methane, nitrogen and carbon dioxide from the triple point to the super critical region.

2)   Check for possible inconsistencies in the PR, BWR, SPHCT, MSPHCT and PRG EOS using the database set up for this purpose.

3)   Make a comparative study of the different EOS models thus studied.

4)   Investigate the effect of tuning of the EOS parameters.

Knowledge gained from this preliminary work should help identify possible inconsistencies in defining the attractive and the repulsive terms in the EOS under study. Once the inconsistencies are identified, new correlations can be developed for the attractive and repulsive terms which will help in developing improved EOS models.

CHAPTER II

EOS EVALUATION STRATEGY

This chapter presents a brief description for the EOS evaluation strategy used in this work. The subject matter relating to EOS evaluation and development is vast. Thus, no attempt was made in this preliminary work to consider the various evaluation methods discussed in the literature.

An EOS is a mathematical relation among the observables: temperature T, pressure p, specific volume v, and composition x expressed as f(T, p, v, x) = 0 or p = f(T, v, x) in a pressure explicit form [11]. The simplest form of an EOS is that of an ideal gas, where pv = RT. An ideal gas represents the case where there are no intermolecular attractions present and the molecular volume is negligible. The non-ideality of a gas at given conditions is reflected in the compressibility factor term. By definition the compressibility factor is given as:

$$Z = \frac{P}{\rho RT} \qquad (1)$$

where $\rho = 1/v$. Ideal gas behavior is indicated when the compressibility factor has a value of one.

Compressibility factors can be determined in two ways. Knowing the experimental values of temperature, pressure and density one can compute the compressibility factor

using Equation (1). Using only the temperature and pressure data, the compressibility factors can be calculated using an EOS, such as the PR EOS [2] given below:

$$P = \frac{RT}{v-b} - \frac{a(T)}{v(v+b)+b(v-b)} \tag{2}$$

For fixed values of the EOS parameters a and b, one can compute the compressibility factors iteratively. By regressing the parameters which define a and b against experimental data, the EOS predictions can be improved significantly.

Deviations in the pvT behavior of any real gas from the ideal gas law are caused by the repulsive and attractive forces acting between molecules. Extensive work has been done to develop theoretically sound correlations for the repulsive and attractive terms. The correlations existing in the literature for the repulsive term represent the molecular forces reasonably well. Various studies (see, e.g., Park [9]), however, have indicated that the attractive term requires further development.

The compressibility factor can be written as the sum of attractive and repulsive terms as defined below:

$$Z_{cal} = 1 + f[Z_{att}(T,p,\rho) + Z_{rep}(T,p,\rho)] \tag{3}$$

Thus, an EOS can be reduced to a compressibility factor form, which is a sum of attractive and repulsive terms. For example, the PR EOS defined in Equation (2) can be written as:

$$Z = \frac{Pv}{RT} = 1 + \frac{b}{v-b} - \frac{av}{RT(v^2 + 2bv - b^2)} \tag{4}$$

where

$$Z_{rep} = \frac{b}{v-b}$$

81

and

$$Z_{att} = -\frac{av}{RT\left(v^2 + 2bv - b^2\right)}$$

Experimental density, temperature and pressure data can be used in the above equation to obtain the calculated value of the compressibility factor [11]. Since the experimental density data are used to compute the attractive and repulsive terms separately, in principle, the sum of the two terms should equal to the experimental compressibility factor within the experimental uncertainty. Thus, significant discrepancies between the calculated and the experimental values will reveal the inconsistencies existing in one or both terms.

In addition, this study explores the predictive capabilities of the various EOS under study, as they appear in the literature. Upon evaluation of the predictive capabilities of these EOS by the above method, the EOS parameters are regressed using experimental data to obtain improved predictions.

The approach used for evaluating the EOS under study is as follows:

1) Where possible, the EOS is written as a sum of Z_{att} and Z_{rep} terms, as defined in Equation (3).

2) Experimental densities are used to calculate the compressibility factors for the selected pure fluids, Z_{expt}.

3) The EOS predictions of the compressibility factors, Z_{cal}, are compared with Z_{expt}.

4) The EOS parameters are then re-optimized ("tuned") using the experimental data and compared to the original EOS performance for the complete data range.

CHAPTER III

REVIEW OF EOS MODELS

This chapter briefly reviews five EOS models selected for evaluation in this work. They are the (1) BWR, (2) PR, (3) SPHCT, (4) MSPHCT and (5) PRG model. The EOS models are presented in terms of the attractive and repulsive terms of the compressibility factor wherever possible.

Classical EOS

The PR EOS represents one of the most commonly used van der Waals type classical equations. Peng and Robinson [2] proposed an equation of the form described below by modifying the attraction pressure term of the semi-empirical van der Waals equation:

$$P = \frac{RT}{v - b} - \frac{a(T)}{v(v + b) + b(v - b)} \tag{6}$$

where v is the specific volume, R is the gas constant, a and b are the EOS parameters defined as:

$$a(T) = a(T_c)\alpha(T_r, \omega) \tag{7}$$

$$b(T) = b(T_c) \tag{8}$$

Following Soave's work, α is defined as

$$\alpha^{\frac{1}{2}} = 1 + \kappa(1 - T_r^{\frac{1}{2}}) \qquad (9)$$

$$\kappa = m_0 + m_1\omega + m_2\omega^2 \qquad (10)$$

$a(T_c)$ and $b(T_c)$ are defined at the critical point as

$$a(T_c) = \Omega_a \frac{R^2 T_c^2}{P_c} \qquad (11)$$

$$b(T_c) = \Omega_b \frac{R T_c}{P_c} \qquad (12)$$

More accurate liquid density values can be obtained with the PR EOS when compared to the SRK EOS, with the other performances being comparable [2]. The inherent simplicity and qualitative success makes it the most attractive EOS industrially. The attractive and repulsive terms for the compressibility factor are presented in Equations (4a) and (4b). The values of EOS parameters available in the literature [6] are included in Appendix A.

Virial-Based EOS

The variation of the BWR EOS used in this work is the form presented by Starling [1]. Thermodynamic property data in the liquid, gas and dense fluid regions were used simultaneously in developing this new model. To ensure consistency between predicted properties, available experimental pvT, enthalpy and vapor pressure data were used simultaneously by the authors in a multi-property analysis to determine the parameters in the EOS for individual materials. The EOS is a pressure-explicit function of temperature T, and molar density ρ. Prediction of density at a given temperature-pressure condition requires a trial and error solution. Starling [1] used thermodynamic property data in the liquid, gas and dense fluid regions to simultaneously develop this new model.

$$P = \rho RT + (B_0 RT - A_0 - \frac{C_0}{T^2} + \frac{D_0}{T^3} - \frac{E_0}{T^4})\rho^2 + (bRT - a - \frac{d}{T})\rho^3$$
$$+ \alpha(a + \frac{d}{T})\rho^6 + \frac{c\rho^3}{T^2}(1 + \gamma\rho^2)\exp(-\gamma\rho^2) \qquad (13)$$

where A_0-E_0, a-d, α and γ are the EOS parameters. As the pressure is a complex function of density, no effort has been made to present this model in terms of attractive and repulsive terms of compressibilities. The values of EOS for the individual components are included in Appendix A.

Perturbed-Hard-Chain Theory EOS

SPHCT EOS

Beret, Donohue and Prausnitz [3] developed the perturbed-hard-chain theory (PHCT) which is applicable to both liquid and gas phases for compounds ranging in structural complexity from methane to heavy hydrocarbons and polymers. The basic approach of the PHCT EOS is to define a canonical partition function of statistical thermodynamics in terms of all the energy states of the molecules and relate it to the classical thermodynamic variables. Kim [14] proposed a simplification to the PHCT equation by replacing the attractive portion of the partition function with the model of Lee, Lombardo and Sandler. The SPHCT equation results in an attractive term with a much simpler density and temperature dependence than the original PHCT equation making it more convenient for engineering calculations.

The SPHCT EOS [8] is given as:

$$Z = 1 + c(Z_{rep} + Z_{att})$$

where

$$Z_{rep} = \frac{4(\tau\tilde{\rho}) - 2(\tau\tilde{\rho})^2}{(1 - \tau\tilde{\rho})^3} \tag{14}$$

$$Z_{att} = -\frac{Z_M cv^* Y}{cv + cv^* Y} \tag{15}$$

$$Y = \exp\left(\frac{1}{2\tilde{T}}\right) - 1 \tag{16}$$

$$\tilde{\rho} = \frac{v^*}{v} \ , \quad \tilde{T} = \frac{T}{T^*} \tag{17}$$

where T^* and v^* are the characteristic temperature and volume respectively, c is the degrees of freedom parameter and Z_M is the maximum coordination number equal to 36. The values of EOS parameters are included in Appendix A.

MSPHCT EOS

Systemic errors have been observed for the vapor pressure and liquid density predictions using the SPHCT for pure fluids near both the triple point and the critical temperatures. Such errors have been attributed to poor characterization of the EOS parameters and tend to make optimization of the EOS parameters more difficult. To address some of these drawbacks, Shaver [8] introduced critical point constraints and modified the attractive term to improve the parameterization of the SPHCT EOS. The MSPHCT equation is given as:

$$Z_{att} = -\frac{Z_M cv^* Y}{cv + cv^* Y} \tag{18}$$

$$Y = \exp(F_t) - 1 \tag{19}$$

$$F_t = \sum_{i=1}^{4} b_i \left(\frac{1}{2\tilde{T}} \right)^{\frac{i}{2}} \tag{20}$$

where b_i are the coefficients of the modifying function F_t. The values of the EOS parameters are included in Appendix A.

PRG EOS

PRG EOS [9] was developed on the same lines as the SPHCT and other similar models. Park and co-workers adopted the attractive term from the generalized cubic and appended a correction term to it. The repulsive term was adopted from the correlation developed by Elliot and co-workers [47]. PRG equation is defined as:

$$Z = 1 + c \left(\frac{a\tau}{v_r - b\tau} - \frac{\alpha Y v_r}{v_r^2 + u v_r + w} - \frac{Q\alpha Y}{v_r + 1} \right) \tag{21}$$

where $\quad \alpha = \alpha_o h(T)$

$$h(T) = 1 + \kappa_1 \tilde{T}^{1/2} + \kappa_2 \tilde{T} + \kappa_3 \tilde{T}^2 + \kappa_4 \tilde{T}^{-1} \tag{22}$$

$$Y = \exp\left(\frac{1}{\tilde{T}} \right) - 1 \tag{23}$$

where $v_r = v/v^*$ and $\tilde{T} = \dfrac{T}{T^*}$ and

$$Z_{rep} = \frac{a\tau}{v_r - b\tau} \tag{24}$$

$$Z_{att} = -\frac{\alpha Y v_r}{v_r^2 + u v_r + w} - \frac{Q\alpha Y}{v_r + 1} \tag{25}$$

The values of EOS parameters are included in Appendix A.

CHAPTER IV

EXPERIMENTAL pvT DATA FOR THE SINGLE PHASE REGION

The present chapter gives a brief description of the database used in the present evaluations. The motivation for selecting the gases under study is also described.

The components chosen for this work are methane, nitrogen and carbon dioxide. These components were chosen because (a) these gases are widely used in the industry, and (b) they provide the necessary information for the experimental adsorption measurements undertaken at OSU. The temperature and pressure ranges considered in this study extend from the triple point to the supercritical region.

Experimental data for pures has been identified in the range of 0-500 bar and 0-500 K. Sources for the available experimental data, along with temperature, pressures and density ranges, are presented in Tables I - III. Figures 1-6 map the compressibility factor data used in this evaluation in terms of temperature and pressure. The critical properties and the other physical property data needed for each component are tabulated in Appendix B.

Table I. Summary of Available Experimental p-ρ-T Data for Methane

Source	Year	Number of Data Points	Pressure Range (bars)	Temperature Range (K)
Keys & Burks [24]	1927	80	32-257	273-473
Kvalnes&Gaddy [25]	1931	182	0-1000	203-473
Michels et al. [26]	1936	175	20-390	273-423
Reamer et al. [27]	1943	294	13-482	294-510
Van Itterbeek et al. [28]	1963	162	9-312	114-188
Douslin et al. [29]	1964	317	16-405	273-623
Kobayashi et al. [30]	1970	262	15-690	150-273
Da Ponte et al. [31]	1978	86	14-1280	110-120

Table II. Summary of Available Experimental p-ρ-T Data for Nitrogen

Source	Year	Number of Data Points	Pressure Range (bars)	Temperature Range (K)
Michels et al. [15]	1934	56	20-80	273-423
Michels et al. [16]	1936	147	200-3000	273-423
Benedict [17]	1937	25	100-1560	90-273
Van Itterbeek & Verbeke [18]	1960	67	13-140	66-91
Kobayashi et al. [19]	1962	152	2-540	133-273
Street & Staveley [20]	1967	107	4-680	77-120
Weber [21]	1970	76	140-2660	80-140
Da Ponte et al. [22]	1978	27	0.5-1	110-120
Straty & Diller [23]	1980	280	0-350	84-300

Table III. Summary of Available Experimental p-ρ-T Data for Carbon Dioxide

Source	Year	Number of Data Points	Pressure Range (bars)	Temperature Range (K)
Michels et al. [32]	1935	239	16-3039	273-423
Kennedy [33]	1954	2222	25-1400	273-1473
Vukalovich et al. [34]	1968	168	7-300	273-308
Golovskii et al. [35]	1969	128	9-600	220-306
Kirillin et al. [36]	1969	21	20-580	433-473
Kirillin et al. [37]	1969	39	16-500	283-308
Kirillin et.al [38]	1970	24	20-500	223-273
Vukalovich et al. [39]	1970	95	7-190	238-273
Popov et al. [40]	1970	117	7-300	283-303
Holste et al. [41]	1987	236	3-477	220-450
Ely et al. [42]	1988	10	58-270	250-330

Figure 1. Experimental Compressibility Factor Data Available for Methane

Figure 2. Experimental Compressibility Factor Data Used in Evaluations for Methane
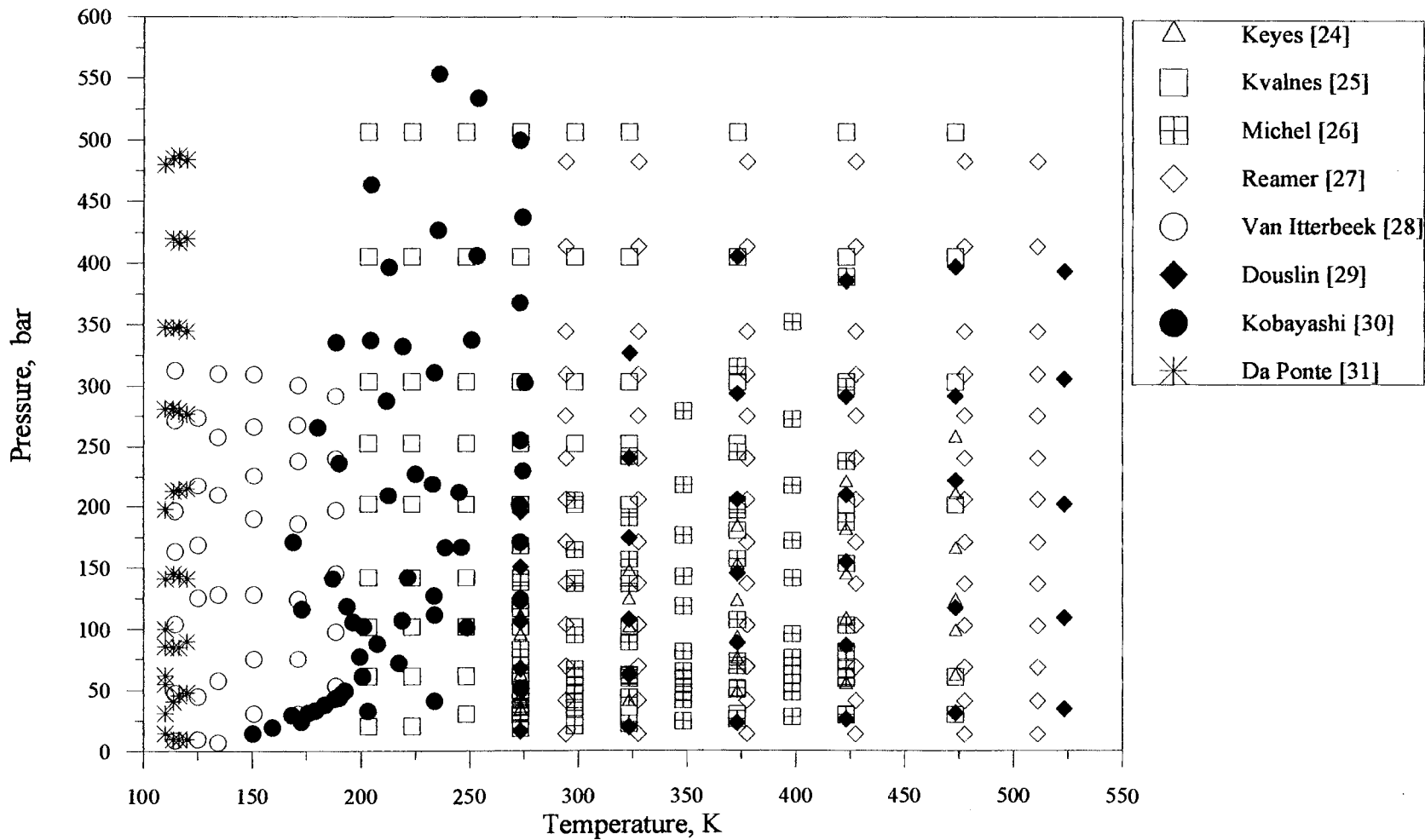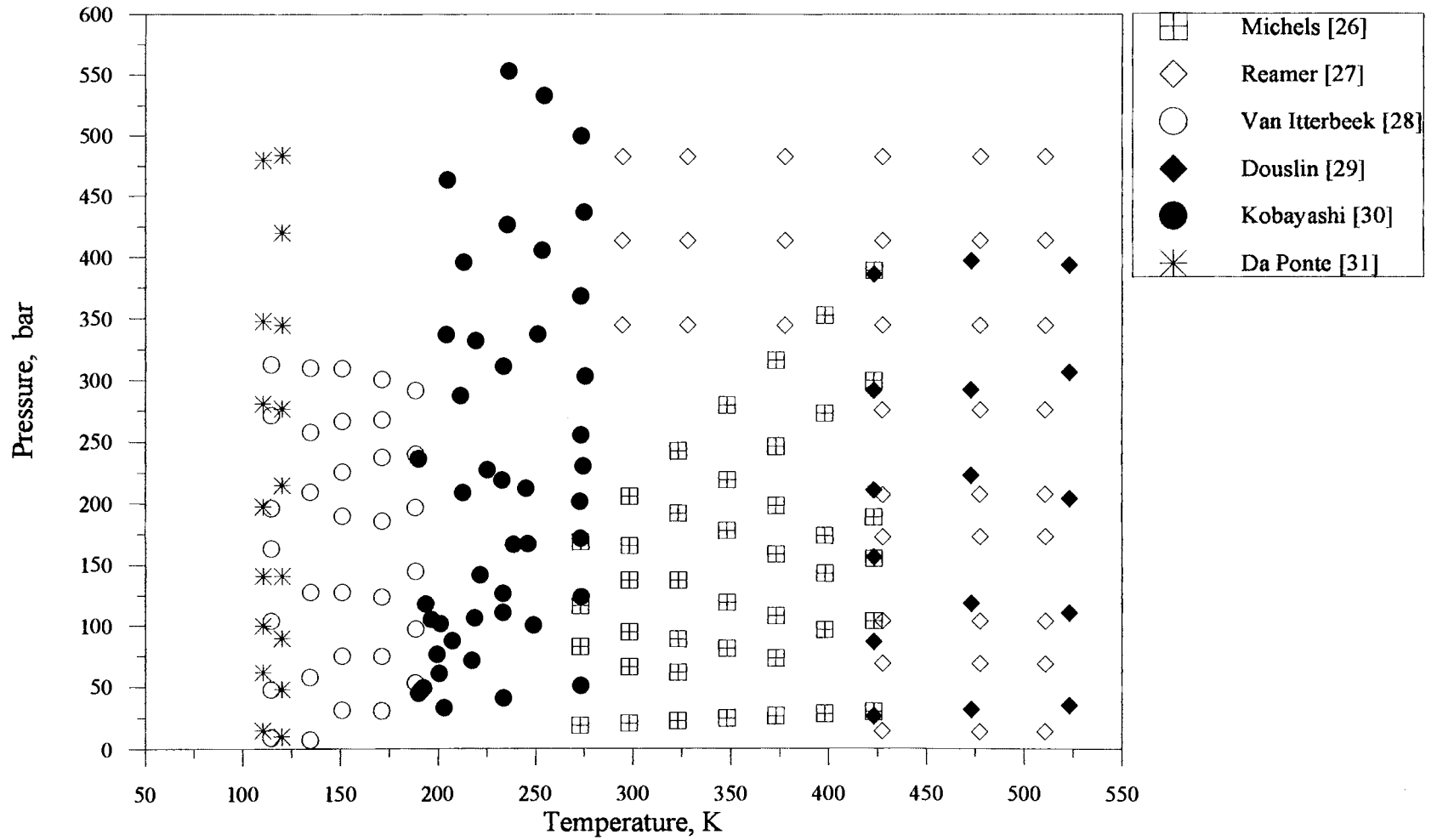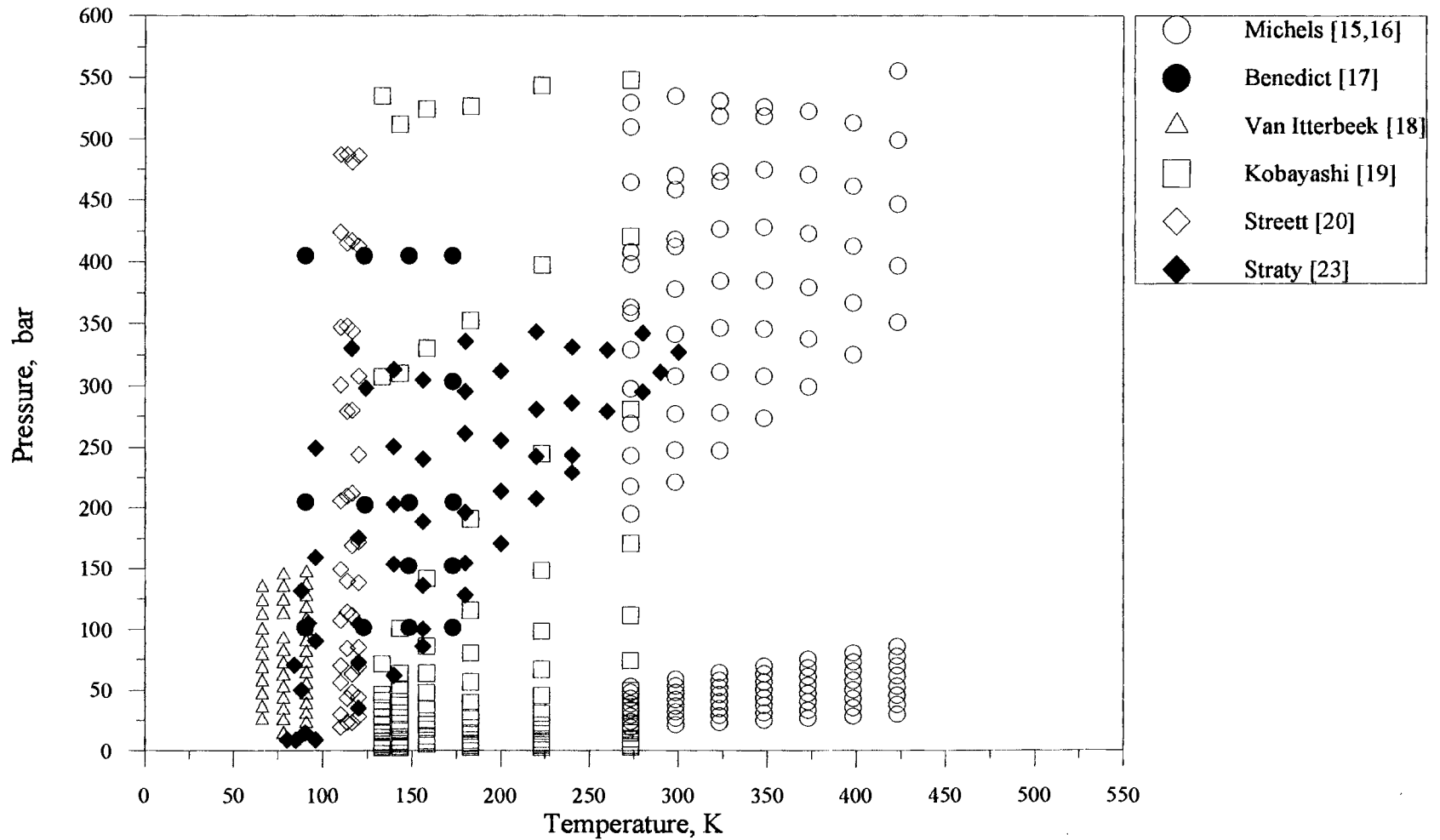
Figure 3. Experimental Compressibility Factor Data Available for Nitrogen
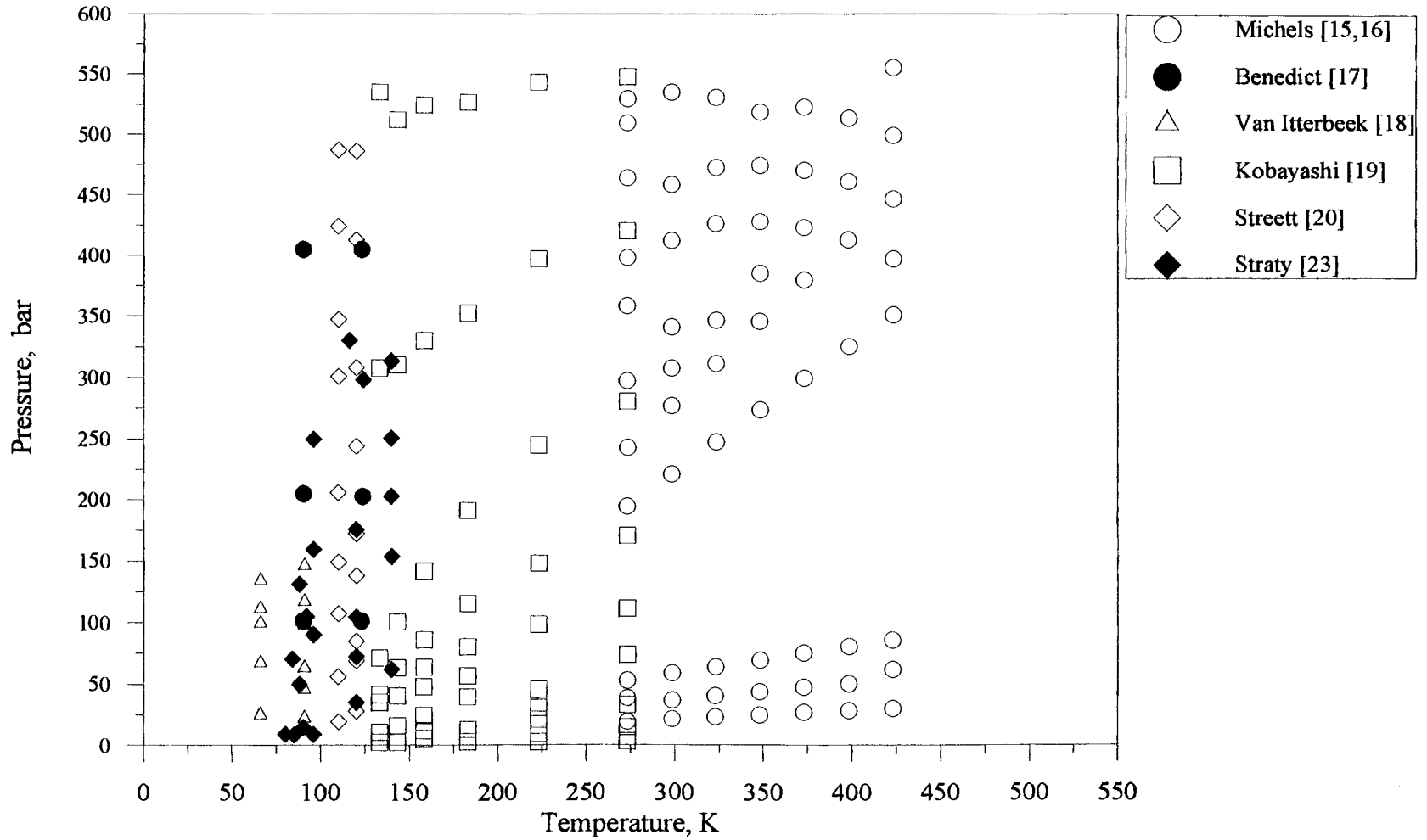
Figure 4. Experimental Compressibility Factor Data Used in Evaluations for Nitrogen
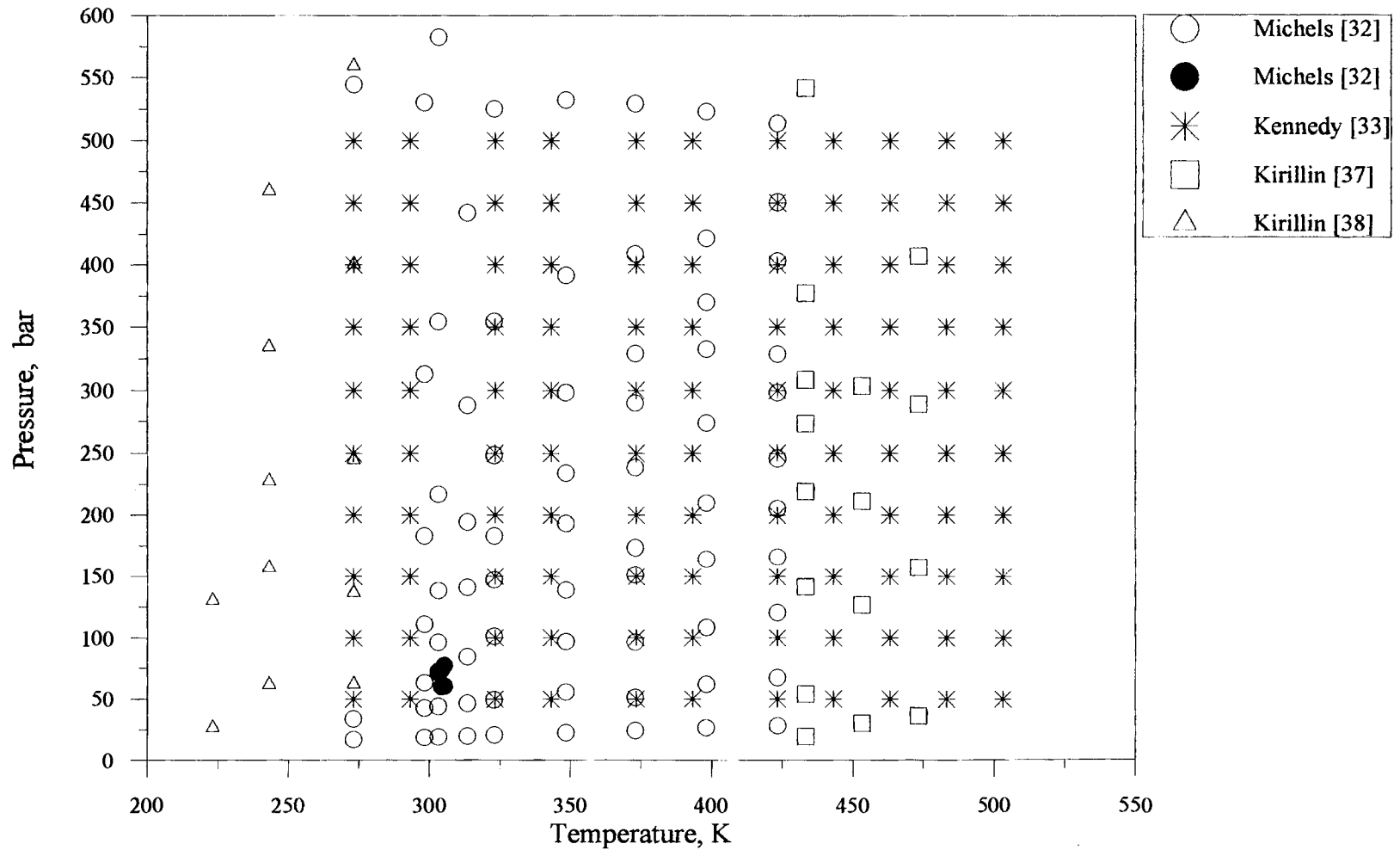
Figure 5. Experimental Compressibility Factor Data Available for Carbon Dioxide
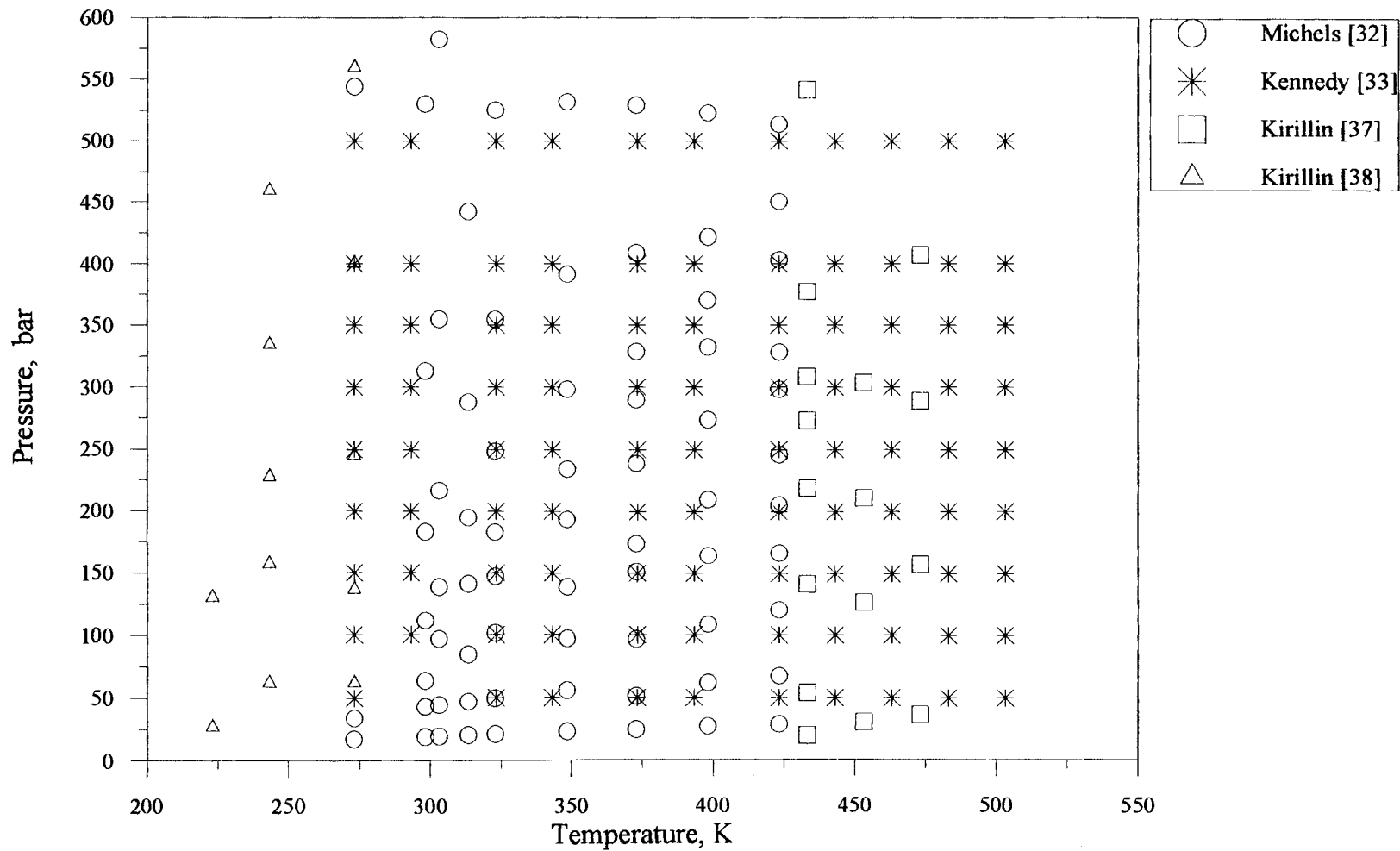
Figure 6. Experimental Compressibility Factor Data Used in Evaluations for Carbon Dioxide

CHAPTER V

RESULTS AND DISCUSSION

Extensive experimental data were used to evaluate the various EOS for the gases

under study. The predictive capabilities of the EOS were evaluated and compared. In

addition, an optimization routine was used to regress the EOS model parameters and to

explore the effect of parameter tuning on the quality of the predictions.

Five EOS models (PR, BWR, SPHCT, MSPHCT and PRG) have been evaluated

in this work. The absolute average percentage deviation (%AAD) in the compressibility

factors are used to assess the EOS predictions and in the model comparisons. FORTRAN

codes for the different models were introduced into the PFP.FOR (Pure Fluid Properties

Program) provided by Gasem [12]. The routine used for linking and compiling various

subroutines is presented in Appendix C.

Results for pure methane, nitrogen and carbon dioxide are summarized in Tables

IV-VI. Table IV indicates that the BWR EOS predictions are better than the other

models. This is expected since the BWR EOS parameters are specific for the component

being considered. The results obtained for methane using the BWR equation are 3/4 of

the %AAD of the other two gases being considered. The results for methane by PRG

model seem abnormal, i.e., a %AAD of 226. Smoothed methane data from NBS was used

to check the predictions and the results obtained (AAD of 195%) indicate that a few data

points near the triple point caused the observed large deviations. When the classical van

der Waals type PR equation is considered, it is seen that the predictions are better for

carbon dioxide than for the other gases. This can be explained by the fact that some data points for methane and nitrogen in the triple point region result in higher %AAD. The PHCT EOS give better predictions for carbon dioxide than methane. The EOS parameters (T^*, v^*, and c) for the SPHCT, MSPHCT and PRG models are not available for nitrogen, therefore predicted values are not included in the table. When the results for these equations for carbon dioxide are compared, it is clear that the MSPHCT model gives worse results than the SPHCT model and the results from PRG model are similar to those of the SPHCT and PR equations.

Table V shows the results obtained on optimizing the EOS parameters for the PR, BWR and SPHCT equations. To regress the EOS parameters, the following objective function was employed to minimize the relative error in the compressibility factors:

$$SS = \sum_{i=}^{n} \left(\frac{Z_{calc} - Z_{exp}}{Z_{exp}} \right)_i^2 \tag{26}$$

For the PR equation, the model parameters m_0, m_1, m_2 were optimized. The results obtained indicate a noticeable improvement in the methane and nitrogen predictions (50% reduction in %AAD). Similarly, when the EOS parameters for the SPHCT equation, T^*, v^* and c were optimized, the deviations for all the pure fluids are reduced by half (47.6% to 22.2% AAD). However, for carbon dioxide, no significant improvement is realized. By comparison, the best results (1% AAD) are obtained from the BWR model on optimizing all the constants.

Table VI presents the results obtained for the MSPHCT and PRG model. Initially, only the characteristic temperature T^*, characteristic volume v^* and the degrees of freedom parameter c were optimized. There was significant improvement in the compressibility factor deviations. On further optimization of all the EOS parameters and

TABLE IV. Summary of Results for EOS Predictions for
Compressibility Factor Data

EOS	No. of Parameters	RMSE	%AAD
Methane			
PR	5	0.57	83.2
BWR	11	0.05	6.1
SPHCT	3	0.38	47.6
MSPHCT	7	0.27	33.5
PRG	14	2.34	226.5*
Nitrogen			
PR	5	0.53	72.6
BWR	11	0.10	10.8
Carbon Dioxide			
PR	5	0.10	11.2
BWR	11	0.14	14.8
SPHCT	3	0.10	15.3
MSPHCT	7	0.23	37.4
PRG	14	0.13	16.0

* A discrepancy has been identified in the PRG EOS constants; however, at the time, the evaluation was completed.

TABLE V. Summary of Results for Regressed-Parameter EOS Predictions for Compressibility Factor Data

EOS	No. of Parameters	RMSE	%AAD
Methane			
PR	5	0.32	30.0
BWR	11	0.02	1.1
SPHCT	3	0.21	22.2
Nitrogen			
PR	5	0.37	30.5
BWR	11	0.02	2.4
SPHCT	3	0.17	17.9
Carbon Dioxide			
PR	5	0.09	9.3
BWR	11	0.01	0.8
SPHCT	3	0.05	7.1

TABLE VI. Results Obtained on Optimization of EOS Parameters for
Compressibility Factor Data

EOS	No. of Parameters	RMSE	%AAD
Methane			
MSPHCT*	3	0.19	18.5
MSPHCT**	7	0.10	7.5
PRG!	3	0.16	14.8
PRG!!	14	0.02	1.5
Nitrogen			
MSPHCT*	3	0.15	14.1
MSPHCT**	7	0.06	5.1
PRG!	3	1.59	84.8
PRG!!	14	0.10	8.6
Carbon Dioxide			
MSPHCT*	3	0.04	4.9
MSPHCT**	7	0.02	2.4
PRG!	3	0.03	4.6
PRG!!	14	0.01	1.1

* Only EOS parameters T^*, v^*, and c were optimized
** All EOS parameters and EOS constants were optimized
! Only EOS parameters T^*, v^*, and c were optimized
!! All EOS parameters and EOS constants were optimized

TABLE VI. Results Obtained on Optimization of EOS Parameters for
Compressibility Factor Data

EOS	No. of Parameters	RMSE	%AAD
Methane			
MSPHCT*	3	0.19	18.5
MSPHCT**	7	0.10	7.5
PRG!	3	0.16	14.8
PRG!!	14	0.02	1.5
Nitrogen			
MSPHCT*	3	0.15	14.1
MSPHCT**	7	0.06	5.1
PRG!	3	1.59	84.8
PRG!!	14	0.10	8.6
Carbon Dioxide			
MSPHCT*	3	0.04	4.9
MSPHCT**	7	0.02	2.4
PRG!	3	0.03	4.6
PRG!!	14	0.01	1.1

* Only EOS parameters T^*, v^*, and c were optimized
** All EOS parameters and EOS constants were optimized
! Only EOS parameters T^*, v^*, and c were optimized
!! All EOS parameters and EOS constants were optimized

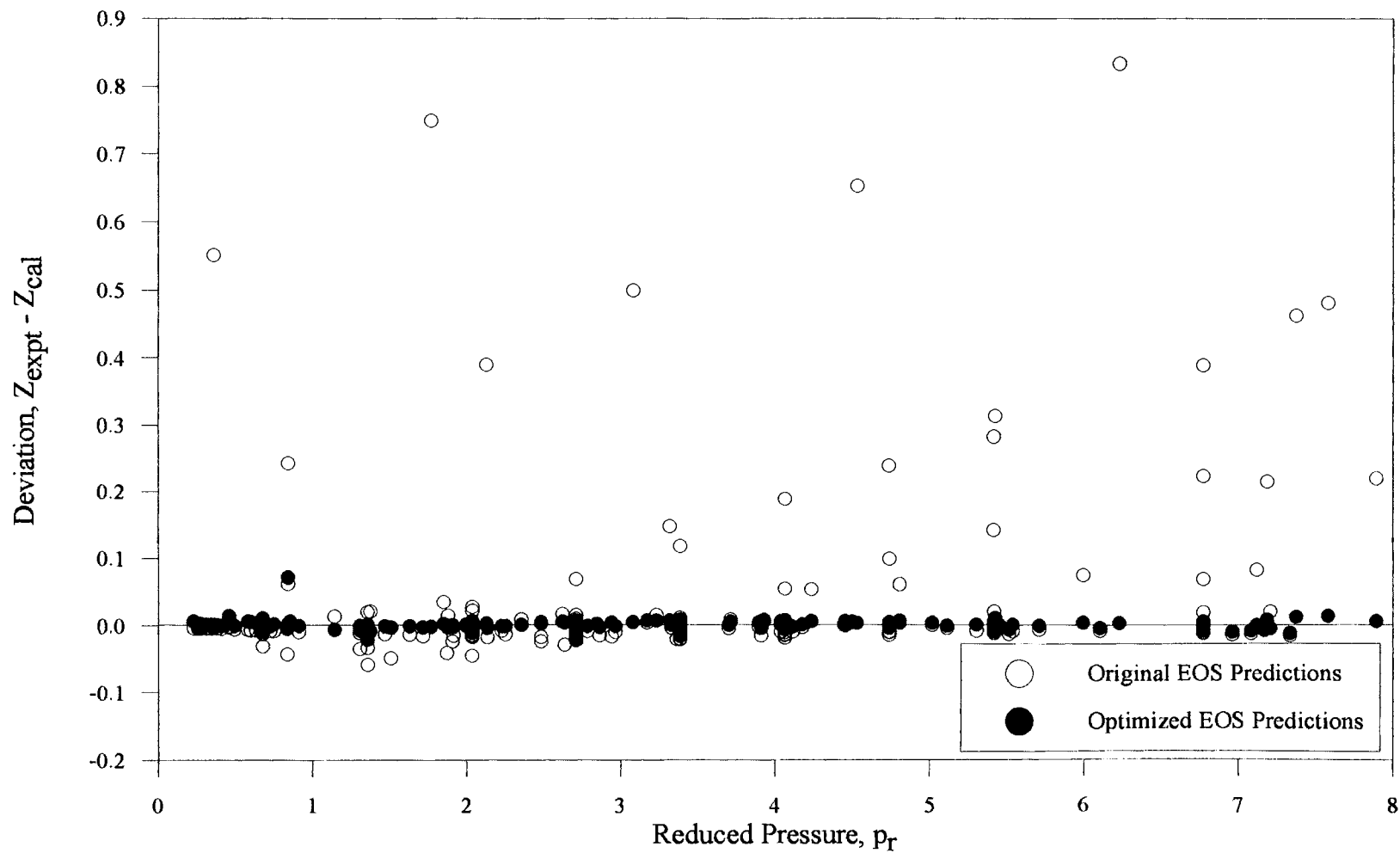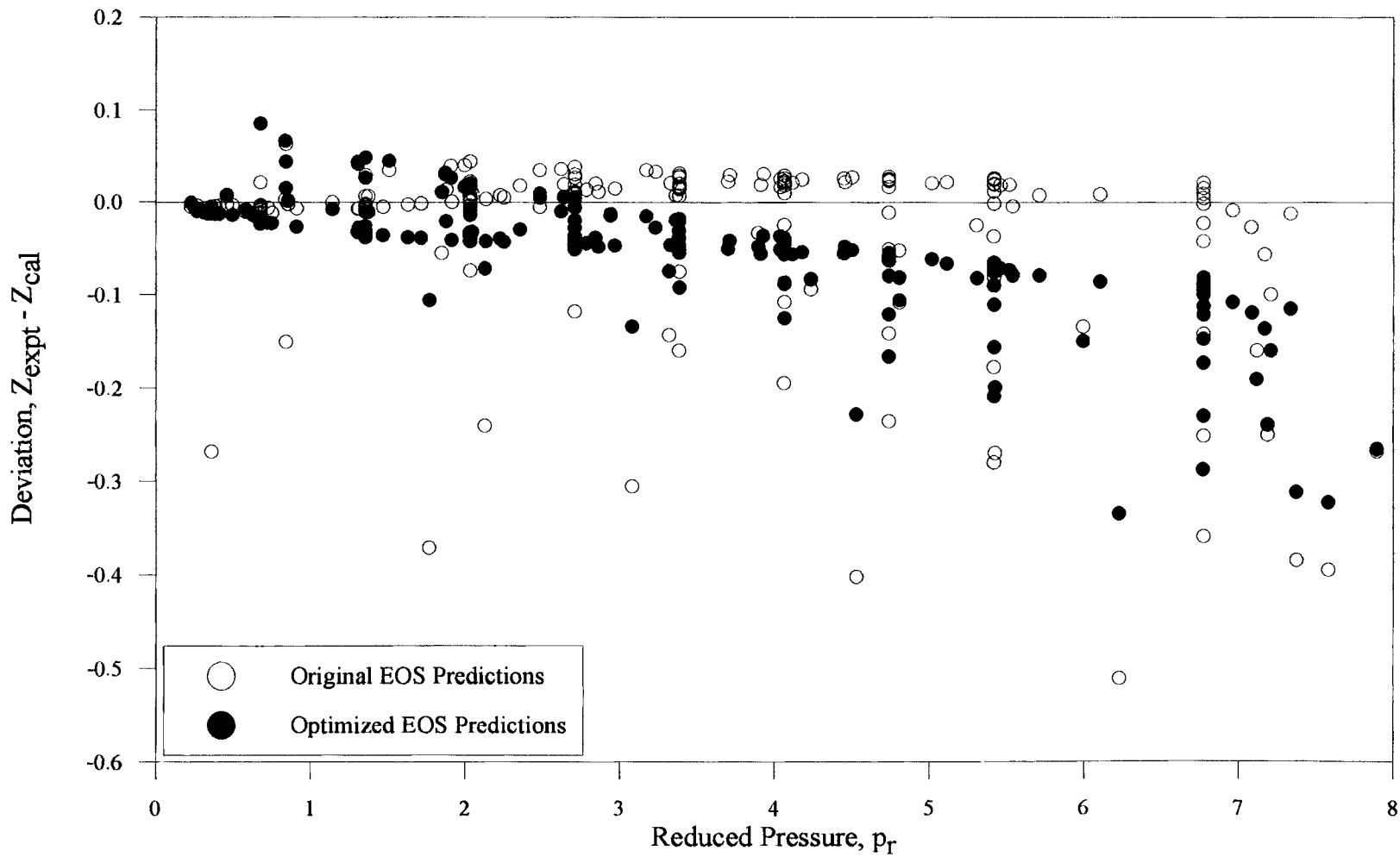Figure 7. Deviations in the Carbon Dioxide Compressibility Factors Using the BWR EOS

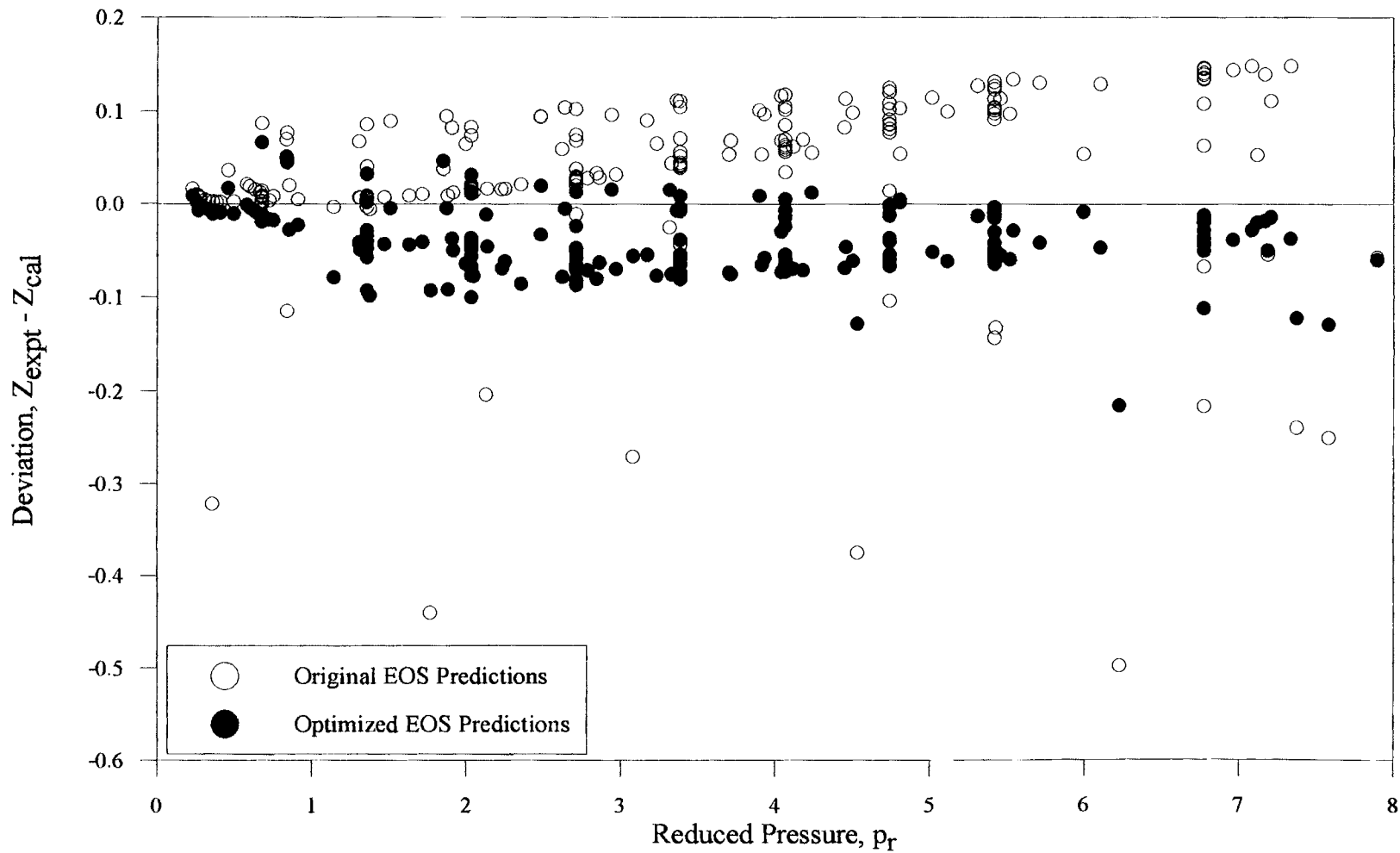Figure 8. Deviations in the Carbon Dioxide Compressibility Factors Using the PR EOS

Figure 9. Deviations in the Carbon Dioxide Compressibility Factors Using the SPHCT EOS
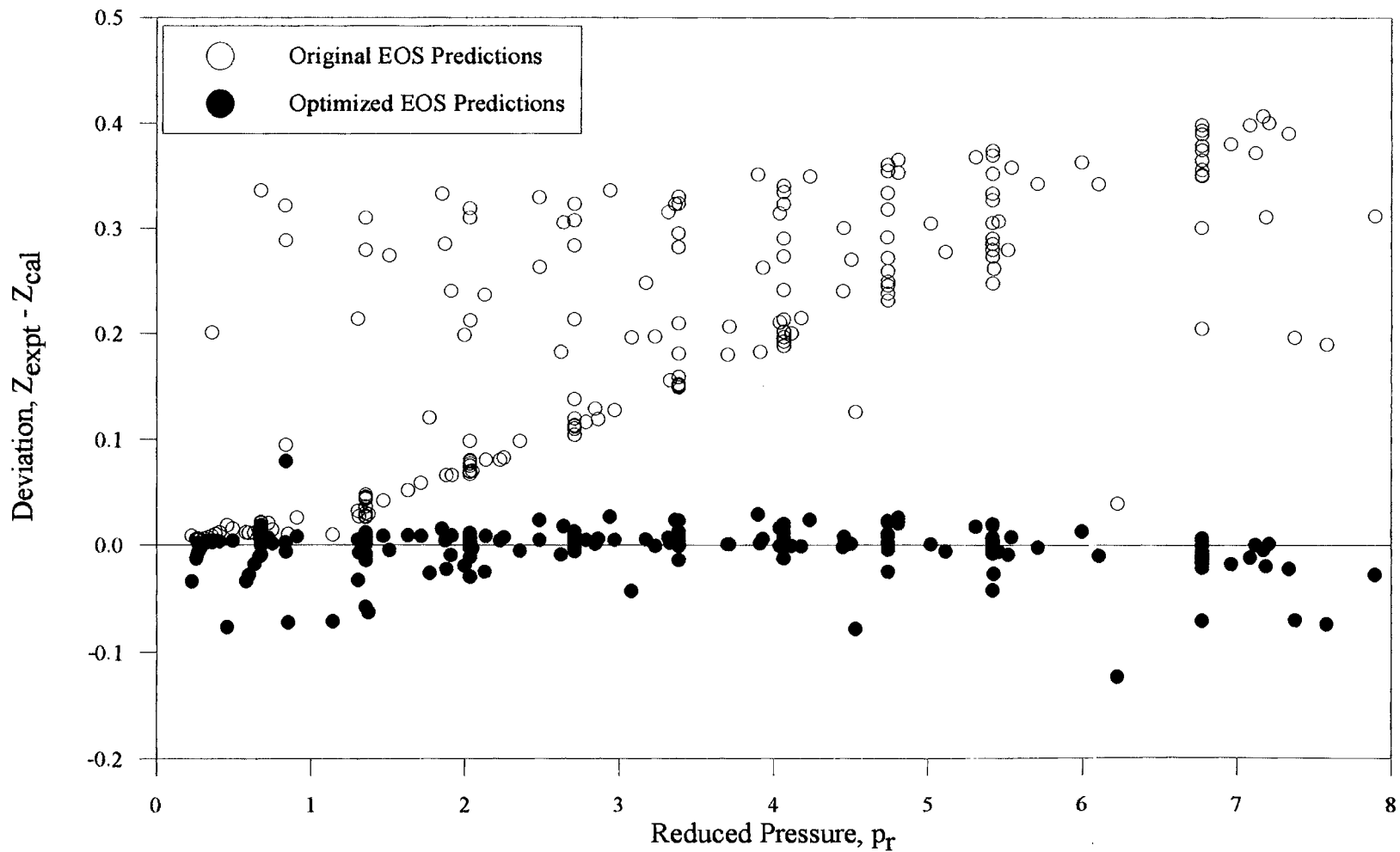
Figure 10. Deviations in the Carbon Dioxide Compressibility Factors Using the MSPHCT EOS
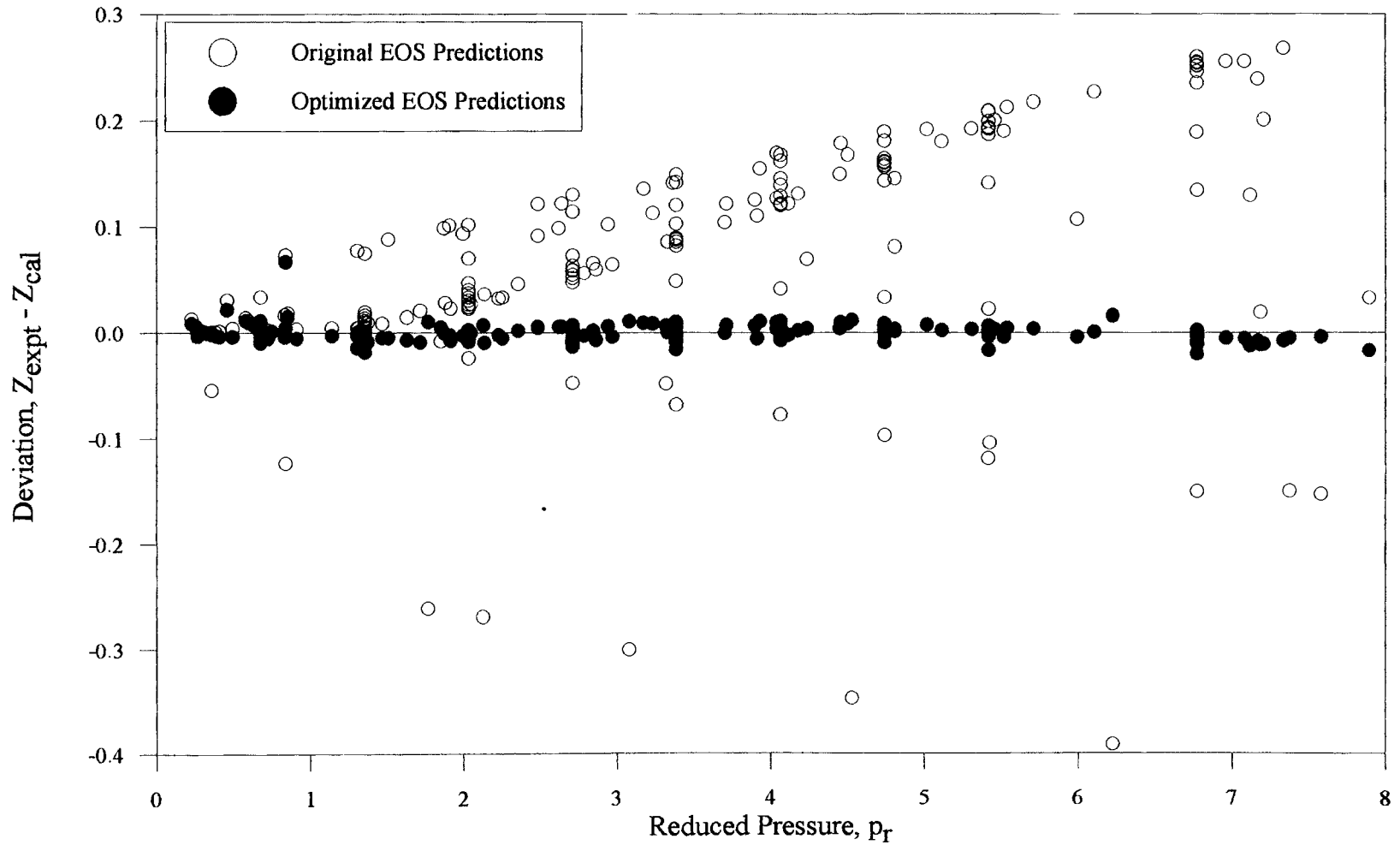
Figure 11. Deviations in the Carbon Dioxide Compressibility Factors Using the PRG EOS

the EOS constants, more improvement in the predictions was observed as indicated in the Tables V and VI.

Based on the results obtained for all the models, it is evident that the BWR and PRG model provide good predictions when all the constants are optimized. This is expected, since a large number of parameters are optimized for these equations.

Figures 7-11 compare the predictive and correlative (optimized) abilities of the various EOS in terms of compressibility factor deviations for carbon dioxide. Similar plots for methane and nitrogen are included in Figures 12-18. These figures show in general that the deviations obtained from the optimized-parameter predictions are relatively small in the subcritical region, but as the reduced pressure increases the deviations also increase. Moreover, while all the EOS evaluated show significant improvements on tuning of the EOS parameters, the BWR equation provides the best predictions.

Figures 19 and 20 illustrate the variation of deviations in the compressibility factors with reduced density and reduced temperature, respectively. Using the SPHCT EOS, a systematic trend is observed in the compressibility factor deviations of carbon dioxide, especially, for reduced densities in the supercritical region. In comparison, Figure 20 indicates that significant deviations in the compressibility factor occur at reduced temperatures in the subcritical region. Moreover, the deviations in the supercritical region are similar in nature and vary widely for a given temperature. Additional plots illustrating the variation of compressibility factor deviations with reduced density for the five EOS models are presented in Appendix D.

It should be noted that the evaluations are performed for the compressibility factor predictions using experimental densities. The viability of the optimized parameters in this work will be decided by the quality of the predictions obtained for the volumetric and equilibrium properties through iterative computations.

Figure 12. Deviations in the Methane Compressibility Factors Using the BWR EOS

Figure 12. Deviations in the Methane Compressibility Factors Using the BWR EOS

Figure 13. Deviations in the Methane Compressibility Factors Using the PR EOS
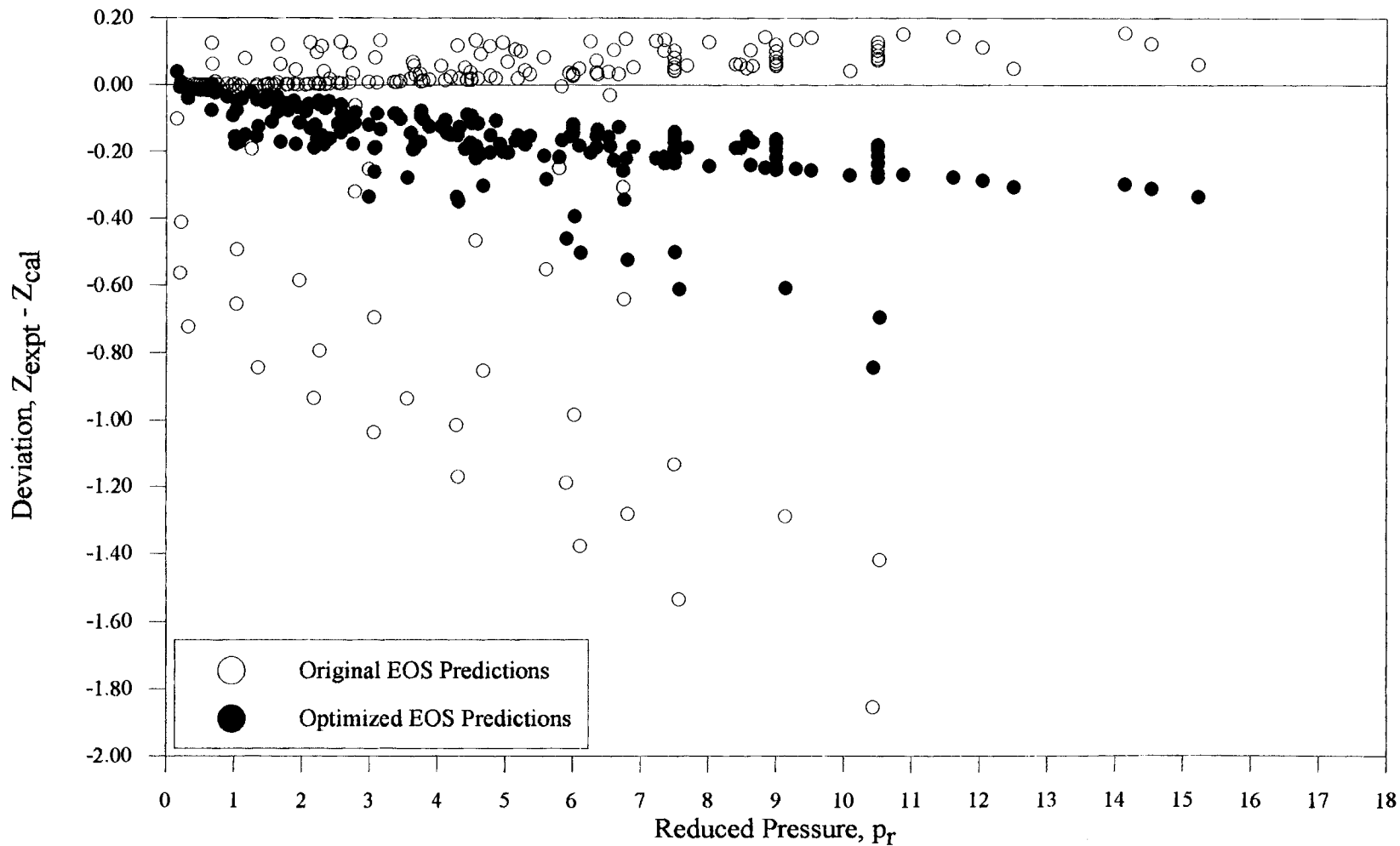
Figure 14. Deviations in the Methane Compressibility Factors Using the SPHCT EOS
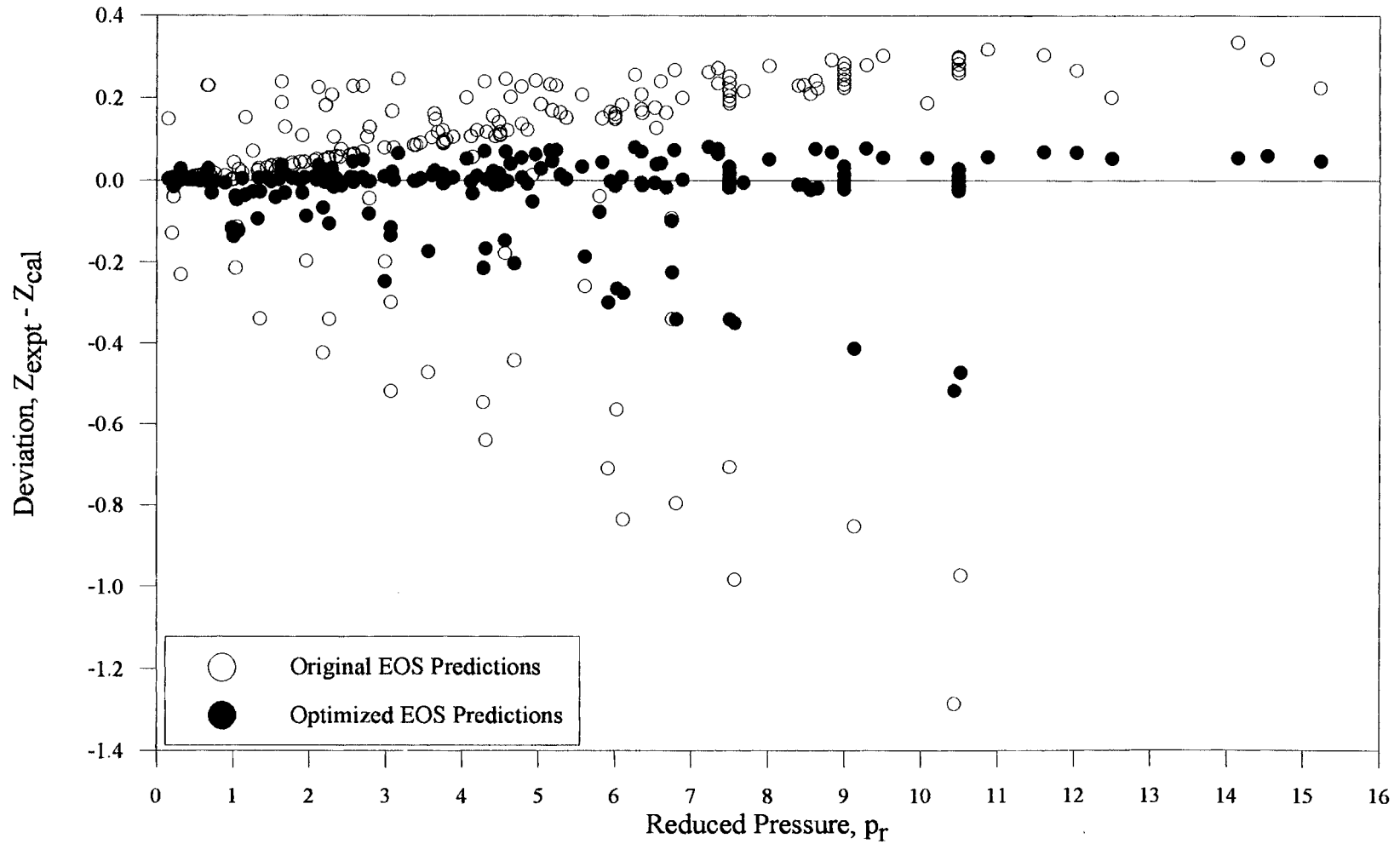
Figure 15. Deviations in the Compressibility Factors Using the MSPHCT EOS
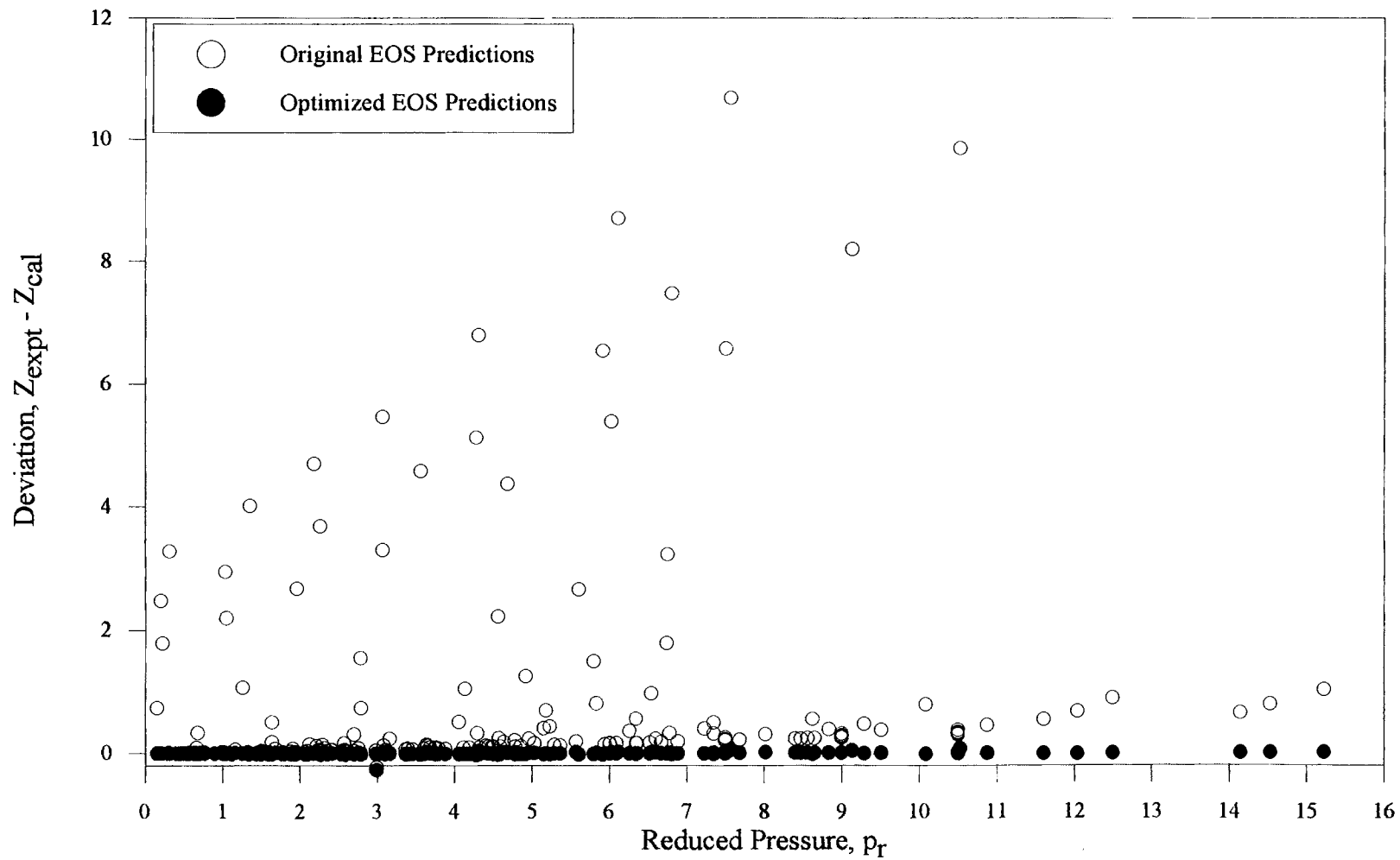
Figure 16. Deviations in the Methane Compressibility Factors Using the PRG EOS
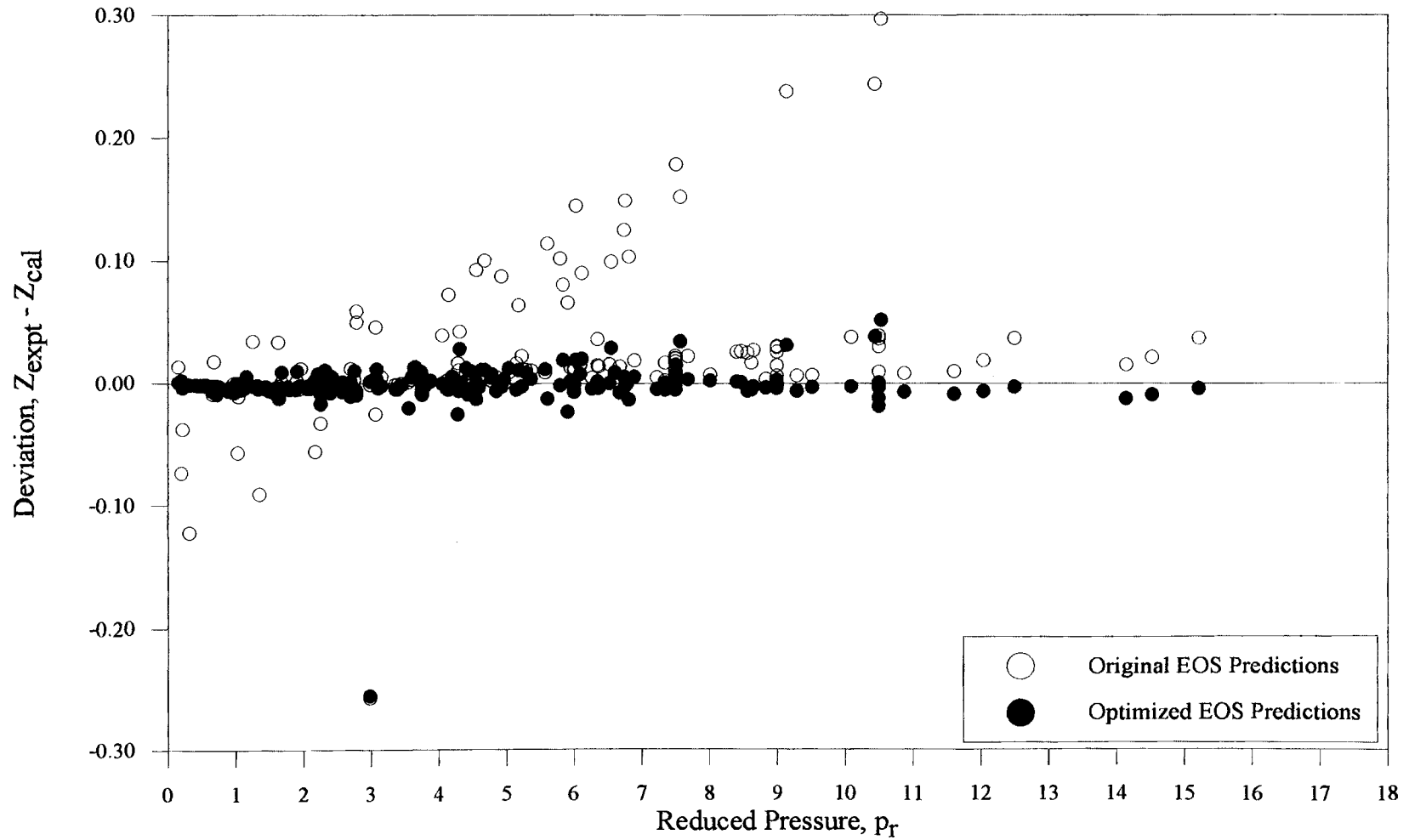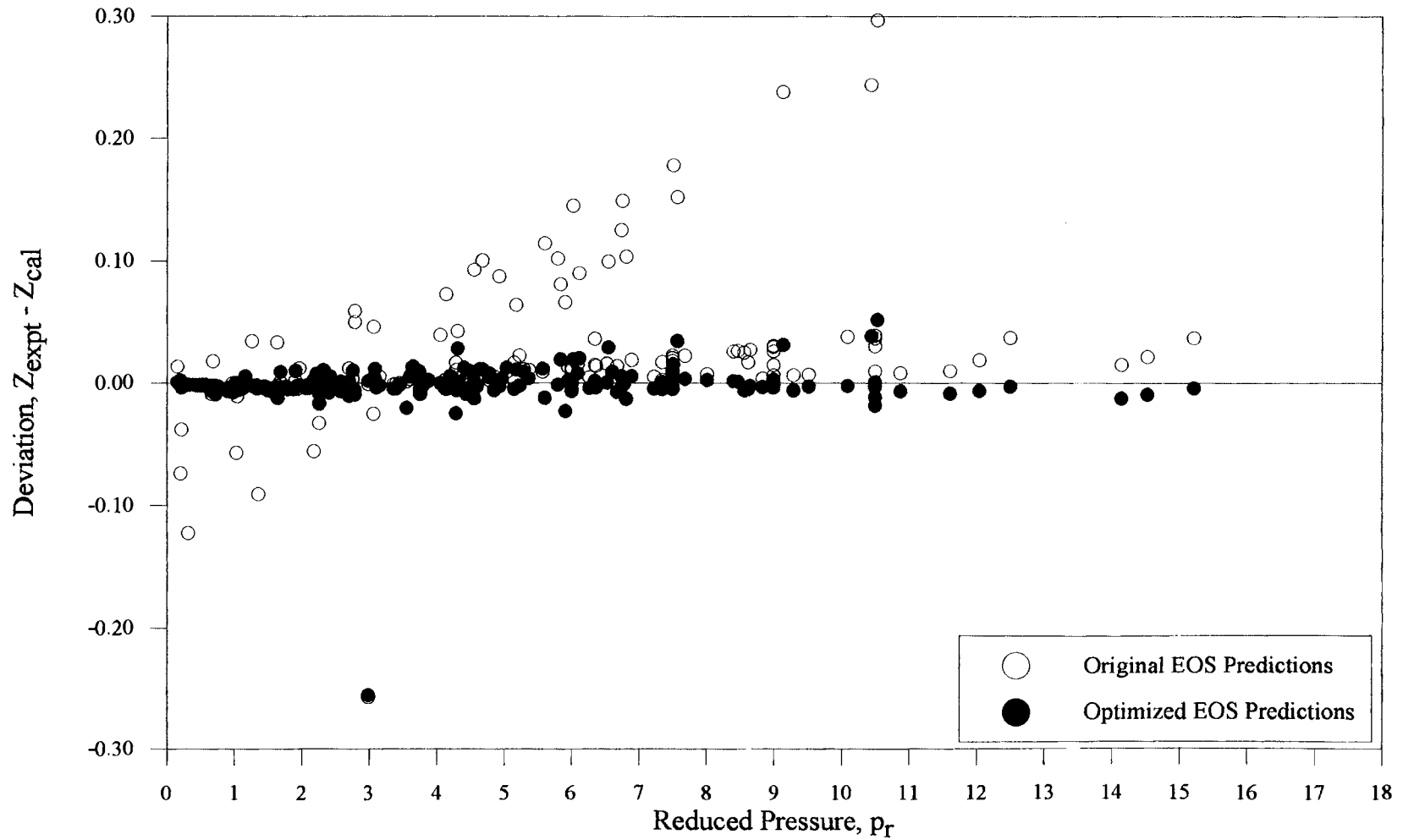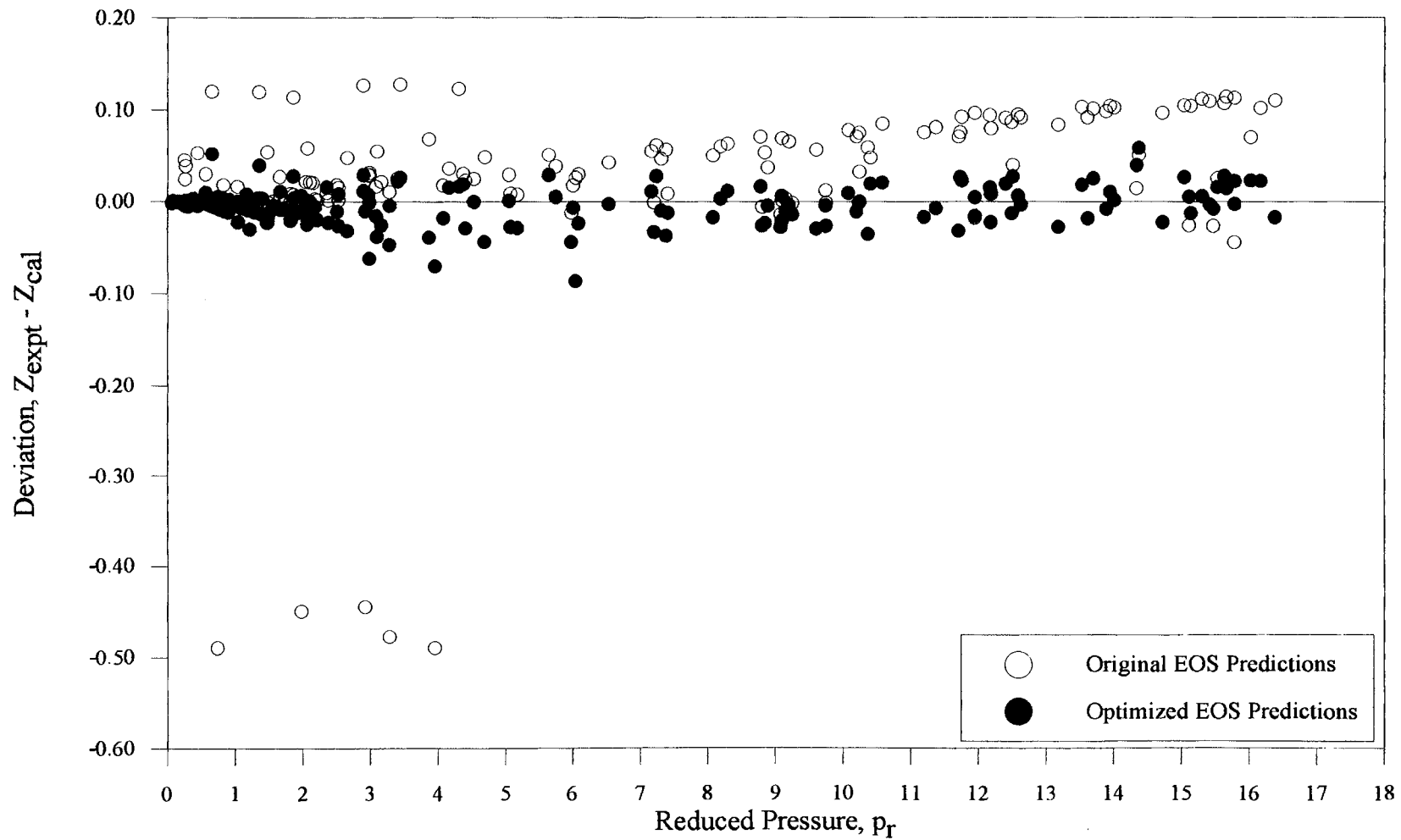
Figure 17. Deviations in the Nitrogen Compressibility Factors using the BWR EOS

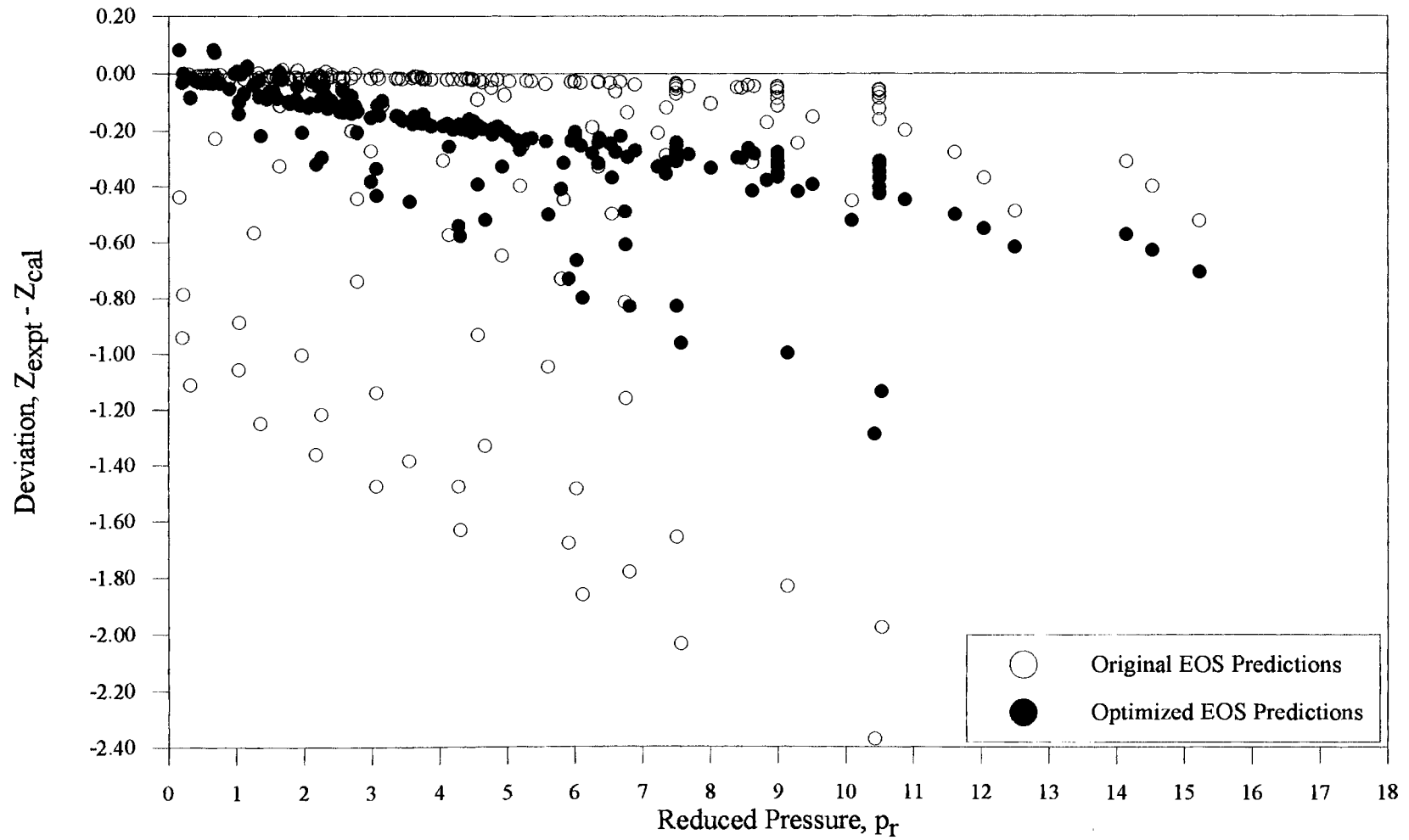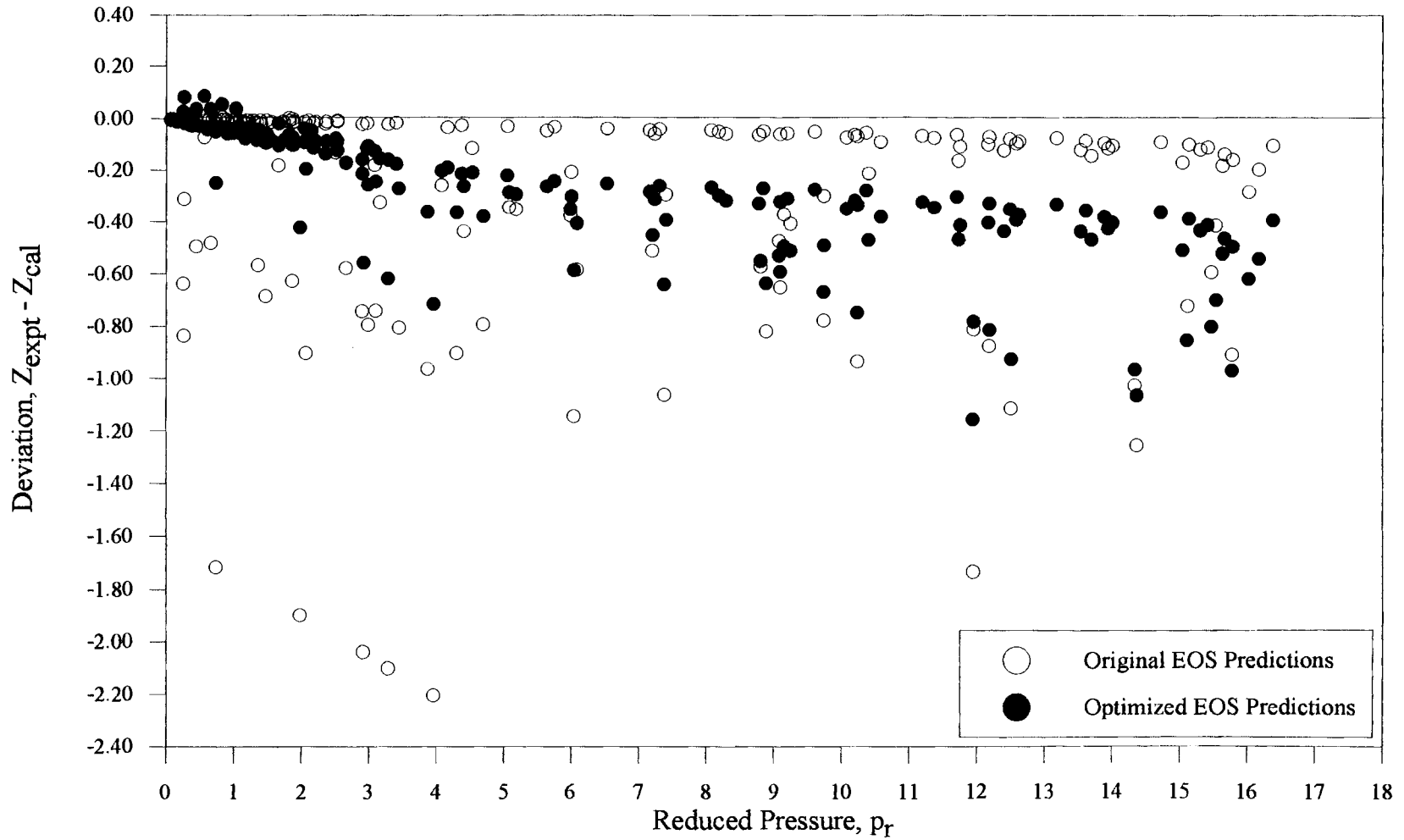Figure 18. Deviation in the Nitrogen Compressibiltiy Factors using the PR EOS
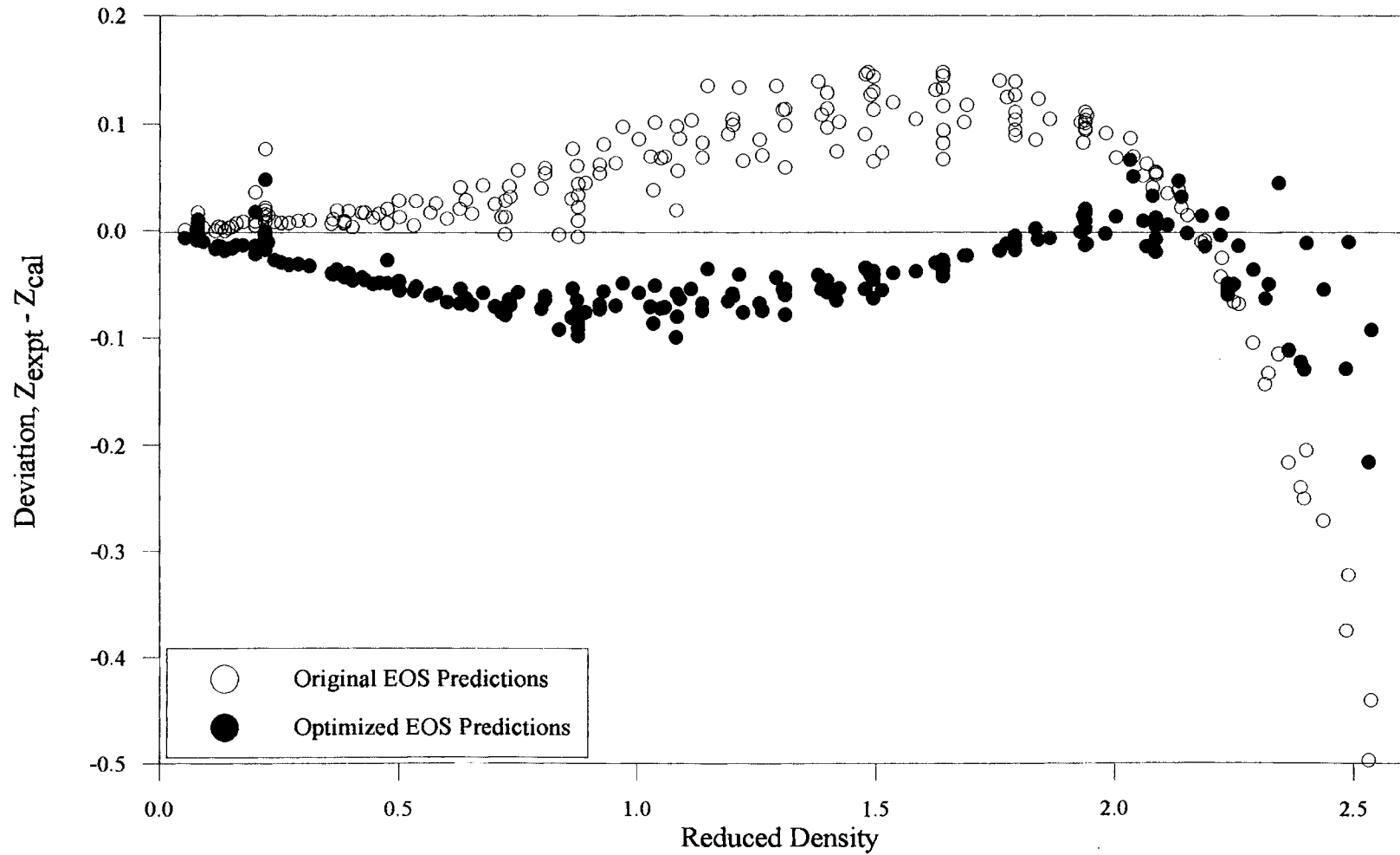
Figure 19. Deviations in the Carbon Dioxide Compressibility Factors Using the SPHCT EOS
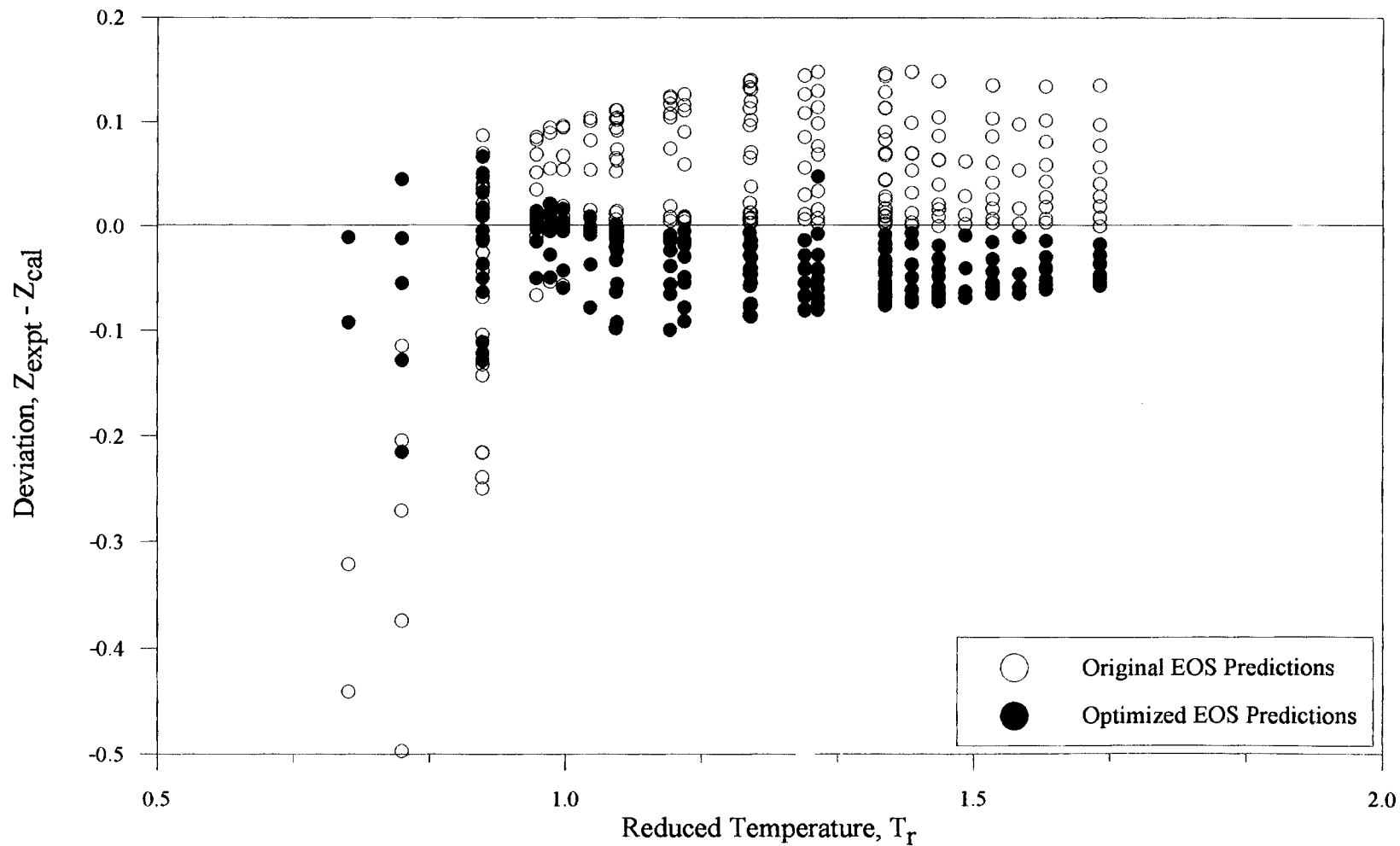
Figure 20. Deviations in the Carbon Dioxide Compressibility Factors Using the SPHCT EOS

CHAPTER VI

CONCLUSIONS AND RECOMMENDATIONS

Five EOS models were evaluated for their abilities to predict compressibility factors. Experimental pvT data were compiled ranging from near the triple point to beyond the critical point region for nitrogen, methane and carbon dioxide. The upper limits for the temperature and pressure are 500 K and 500 bars. For some data sets, measurements near the triple point were not available; thus, the evaluations were performed based on the best available data. Following are specific conclusions and recommendations which can be made based on this preliminary work.

Conclusions

1)   The substance-specific BWR model was found superior to the other models. All five models predicted poorly near the triple point region. The results improved as the critical region was approached but worsened at the upper limits of the temperature and pressure.

2)   Although all the optimized EOS models produced significant improvement in the compressibility factor predictions, the BWR equation gave the best results.

3)   The EOS prediction results were highly dependent on the number of regressed parameters.

Recommendations

1) This preliminary evaluation of the five models was restricted to only three pure fluids. The pure database should be expanded to include more types of chemical compounds for future EOS evaluations.

2) It has been observed that the deviations vary widely depending on the temperature, pressure and density ranges considered. Comprehensive evaluation of the five models covering the full temperature and pressure ranges should be performed using other fluids for which data are available near the triple point.

3) The EOS parameters were optimized for all the EOS models and a significant improvement in the results was observed. Efforts should be directed to include all the pure fluids being considered and simultaneously regress the parameters, thus making the EOS more general.

4) Mixtures were not considered in the present evaluations. The predictive capabilities of the five models for mixtures commonly encountered in the chemical industry should be studied.

5) All five models considered predicted poorly near the triple point region and at very high pressures. Efforts should be directed to improve the model predictions in these limiting regions.

6) The usefulness of newly regressed EOS parameters should be verified through iterative volumetric and equilibrium computations.

LITERATURE CITED

1. Starling, K., "Fluid Thermodynamic Properties for Light Petroleum Systems," Gulf Publishing Company, Houston, (1973).

2. Peng, D. and Robinson D. B., "A New Two-Constant Equation of State," Industrial and Engineering Chemistry Fundamentals, Vol. 15, No. 1, 59-64, (1976).

3. Beret, S. and Prausnitz, J. M., "Perturbed Hard-Chain Theory: An Equation of State for Fluids Containing Small or Large Molecules," AIChE Journal, Vol. 21, No. 6, 1123-1132, (1975).

4. Donohue, M. D. and Prausnitz, J. M., "Perturbed Hard Chain Theory for Fluid Mixtures: Thermodynamic Properties for Mixtures in Natural Gas and Petroleum Technology," AIChE Journal, Vol. 24, No. 5, (1978).

5. Vimalchand, P. and Donohue, M. D., "Thermodynamics of Quadrupolar Molecules: The Perturbed-Anisotropic-Chain Theory," Industrial and Engineering Chemistry Fundamentals, Vol. 24, 246-257, (1985).

6. Vimalchand, P., Donohue, M. D. and Sandler S. I., "Local Composition Model for Chain like Molecules: A New Simplified Version of the Perturbed Hard Chain Theory," AIChE Journal, Vol. 32, No. 10, 1726-1734, (1986).

7. Donohue, M. D. and Vimalchand, P., "The Perturbed-Hard-Chain Theory Extensions and Applications," Fluid Phase Equilibria, Vol. 40, 185-211, (1988).

8. Shaver, R. D., "Modification of the SPHCT Equation of State," Ph.D. Dissertation, Oklahoma State University, Stillwater, Oklahoma, (1990).

9. Park, J. K., "Binary Vapor-Liquid Equilibrium Measurements for Selected Asymmetric Mixtures and Equation of State Development", Ph.D. Dissertation, Oklahoma State University, Stillwater, Oklahoma, (1993).

10. Hall, F. E., "Adsorption of Pure and Multicomponent Gases on Wet Fruitland Coal," Masters Thesis, Oklahoma State University, Stillwater, Oklahoma, (1993).

11. Gasem, K. M., Personal Communication, Oklahoma State University, Stillwater, Oklahoma, (1992-1994).

12.   Gasem, K. M., Pure Fluid Properties Software, Oklahoma State University, Stillwater, Oklahoma, (1992-1994).

13.   Gasem, K. M., "Thermodynamics Class Notes for CHENG 5843," Oklahoma State University, Stillwater, Oklahoma, (1992-1994).

14.   Kim, C. H, P. Vimalchand, M. D. Donohue and S. I. Sandler, "Local Composition Model for Chain-like Molecules: A New Simplified Version of the Perturbed Hard Chain Theory," AICHE Journal, 32(10), 1726, (1986).

15.   Michels, A., Wouters, H. and Boer J., "Isotherms of Nitrogen between 0°C and 150 $^{\circ}$C and at Pressures from 20 to 80 Atm," Physica I, 587-594, (1934).

16.   Michels, A., Wouters, H. and Boer J., "Isotherms of Nitrogen between 0° and 150° and at Pressures from 20 to 80 Atm," Physica III, 585-589, (1934).

17.   Benedict, M., "Pressure, Volume, Temperature Properties of Nitrogen at High Density I. Results Obtained with a Weight Peizometer," J. Chem. Soc., Vol. 59, 2224-2233, (1937).

18.   Van Itterbeek, A. and Vebeke, O., "Density of Liquid Nitrogen and Argon as a Function of Pressure and Temperature," Physica 26, 931-938, (1960).

19.   Kobayashi, R., Canfield F. and Leland, T. W., "Compressibility Factors for Helium-Nitrogen Mixtures," J. Chem. Eng. Data, Vol. 10, No. 2, 92-96, (1965).

20.   Streett, W. B. and Staveley, L. A. K., "The P-v-T Behavior of Liquid Nitrogen at Temperatures from 77 to 120 K and Pressures to 680 Atmospheres," Adv. Cryog. Eng., Vol. 13, 363-374, (1967).

21.   Weber, L. A., "Some Vapor Pressure and P, V, T Data on Nitrogen in the Range 65 to 140 K," J. Chem. Thermodynamics, Vol. 2, 839-846, (1970).

22.   Da Ponte M., Streett, W. and Staveley, L., "An Experimental Study of the Equation of State of Liquid Mixtures of Nitrogen and Methane, and the Effect of Pressure on their Excess Thermodynamic Functions," J. Chem. Thermodynamics, Vol. 10, 151-168, (1978).

23.   Straty, G. and Diller, D., "(P, v, T) of Saturated and Compressed Fluid Nitrogen," J. Chem. Thermodynamics, Vol. 12, 927-936, (1980).

24.   Keyes, G. and Burks, H., "The Isometrics of Gaseous Methane," J. Am. Chem. Soc., Vol. 49, 1403-1411, (1927).

25. Kvalnes, H. and Gaddy, V., "The Compressibility Isotherms of Methane at Pressures to 1000 Atmospheres and at Temperatures From -70 to 200°C," J. Amer. Chem. Soc., Vol. 49, 394-399, (1931).

26. Michels, M. and Nederbragt, G., "Isotherms of Methane between 0 and 150°C for Densities up to 225 Amagat, Calculated Specific Heat, Energy and Entropy in the same Region," Physica III, No. 7, 569-577, (1936).

27. Reamer, H., Olds, R., Sage, B. and Lacey, W., "Volumetric Behavior of Methane," Industrial and Engineering Chemistry, Vol. 35, No. 8, 922-924, (1943).

28. Van Itterbeek, A., Verbeke, O. and Staes, K., "Measurements on the Equation of State of Liquid Argon and Methane up to 300 kg cm^{-2} at Low Temperatures," Physica 29, 742-754, (1963).

29. Douslin, D., Harrison, R., Moore, R. and McCullough, "P-V-T Relations for Methane," J. Chem. and Eng. Data, Vol. 9, No. 3, 358-363, (1964).

30. Kobayashi, R., Vennix, A. and Leland, T., "Low-Temperature Volumetric Properties of Methane," J. Chem. Eng. Data, Vol. 15, No. 2, 238-243, (1970).

31. Da Ponte M., Streett, W. and Staveley, L., "An Experimental Study of the Equation of State of Liquid Mixtures of Nitrogen and Methane, and the Effect of Pressure on their Excess Thermodynamic Functions," J. Chem. Thermodynamics, Vol. 10, 151-168, (1978).

32. Michels, M. and Mrs. Michels, "Isotherms of CO_2 between 0°C and 150°C and Pressures from 16 to 250 Atm (Amagat Densities 18-206)," Proc. Roy. Soc., A-153, 201-224, (1935).

33. Kennedy, G. C., "Pressure-Volume-Temperature Relations in CO_2 at Elevated Temperatures and Pressures," Amer. J. Sci, Vol. 252, 225-241, (1954).

34. Vukalovich, M. P., Kobelev, V. P. and Timoshenko, N. I., "Experimental Investigation of CO_2 Density at Temperatures from 0 to 35°C and Pressures of up to 300 bar," Thermal Engineering, Vol. 15, No. 4, 103-106, (1968).

35. Golovskii, E. V., Elema, V., Zagoruchenk, V. A. and Tsimarnii, V., "Experimental Study of Specific Volumes of Liquid CO_2," Thermal Engineering, Vol. 16, No. 1, 102-105, (1969).

36. Kirillin, V. A., Ulybin, S. A. and Zherdev, E. P., "An Experimental Study of Density of Carbon Dioxide," Thermal Engineering, Vol. 16, No. 2, 133-134, (1969).

37. Kirillin, V. A., Ulybin, S. and Zherdev, E., "CO_2 Density on 35,30,20 and $10°C$ Isotherms at Pressures up to 500 bar," Thermal Engineering, Vol. 16, No. 6, 137-139, (1969).

38. Kirillin, V. A., Ulybin, S. A. and Zherdev, E. P., "Experimental Determination of the Density of Carbon Dioxide at Temperatures from 0 to $-50°C$ and Pressures up to 500 bar," Thermal Engineering, Vol. 17, No. 5, 99-100, (1970).

39. Vukalovich, M. P., Kobelev, V. P. and Timoshenko, N. I., "Experimental Investigation of CO_2 Density at Temperatures below $0°C$," Thermal Engineering, Vol. 17, No. 12, 82-83, (1970).

40. Popov, V. N. and Sayapov, M. K. H., "The Density of Carbon Dioxide in the Liquid Phase," Thermal Engineering, Vol. 17, No. 4, 114-115, (1970).

41. Holste, J., Hall, K., Eubank, P., Esper G., Watson, M., Warowny, W., Bailey, D., Young, J. and Bellomy, M., "Experimental (P, V_m,T) for Pure CO_2 between 220 and 450 K," J. Chem. Thermodynamics, Vol. 19, 1233-1250, (1987).

42. Magee, J. and Ely, J., "Isochoric (P, v, T) Measurements on CO_2 and (0.98 CO_2 + 0.02 CH_4) from 225 to 400 K and Pressures to 35 Mpa," International Journal of Thermophysics, Vol. 9, No. 4, 547-557, (1988).

43. Ely, J. F., and Hanley H. J. M., NBS TN 1039, (1992).

44. Goodwin, R. D., "Thermophysical Properties for Methane, from 90 to 500 K at Pressures to 700 Bar," NBS TN 653.

45. Jacobsen, R., Stewart, R. and Jahangiri, M., "Thermodynamic Properties of Nitrogen from the Freezing line to 2000 K at Pressures to 1000 MPa," J. Phys. Chem. Ref. Data, Vol. 15, No. 2, 735-909, (1986).

46. Angus, S., K. M. de Reuck, and B. Armstrong, "International Thermodynamic Tables of the Fluid State Carbon Dioxide," International Union of Pure and Applied Chemistry, Pergamon Press, New York (1977).

47. Elliott, Jr., J. R., S. J. Sresh and M. D. Donohue, "A Simple Equation of State for Nonspherical and Associating Molecules," Industial and Engineering Chemistry Research, 29, 1476, (1990).

48. Soave, G., "Equilibrium Constants from a Modified Redlich-Kwong Equation of State," Chemical Eng. Science, 27, 1197, (1972).

APPENDIX A

EQUATION OF STATE PARAMETERS USED

This Appendix contains the original EOS parameters which were used in the predictions of compressibility factors. Table A.1 contains the PR EOS parameter values as available in the literature [2]. Table A.2 contains the EOS parameters for the modified version of BWR EOS, as given by Starling [1]. Table A.3 contains the SPHCT EOS parameters for methane and carbon dioxide as found in the literature [14]. Table A.4 contains the EOS parameters for the MSPHCT equation [8]. Table A.5 contain the pure fluid parameters for methane and carbon dioxide for PRG EOS [9]. Table A.6 contain the PRG EOS constants. The EOS parameter values for nitrogen were not available for the SPHCT, MSPHCT and PRG EOS.

TABLE A.1. PR EOS Parameter Values

m_0	m_1	m_2	Ω_a	Ω_b
0.37464	1.54226	-0.26992	0.45724	0.07780

Table A.2. BWR EOS Pure Fluid Parameters

Parameter*	Methane	Nitrogen	Carbon dioxide
B_0	0.723251	0.677022	0.394117
A_0	0.752029E+04	0.418505E+04	0.659203E+04
C_0	0.271092E+09	0.137936E+09	0.295902E+10
D_0	0.107737E+11	0.195183E+11	0.409151E+12
E_0	0.301122E+11	0.121648E+13	0.102898E+11
b	0.925404	0.833470	0.971443
a	0.257489E+04	0.140459E+04	0.5632.85E+04
d	0.474891E+05	0.311894E+05	0.59929.7E+05
α	0.468828	0.302696	0.395525
c	0.437222E+09	0.844317E+08	0.274668E+10
γ	0.148640E+01	0.110011E+01	0.164916E+01

* The EOS constants are based on units of °R, psia and lbmole

Table A.3. SPHCT Pure Fluid Parameters

Component	T^* (K)	v^* (cm^3/mol)	c
Methane	80.05	18.889	1.0298
Nitrogen	-	-	-
Carbon dioxide	104.32	14.486	1.9258

Table A.4. MSPHCT Pure Fluid Parameters

Component	T^* (K)	v^* (cm^3/mol)	c
Methane	95.23	18.858	1.0003
Nitrogen	-	-	-
Carbon dioxide	131.05	15.858	1.6258

Table A.5. PRG EOS Pure Fluid Parameters

Component	T^* (K)	v^* (cm^3/mol)	c
Methane	81.287	23.180	1.0000
Nitrogen	-	-	-
Carbon dioxide	111.31	18.052	1.6565

Table A.6. PRG EOS Constants

Constant[*]	Value
τ	0.74048
a	4.0000
b	1.9000
u	-2.6192
w	2.0000
Q	7.3708
α_0	1.4000
κ_1	0.092687
κ_2	0.18011
κ_3	-0.030748
κ_4	-0.33149

* The EOS constants are based on units of K, bar and cm^3/mole

APPENDIX B

PHYSICAL PROPERTY DATA

This appendix contains the physical property data of the pure fluids used in the present work. The critical property values along with the acentric factor and the molecular weight are given in Table B. The critical temperature, critical pressure, acentric factor and molecular weight data were obtained directly from the LIB.FOR routine [43]. The triple point temperatures and pressures were obtained from the literature as indicated by the references.

Table B. Physical Property Data Used in this Work [43]

Physical Property	CH_4	N_2	CO_2
Critical Temperature (K)	190.555	126.200	304.210
Critical Pressure (bars)	45.9884	33.9003	73.8254
Triple Point Temperature (K)	90.680 [44]	63.148 [45]	216.580 [46]
Triple Point Pressure (bars)	0.1174 [44]	0.1252 [45]	5.180 [46]
Accentric factor	0.0113	0.0390	0.2251
Molecular Weight	16.043	28.010	44.010

APPENDIX C

MAKEFILE ROUTINE

This appendix contains a brief description of the Makefile routine used in the present work. A Makefile is similar to a batch file in DOS, which facilitates compiling and linking multiple Fortran files with ease in an unix environment. The first line consists of SUFFIXES term, which identifies the type of files one will encounter in the Makefile. The second term SOURCE identifies the different object files which will result in the final executable file. The third term, LIBS identifies the type of libraries which are used by the Makefile. For example, Fortran libraries, system libraries, math libraries and X11 libraries are invoked when the Makefile is executed. The fourth term contains the syntax for compiling multiple Fortran files.

A tab symbol, as shown in the Makefile, is necessary for any type of syntax to be executed while running a Makefile. The syntax 'xlf' compiles XL Fortran source files. The '-c' option compiles the Fortran files without calling the linkage editor. The '-g' option produces the debug information which can be used with the 'xde', i.e., the windows debugger. The '-NQ20000' flag indicates the size of the table to be used. Depending on the size of the routine used, a bigger table size may have to be used. The 'O3' option optimizes the code generated by the compiler and also performs additional optimizations which are compiler and memory time intensive. The '-qflag = I:I' flag specifies the severity level of diagnostics to be reported in the listing. This syntax is used in compiling all the files with extension *.f.

The 'a.out' file contains the final executable code. The 'clean' command is used to delete all the object files when the syntax 'make clean' is executed at the unix prompt. The last few lines are used to create object files from source files. The mode of the Makefile should be changed to an executable type and run from the unix prompt by typing 'make'.

.SUFFIXES: .o .c .f

SOURCE= pfp.o files.o sort.o que2.o optin.o xydat2.o zf1.o title.o error.o \
^I   regfun.o func.o tbfun.o tcfun.o pcfun.o vcfun.o wfun.o vpfun.o ldfun.o spfun.o \
^I   stfun.o mix.o cubic.o lib.o vmarg.o slfun.o vzcal.o
LIBS= -lxlf -lsys -lm -lX11

.f.o:
^I   xlf -c -g -NQ20000 $*.f -O3 -qflag=I:I

a.out: $(SOURCE)
^I   xlf -g -o $@ $(SOURCE) $(LIBS)
clean:
^I   rm *.o

pfp.o: pfp.f COMMON.AAA
files.o: files.f COMMON.AAA
sort.o: sort.f COMMON.AAA
que2.o: que2.f COMMON.AAA
optin.o: optin.f COMMON.AAA
xydat2.o: xydat2.f COMMON.AAA
zf1.o: zf1.f COMMON.AAA
title.o: title.f
error.o: error.f COMMON.AAA
regfun.o: regfun.f COMMON.AAA
func.o: func.f
tbfun.o: tbfun.f COMMON.AAA
tcfun.o: tcfun.f COMMON.AAA
pcfun.o: pcfun.f COMMON.AAA
vcfun.o: vcfun.f COMMON.AAA
wfun.o: wfun.f COMMON.AAA
vpfun.o: vpfun.f COMMON.AAA
ldfun.o: ldfun.f COMMON.AAA
spfun.o: spfun.f COMMON.AAA
stfun.o: stfun.f COMMON.AAA
mix.o: mix.f COMMON.AAA
cubic.o: cubic.f
lib.o: lib.f
vmarg.o: vmarg.f
slfun.o: slfun.f COMMON.AAA
vzcal.o: vzcal.f COMMON.AAA

APPENDIX D

ADDITIONAL FIGURES FOR COMPRESSIBILITY FACTOR PREDICTIONS

This Appendix contains additional figures illustrating the variation of compressibility factor deviations with reduced density for the five EOS models studied. Figures D.1 to D.4 illustrate the compressibility factor deviations for carbon dioxide as a function of reduced density. The results for BWR EOS and PR EOS illustrated in Figures D.1 and D.2 show large deviations in compressibility factors when the original EOS parameters were used for the predictions in the subcritical regions. However, the MSPHCT EOS and PRG EOS predictions illustrated in Figures D.3 and D.4 show considerable deviations in compressibility factor in the subcritical region and in the supercritical regions as well. The predictions improved when the EOS constants and parameters were reoptimized with the BWR model resulting in better predictions than the other models.

Figures D.5 to D.9 illustrate the variation of deviations in the compressibility factors with reduced density for methane. The compressibility factor predictions using the original EOS parameters were similar to those observed for carbon dioxide for all the models except for PRG EOS, which gives worse predictions in the subcritical region.

Figures D.10 and D.11 illustrate the variation of deviations in the compressibility factors with reduced density for nitrogen. The original EOS parameters were not available for the SPHCT, MSPHCT and PRG models, therefore no effort was made to present these models here. Both the models show similar behavior to that observed for methane and carbon dioxide, and upon reoptimizing the EOS parameters and the EOS constants the predictions improved significantly.
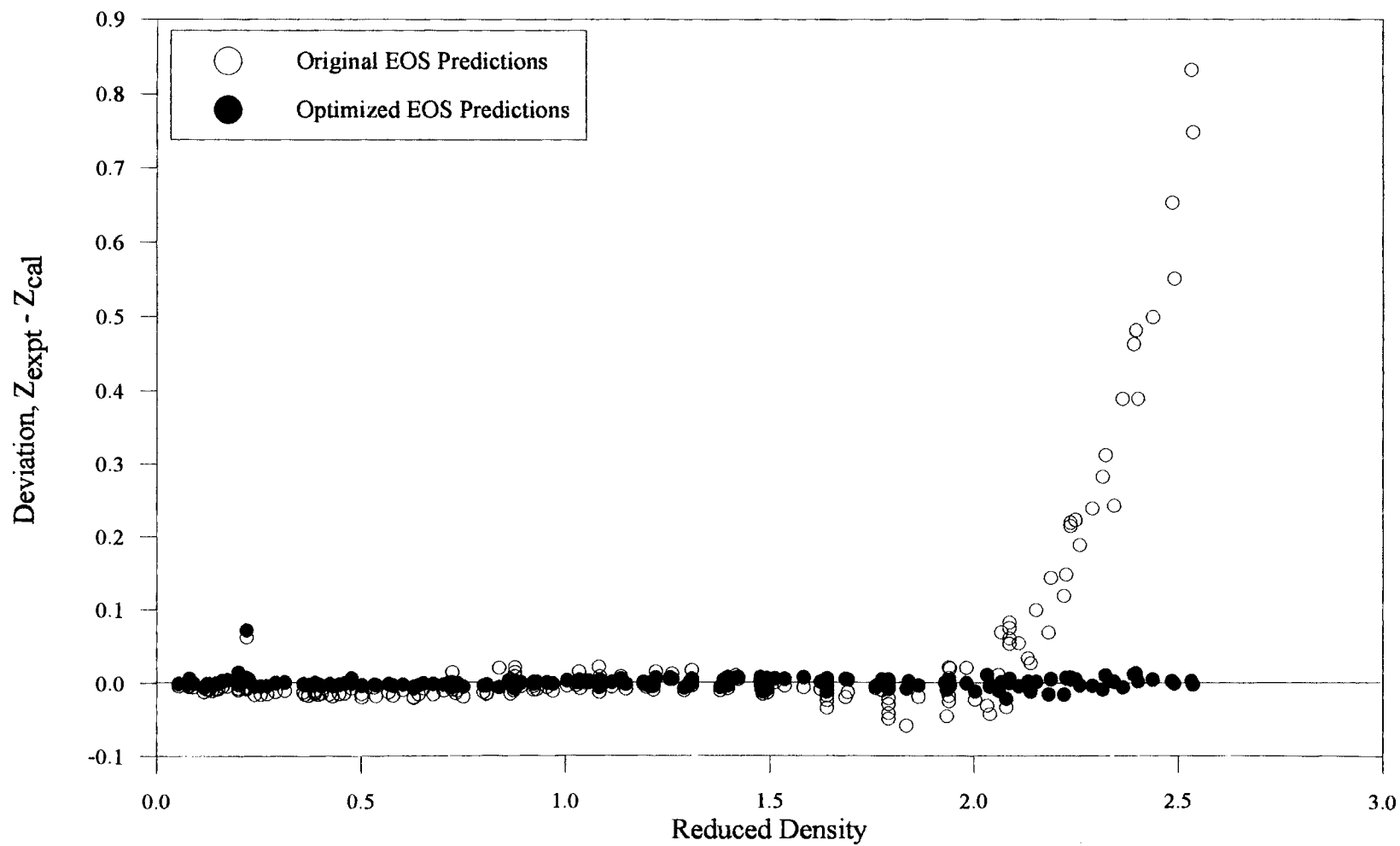
Figure D.1. Deviations in the Carbon Dioxide Compressibility Factors Using the BWR EOS
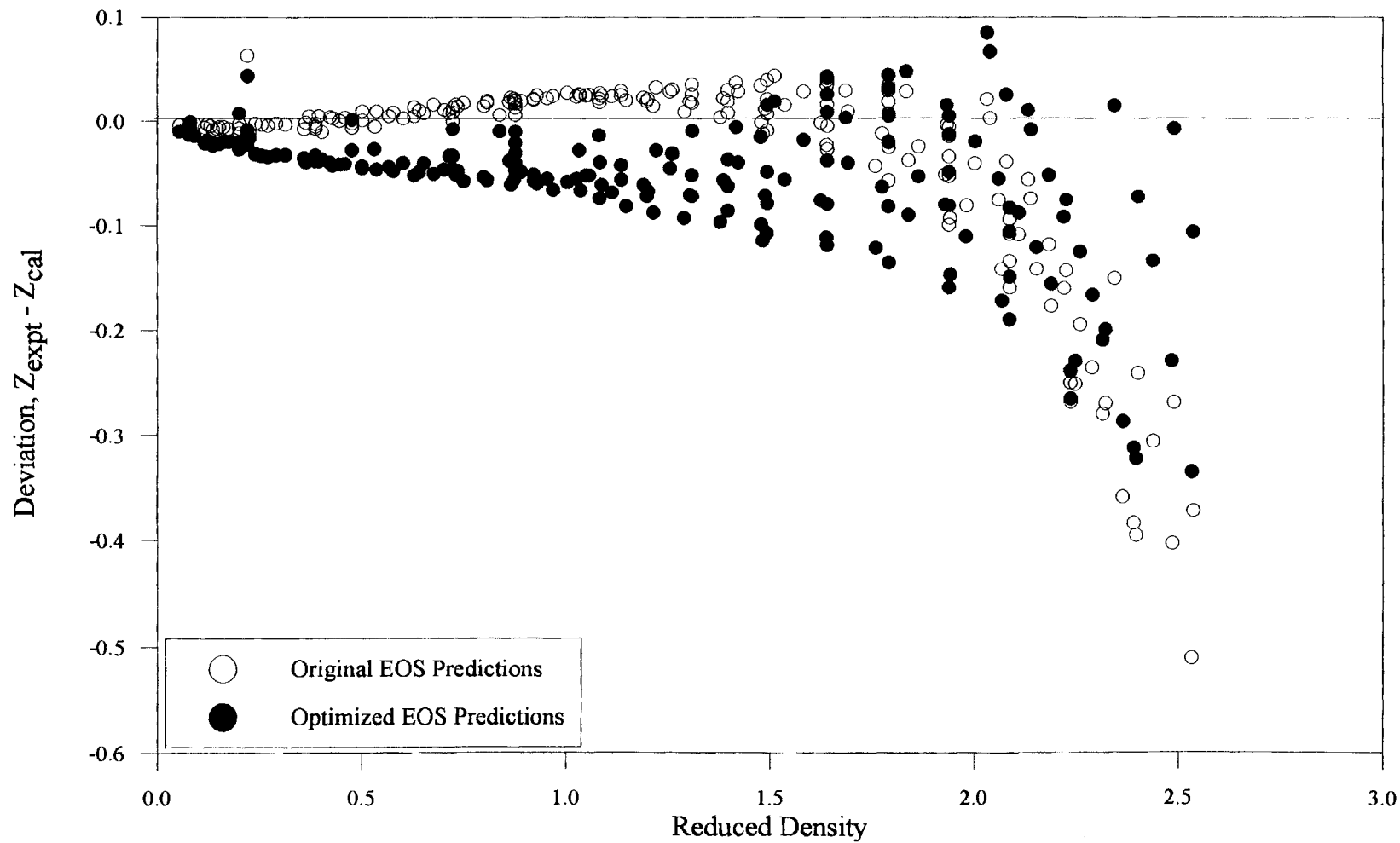
Figure D.2. Deviations in the Carbon Dioxide Compressibility Factors Using the PR EOS
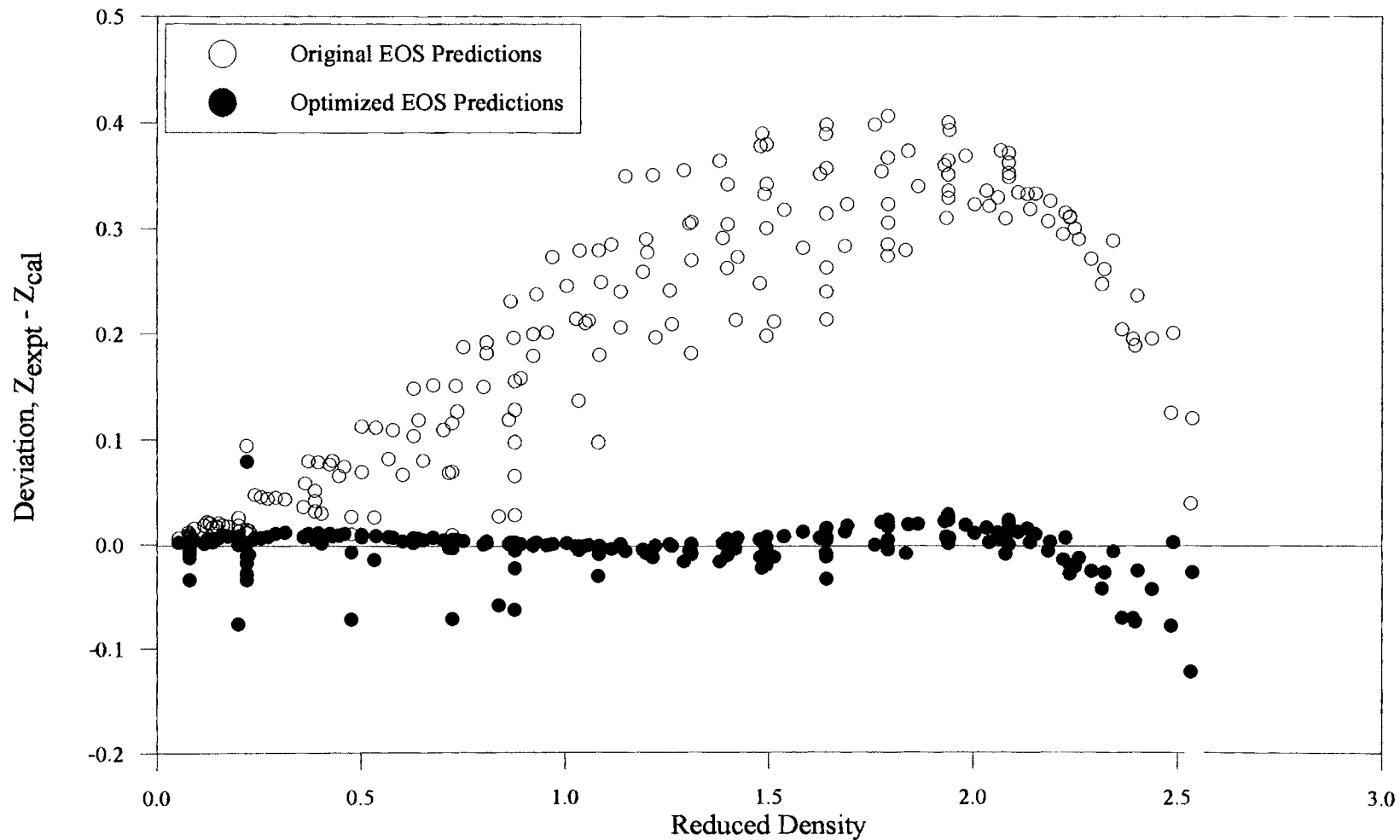
Figure D.3. Deviations in the Carbon Dioxide Compressibility Factors Using the MSPHCT EOS
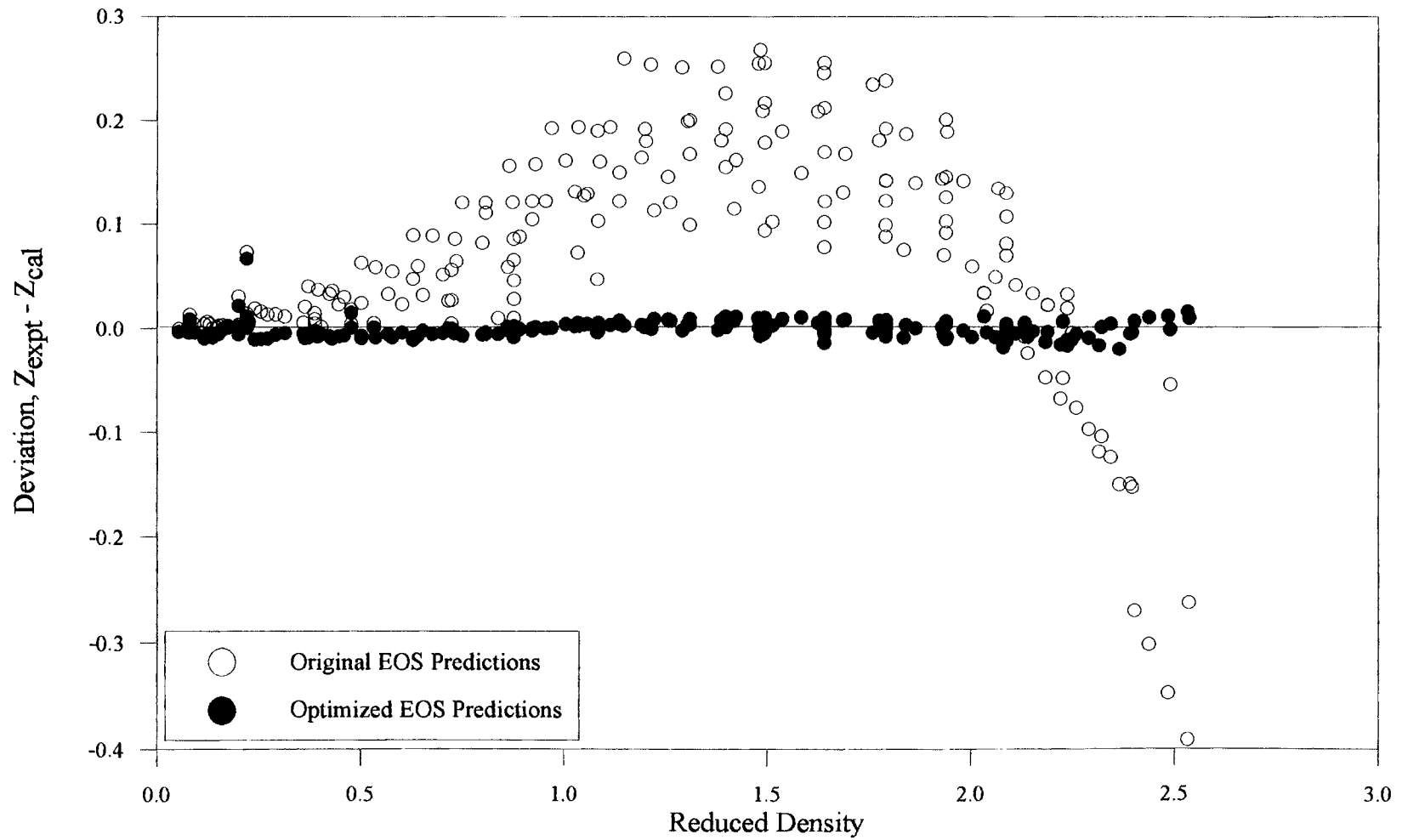
Figure D.4. Deviations in the Carbon Dioxide Compressibility Factors Using the PRG EOS
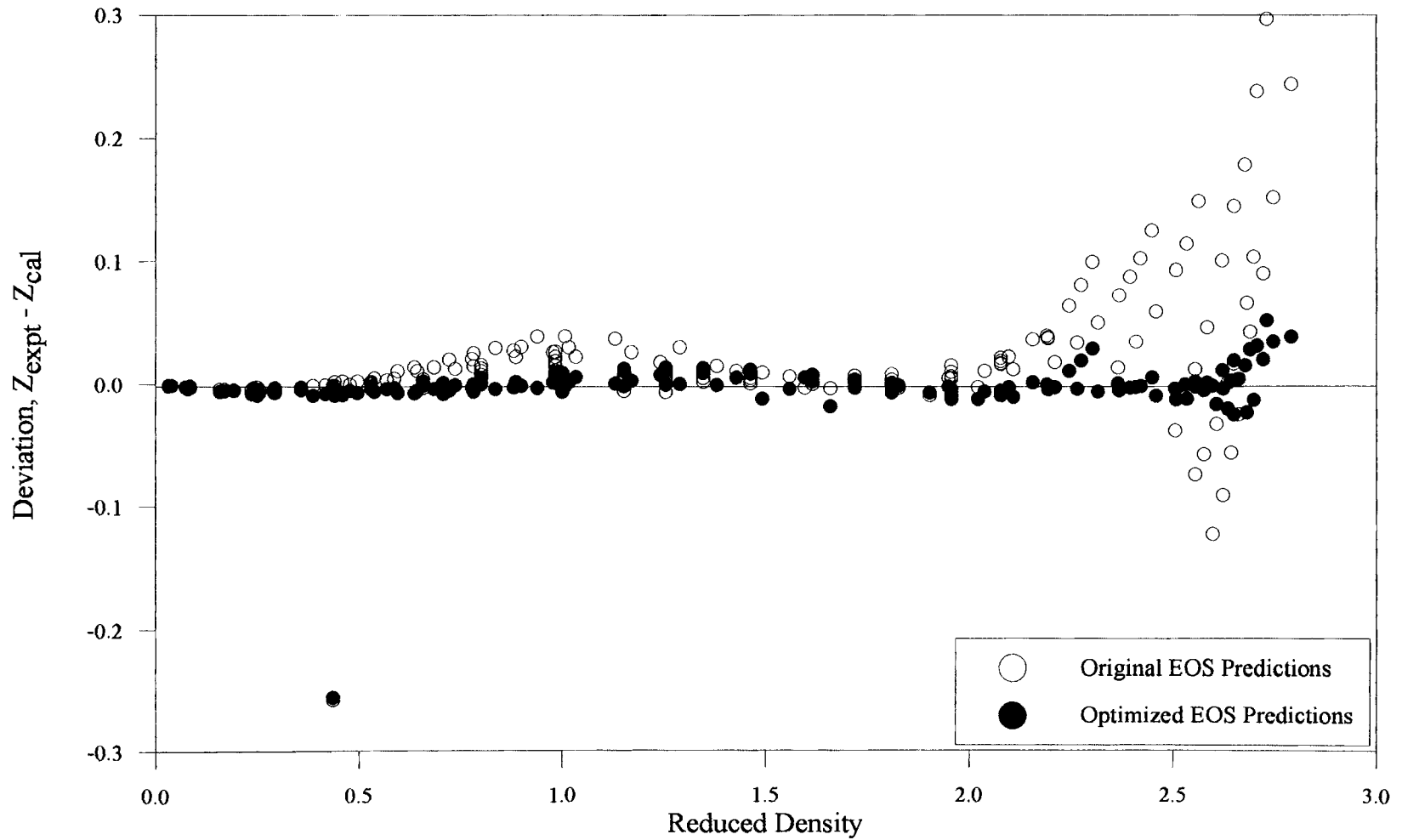
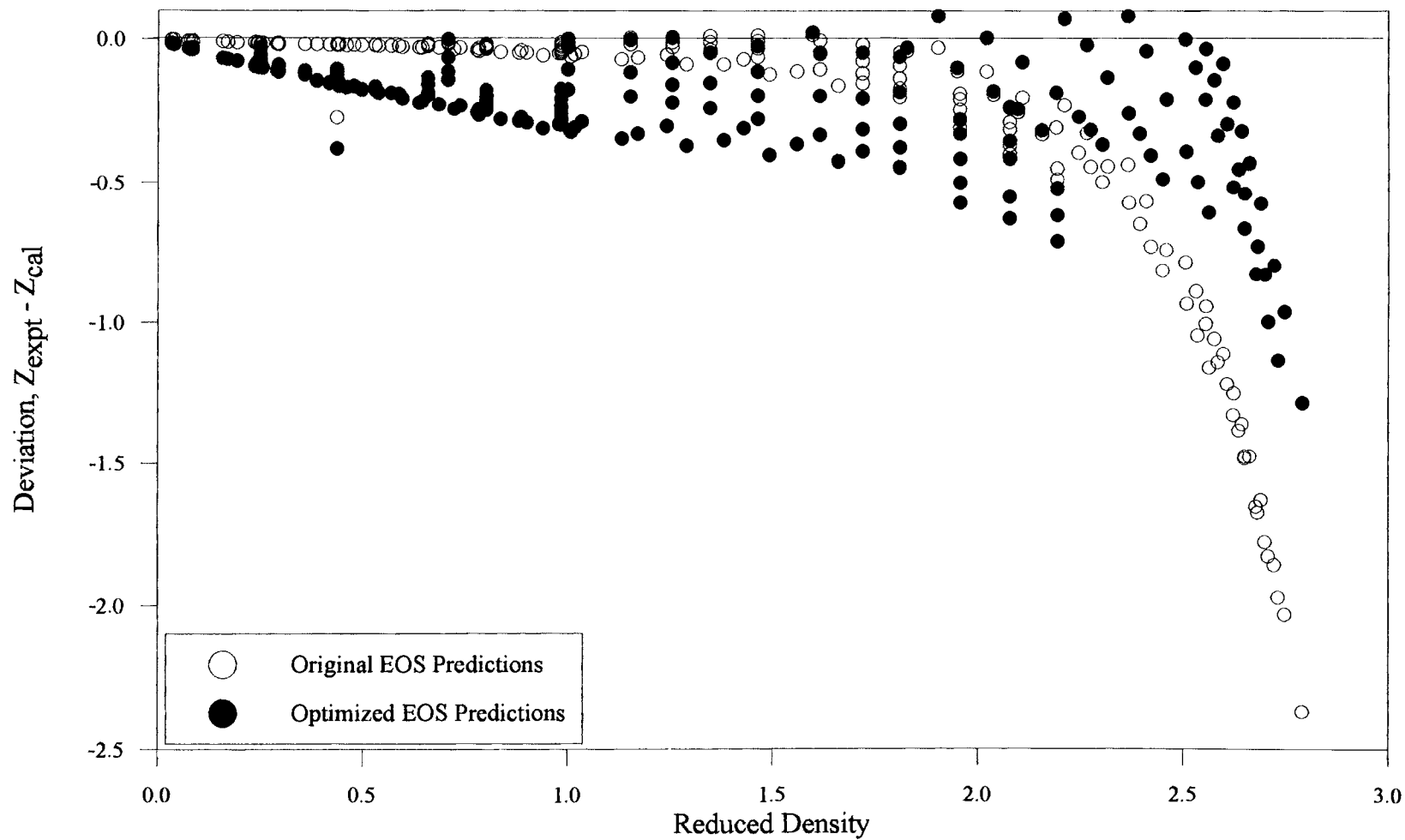Figure D.5. Deviations in the Methane Compressibility Factors Using the BWR EOS

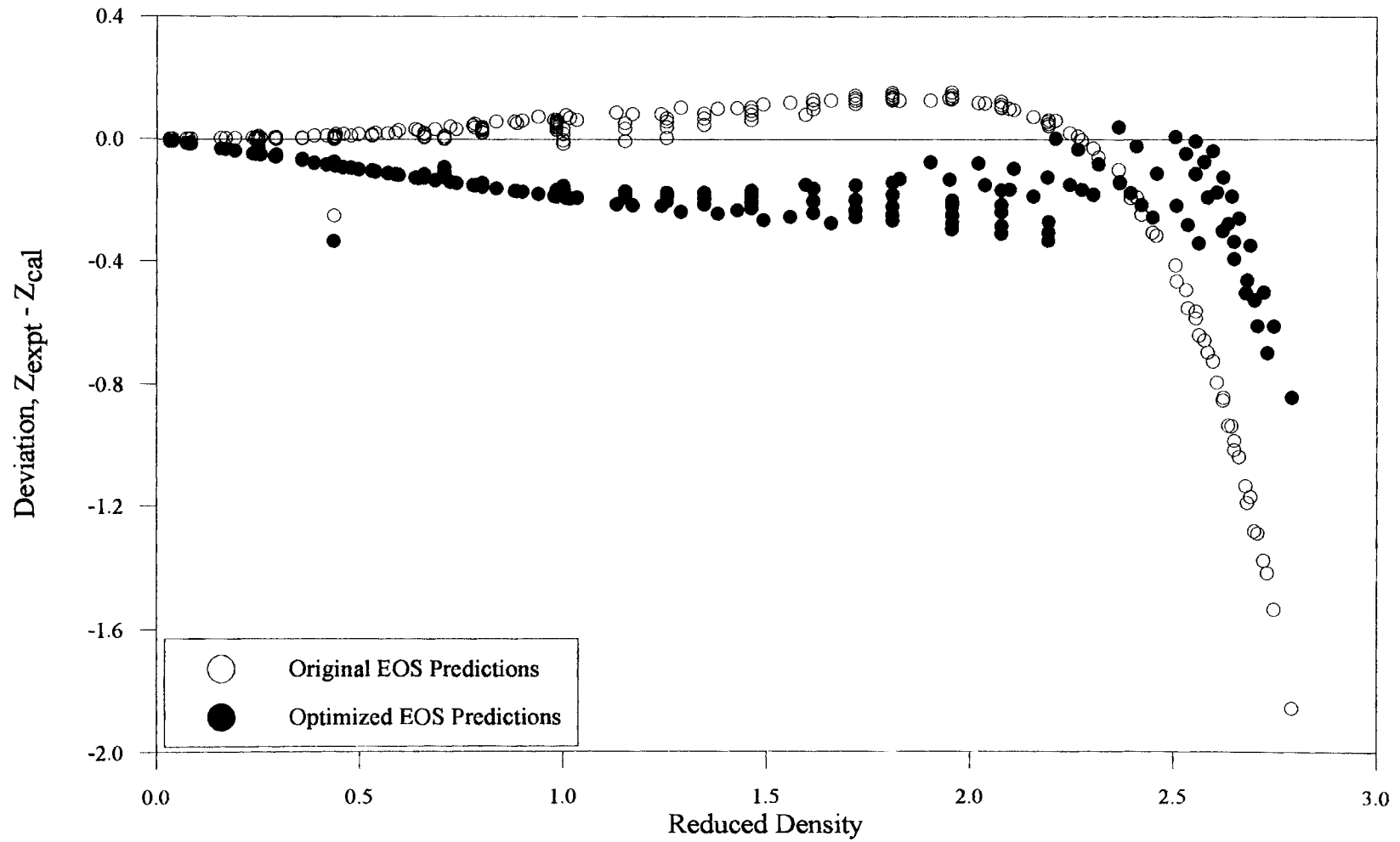Figure D.6. Deviations in the Methane Compressibility Factors Using the PR EOS

Figure D.7. Deviations in the Methane Compressibility Factors Using the SPHCT EOS
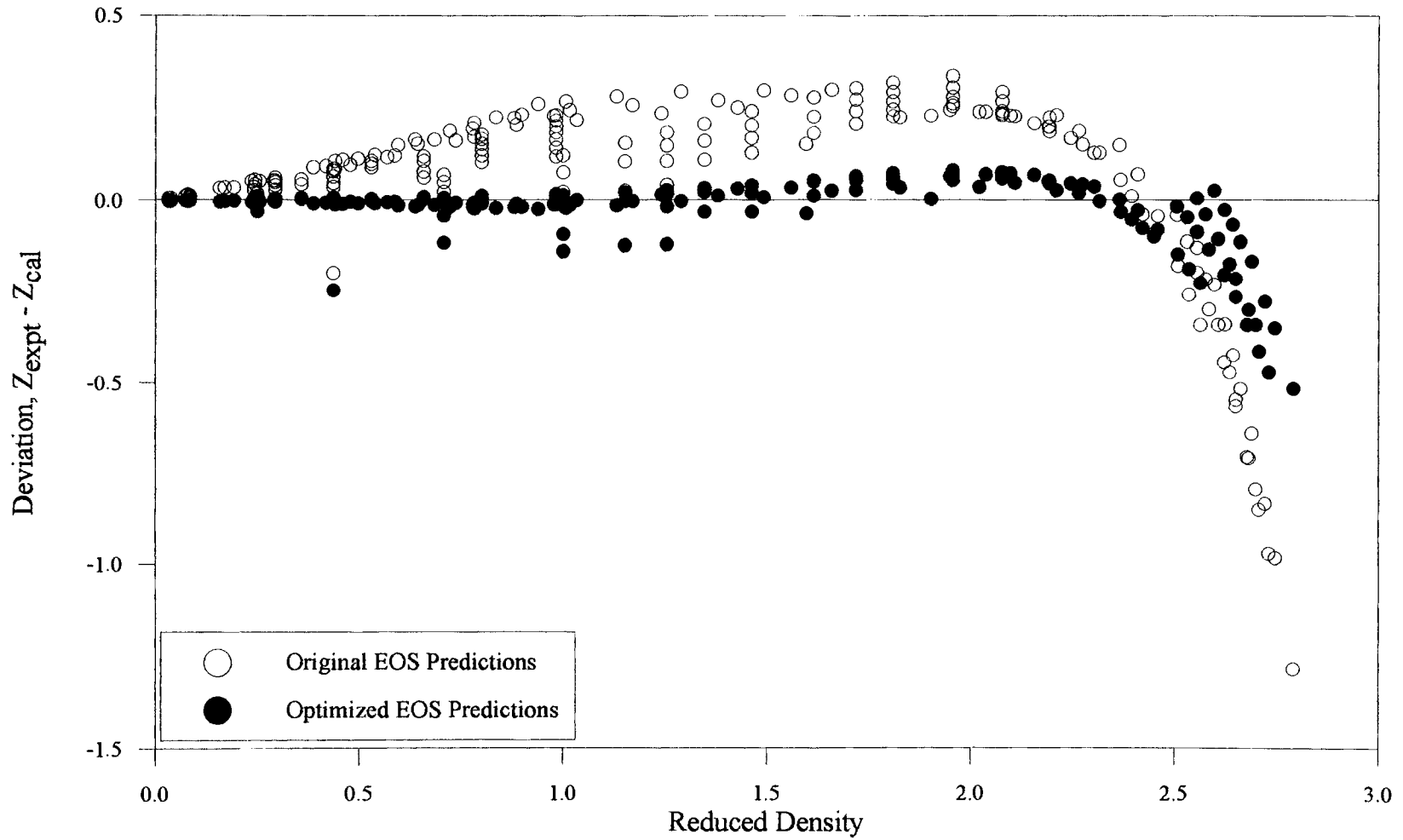
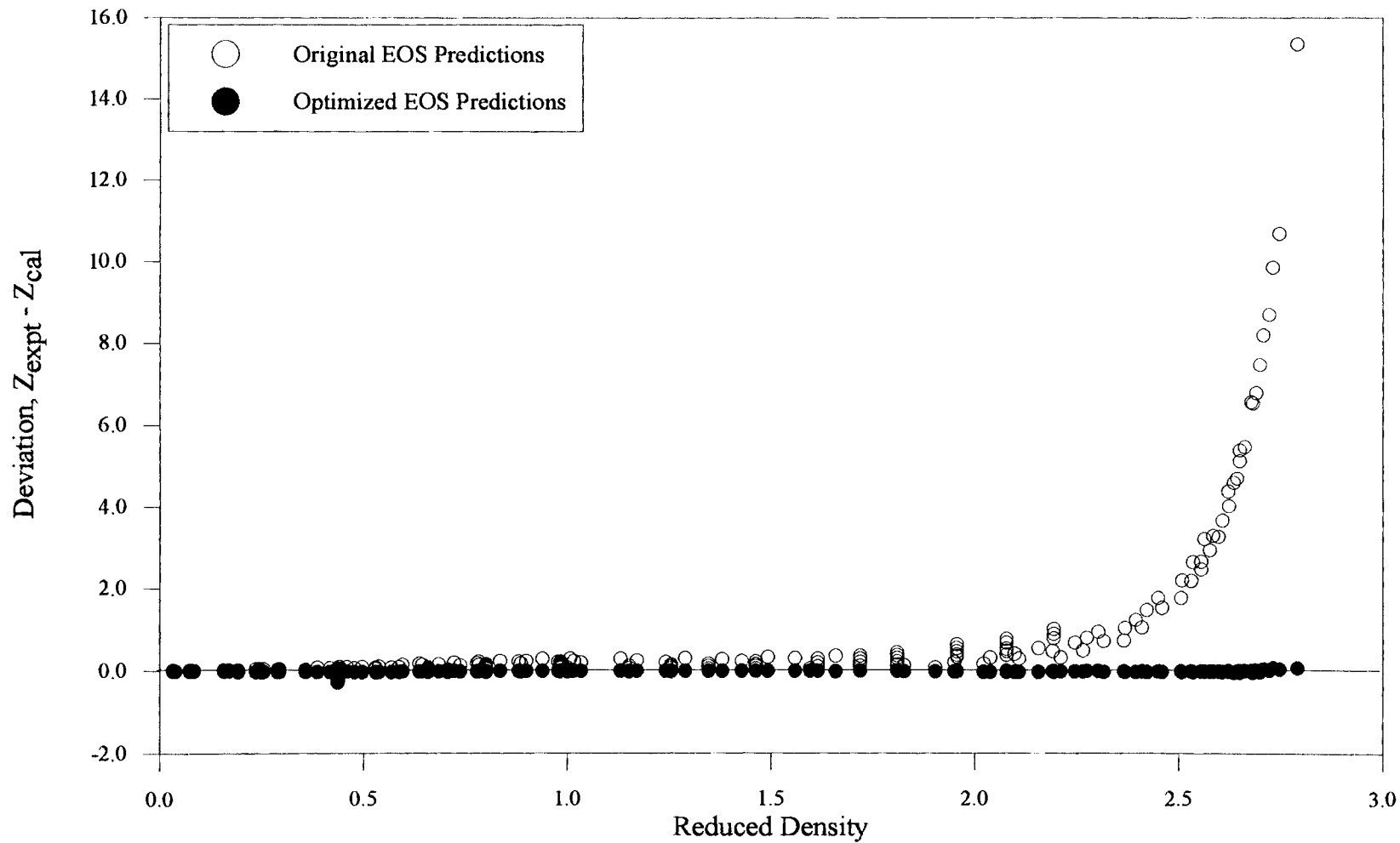Figure D.8. Deviations in the Methane Compressibility Factors Using the MSPHCT EOS

Figure D.9. Deviations in the Methane Compressibility Factors Using the PRG EOS
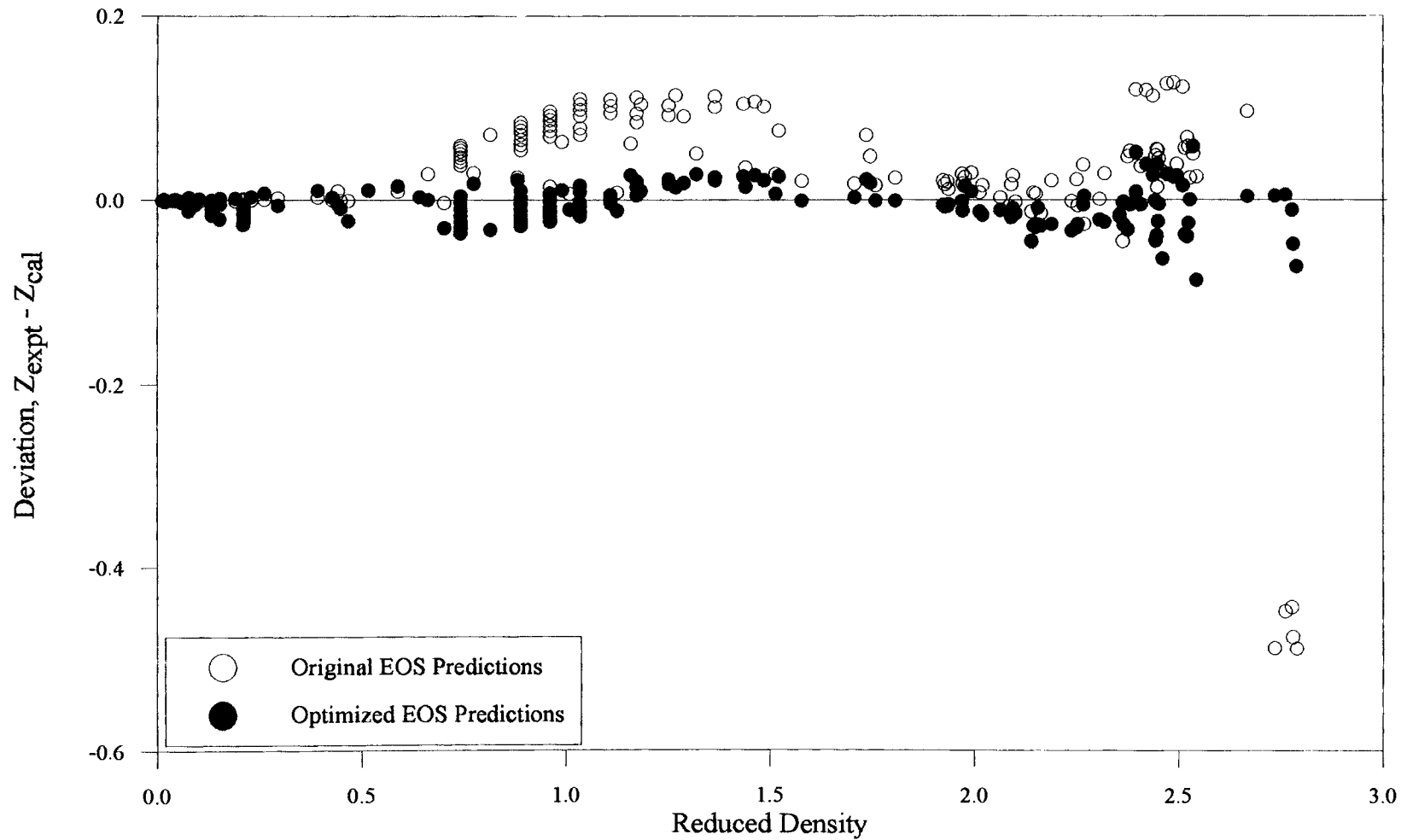
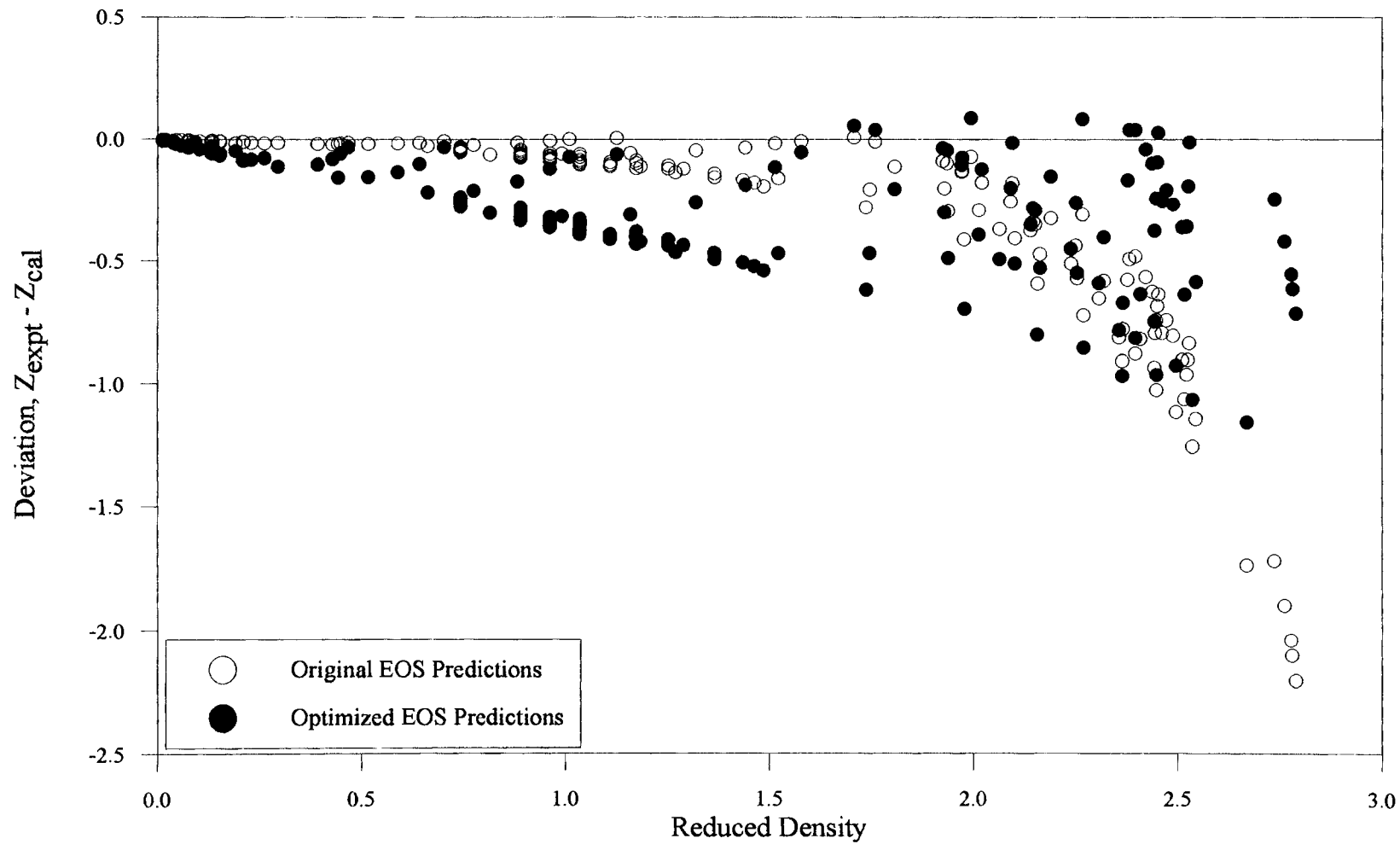Figure D.10. Deviations in the Nitrogen Compressibility Factors Using the BWR EOS

Figure D.11. Deviations in the Nitrogen Compressibility Factors Using the PR EOS

VITA

Suresh Babu Vellanki

Candidate for the Degree of

Master of Science

Thesis: ADSORPTION OF BINARY GAS MIXTURES ON WET FRUITLAND COAL AND COMPRESSIBILITY FACTOR PREDICTIONS

Major Field: Chemical Engineering

Biographical:

    Personal Data: Born in Vijayawada, Andhra Pradesh, India, July 28, 1969, the son of Kasturi and Sankara Rao Vellanki.

    Educational: Graduated from Andhra Loyola College, Vijayawada, Andhra Pradesh, India, in May 1986; received Bachelor of Engineering Degree in Chemical Engineering and Master of Science (Honors) Degree in Chemistry from Birla Institute of Technology and Sciences in June 1991, completed requirements for the Master of Science degree with a major in Chemical Engineering at Oklahoma State University in May 1995.

    Experience: Summer internship at Center for Cellular and Molecular Biology, Hyderabad, 1988, Curricular Practical Training at Indian Rayon Industries, Veraval, 1990. Employed as a Research Assistant, School of Chemical Engineering, Oklahoma State University, August 1992 to July 1993. Employed as a Teaching Assistant, School of Chemical Engineering, Oklahoma State University, August 1993 to December 1993. Employed by College of Engineering , Architecture and Technology as a Research Assistant, January 1994 to December 1994.